

AN OVERVIEW OF RESID CHARACTERIZATION BY MASS SPECTROMETRY AND SMALL ANGLE SCATTERING TECHNIQUES

R. E. Winans and J. E. Hunt
Chemistry Division
Argonne National Laboratory
Argonne, IL 60439

Keywords: petroleum asphaltene, mass spectrometry, small angle X-ray and neutron scattering

ABSTRACT

The purpose of this presentation is to discuss what is known about the molecular structures found in petroleum resid from mass spectrometry and small angle neutron and X-ray scattering methods. The question about molecular size distributions and the occurrence of aggregation in the asphaltene fraction will be examined. Our understanding of this problem has evolved with the application of new analytical methods. Also, correlations with results from other approaches will be discussed. In addition, the issue of the nature of the heteroatom-containing molecules will be examined and the challenges that remain in this area.

INTRODUCTION

As light crudes disappear, there is a need to process heavier crudes with increasing amounts of resid. Petroleum resids can be fractionated by solubility with asphaltenes, the heptane insoluble fraction being the greatest problem in upgrading processing. This fraction is more aromatic than any of the other fractions and contains much of the heteroatoms and metals. Speciation of asphaltenes is extremely difficult and even measuring an accurate molecular weight distribution is problematic. As more is learned about the nature of petroleum asphaltenes, their apparent molecular weights are being lowered. Much of this information is the result of mass spectrometric and small angle X-ray and neutron scattering measurements. These studies suggest that asphaltenes are comprised of molecules with molecular weights less than 1500 and typically are aggregated even in high temperature processing.

Mass Spectrometry

Because of the low volatility of the various components of resid, direct thermal or laser desorption in the MS source has been the most successful MS method to characterize these complex mixtures. Various MS methods have been used including: field ionization mass spectrometry (FIMS), low-voltage (LVMS) and chemical ionization (CIMS), laser desorption mass spectrometry (LDMS), and high resolution mass spectrometry (HRMS).

Some of the first work using this method was reported by Boduszynski, who described a multistep separation followed by characterization of a series of atmospheric resids. The volatile fractions were separated by vacuum distillation and the non-distillable fraction was separated by a sequential elution fractionation (SEF).¹ FIMS data was shown for one of the suite of separation fractions. The mass ranges broaden with succession fractions and the average molecular mass increased until they reached the first SEF fraction, then there was a decrease in subsequent fraction. It was stated that the mass distribution varied with the petroleum source. No significant amount of ions were observed at over a mass of 1900. Although no data was shown, it was stated that field desorption MS gave similar results to FIMS. A more recent FIMS study looked at high molecular weight hydrocarbons from a crude oil and solid bitumen.² Several series of hydrocarbons up to C₁₀ were observed, which corresponds to an upper mass of ~1500, consistent with what has been seen in other studies.

A Middle East vacuum resid was separated by solubility into four fractions: pentane soluble oil, heptane soluble pentane insoluble resins, cyclohexane soluble/heptane insoluble asphaltenes [1], and cyclohexane insoluble asphaltenes [2].³ These fractions were analyzed by thermal volatilization (50-300 °C), low voltage low resolution, mass spectrometry (triple quadrupole MS). The measured average mass decreased within the series: oil (615), resin (485), asphaltene 1 (440) and asphaltene 2 (410). Also, the yields from the thermolysis decreased with an increase in the series and they speculated that upper bounds molecular mass may be higher. However, since the FIMS data showed the same trends, the relative ratios of molecular weights between the fractions may not change even if the entire sample was ionized. CIMS gave similar results to the low voltage experiment.

Although HRMS has been one of the methods of choice for characterizing volatile petroleum fractions, it has only more recently been applied to the complex polar resid fractions.^{4,5} In the HRMS studies, the samples were desorbed from a high temperature probe that was heated from 200-700 °C. Quantitative experiments showed that >95% of the samples, even the asphaltenes, were desorbed. In both HRMS and LDMS, the oil samples gave a larger average molecular weight⁵ distribution compared to the asphaltene samples. This was also the case in the comparison of a non-colloidal (soxhlet extractable) asphaltene. However, the size of the aromatic rings were larger for the asphaltene compared to the oil, as seen in Figure 1. From HRMS data, formulae can be calculated that can yield the type of data shown in Figure 1. The oil, aromatic cores, contained on an average, longer aliphatic side chains that increased the average molecular weight and decreased the tendency for forming colloids. Also, the yield of heteroatom containing molecules was much greater for the asphaltene, as is shown for sulfur in Figure 1.

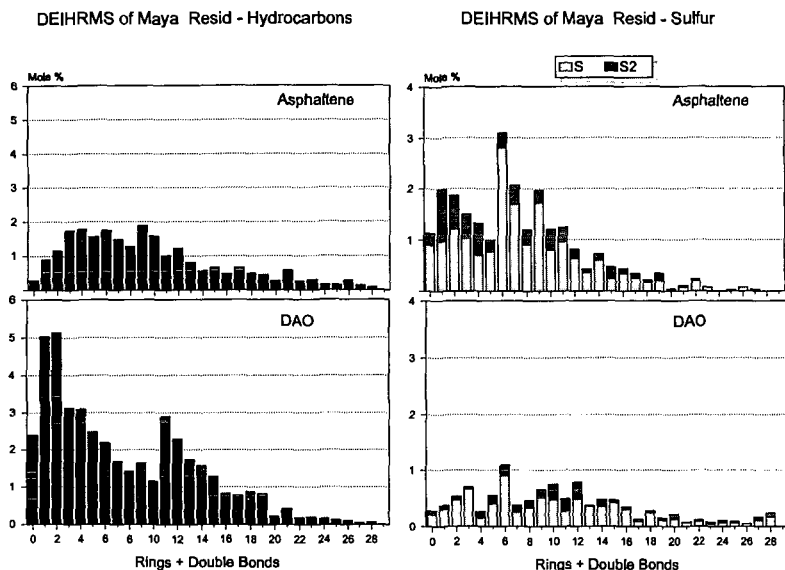


Figure 1. Double bond equivalent distributions for hydrocarbons and sulfur compounds from DEIHMS analysis.

Small Angle Scattering

Using small angle X-ray and neutron scattering methods, the nature of disordered materials over length scales of 6-6000 Å can be observed. Depending on the system, the methods can provide information on molecular or particle size, shape, and surface properties. X-rays scatter off electrons, which are z number dependent phenomena, while neutrons scatter off the nucleus and are dependent on the scattering length density, which can even vary between isotopes such as hydrogen and deuterium.

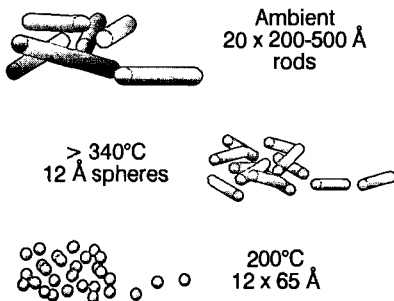
Initial studies using SAXS suggest that vacuum resid asphaltene particles dispersed in resid oil are spherical aggregates that range in radii from 30-60 Å with a polydispersity of 15-20%, depending on the petroleum source.⁶ Using SANS, it has been shown that the size of the asphaltene aggregates do not change with variation of solvent composition for toluene/pyridine mixtures and concentrations of asphaltene in solution. However, from SANS analyses of coal pyridine extracts, it has been shown that pyridine is not a good solvent for complex polar mixtures and does not yield true solutions.⁷

Maya-derived asphaltenes were studied by SANS in *d*₁₀-1-methylnaphthalene from 20-400 °C. Using a modified Guinier analysis, it was shown that the colloidal materials were rod-shaped at the lower temperatures.⁸ These rod-shaped particles had a fairly uniform radius but were polydispersed in length. At high temperature, spherical particles formed resulting in uniform 12 Å spheres at 400 °C. Scheme 1 depicts changes in particle shape and size with temperature. The changes at high

temperature were irreversible and secondary density with covalent bond formation probably occurred. The oils were non-aggregated and showed no scattering.

SCHEME 1

5% wt asphaltenes in
1-methylnaphthalene



Also using SANS, it was found that the size of the colloidal asphaltene particles decreasing with heating as with increasing with dilution with resin material, and increase with the addition of n-hexane.⁹ Apparently resin makes a better solvent than pyridine. Recently, the age hardening of resin was followed by both SAXS and SANS.¹⁰ The asphaltene macrostructure appears not to change with aging and the major effect is the changes in the maltenes.

CONCLUSIONS

From MS and small angle scattering studies, it is apparent that petroleum asphaltenes are colloidal in nature even in "good" solvents and at high temperatures. They are not large polycyclic aromatics, but instead have a maximum ring number of typically 10-11, with the average being 5-6. Asphaltenes are rich in heteroaromatic compounds.

ACKNOWLEDGMENTS

This work was performed under the auspices of the Office of Basic Energy Sciences, Division of Chemical Sciences, U.S. Department of Energy, under contract number W-31-109-ENG-38.

REFERENCES

1. Boduszynski, M. M. *Energy Fuels* **1987**, *1*, 2-11.
2. del Rio, J. C.; Philp, R. P. *Org. Geochem.* **1999**, *30*, 279-286.
3. DeCanio, S. J.; Nero, V. P.; DeTar, M. M.; Storm, D. A. *Fuel* **1990**, *69*, 1233-1236.
4. Miller, J. T.; Fisher, R. B.; Thiyagarajan, P.; Winans, R. E.; Hunt, J. E. *Energy Fuels* **1998**, *12*, 1290-1298.
5. Hunt, J. E.; Winans, R. E.; Miller, J. T. *Prepr. Pap. - Am. Chem. Soc., Div. Fuel Chem.* **1997**, *42*, 427-430.
6. Storm, D. A.; Sheu, E. Y.; DeTar, M. M. *Fuel* **1993**, *72*, 977-981.
7. Storm, D. A.; Sheu, E. Y. *Fuel* **1995**, *74*, 1140-1145.
8. Thiyagarajan, P.; Hunt, J. E.; Winans, R. E.; Anderson, K. B.; Miller, J. T. *Energy Fuels* **1995**, *9*, 829-33.
9. Espinat, D.; Ravey, J. C.; Guille, V.; Lambard, J.; Zemb, T.; Cotton, J. P. *J. Phys. IV* **1993**, *3*, 181-184.
10. Scarsella, M.; Mastrofino, D.; Barre, L.; Espinat, D.; Fenistein, D. *Energy Fuels* **1999**, *13*, 739-747.

PETROLEUM ASPHALTENE MOLECULAR SIZE AND STRUCTURE

Henning Groenzin and Oliver C. Mullins

Schlumberger-Doll Research

Ridgefield, CT 06877

Key words: Asphaltene molecular size, Asphaltene molecular structure, Fluorescence depolarization

Abstract

The rotational correlation times of individual petroleum asphaltene molecules have been determined using fluorescence depolarization techniques, addressing an active, long standing controversy. Using simple theoretical models and using model independent comparisons with known chromophores, a range of asphaltene molecular diameters is obtained of 12 Å to 24 Å and indicates a molecular mass for asphaltene molecules of 500 to 1000 amu. An alkyl-substituted aromatic hydrocarbon with 7 fused rings is shown to correspond to the average molecular size of asphaltenes. Furthermore, the very strong correlation between molecular size and individual chromophore size establishes that the bulk of asphaltene molecules possess 1 or 2 aromatic chromophores per molecule.

I. INTRODUCTION

Petroleum asphaltenes are the heaviest, most aromatic component of crude oil. Asphaltenes are a complex molecular mixture which are colloiddally dispersed in crude oil with a mass fraction of 0 to 10% or more.¹⁻⁶ Asphaltenes generally impede producing, transporting and refining of crude oil resources for a variety of reasons; mitigation of deleterious effects requires a thorough knowledge of the chemical and physical properties of asphaltenes. In addition, the heavy ends of crude oils have many familiar applications related to protective coatings and road paving which can be enhanced by judicious application of asphaltene science. Many bulk properties of asphaltenes have been extensively studied by traditional methods such as NMR, IR, EPR, XANES and optical spectroscopy revealing a great deal about their molecular structure and aggregation propensities.¹⁻⁶

In spite of the wealth of information about asphaltenes, several fundamental properties are not known. The molecular weight of asphaltene molecules has been a matter of controversy for more than a decade. Colligative methods such as vapor pressure osmometry (VPO) generally yield high values¹⁻⁶ quite possibly due to aggregation. Mass spectral techniques yield much lower values (in spite of significant effort to rule out fragmentation).⁷⁻⁹ In addition, there has been considerable uncertainty about the (dominant) number of fused aromatic rings in the asphaltene moieties; estimates have ranged from 4 to >20.¹⁻⁶ Scanning tunneling microscopy (STM) has been used to image directly the aromatic (conductive) components of asphaltene molecules.¹⁰ Size estimates of the fused aromatic ring moieties from these images are approximately 10 Å. NMR¹¹ and optical techniques¹² indicate 7 fused rings on average. Furthermore, there has been uncertainty in the number of fused ring systems per asphaltene molecule with estimates varying widely.

Here, we analyze the fluorescence depolarization rates of very dilute solutions of asphaltenes. These rates give the molecular size with a robust, widely used model. In addition, we analyze known chromophores to provide a model independent analysis of these results. Furthermore, the known dependence of chromophore size to spectral properties has allowed us to correlate the rotation rate of chromophores imbedded in asphaltene molecules with the rotation rate of the molecule as a whole. The excellent correlation of chromophore size to total molecular size over a very broad range strongly implies that asphaltene molecules have one or two fused ring systems per molecule.

II. EXPERIMENTAL SECTION

For all solutions used for fluorescence work, we checked optical densities using a CARY 5 UV-visible-NIR spectrometer. For collection of fluorescence spectra, we employed the PTI C-72 + A-720 fluorescence spectrometer using a 75 watt Xe compact arc lamp source.

The PTI C-72 system was used for collection of fluorescence time-dependent depolarization spectra. This system employs a PTI GL-3300 nitrogen laser source along with a PTI GL-302 high-resolution dye laser with a fiber optic coupling to the measurement cell to excite the

fluorescence. The excitation and emission light from the cell are oriented 90° from each other with vertical polarization defined to be perpendicular to this plane. The wavelength of the PTI model 101 M emission monochromator is fixed while two Glan-Thompson polarizers are used to select the polarizations. One polarizer is placed at the output of the fiber optic, immediately before the measurement cell, and the other polarizer is placed at the entrance to the emission monochromator. Fluorescence time decay curves are collected for four polarizations; vertical on the source side, vertical on the emission side (v-v), vertical-horizontal (v-h), horizontal-vertical (h-v), and horizontal-horizontal (h-h).

The following procedure is used to acquire the time decay spectra; the laser firing triggers a box car delay gate which then triggers a high voltage pulse at known delay to the PMT. The short duration of the high voltage pulse "turns on" the PMT for a short time interval. The integrated current over this time interval from the PMT is detected. The delay time is sequentially scanned over the desired time range providing the fluorescence decay curve. The time resolution of the system is about 80 picoseconds.

A complete data set for one excitation and emission wavelength pair corresponds to acquisition of the four polarization combinations mentioned above. Typically, the total acquisition time for the four curves is 2 hours. Reproducibility of signal levels were checked periodically during the acquisition time to validate the data. Duplicate (or more) runs were performed for all wavelength pairs to assure precision. Typically, chi-square values of 1.2 or less were obtained for a good run. Changes in laser power during the run was associated with large values of chi-square.

The v-h curve has a higher intensity than the v-v curve. This is due to the fact that horizontal and vertical polarized light have different transmission efficiencies through the emission channel of the instrument. This effect can be compensated by introducing a calibration factor, which is usually denoted with a capital *G* and is defined as $G = I_{hv} / I_{vh}$. Where I_{ij} refers to excitation with *i* polarization and emission with *j* polarization. All experimental data sets are corrected by multiplication of *G* with I_{vh} . I_{vh} then refers to I_h , and $I_{hv} \cdot G$ to I_v .

The crude oil sample we used was obtained from Kuwait (UG8). We prepared the n-heptane insoluble asphaltenes from this oil. Optical densities of all solutions were kept below 0.2 OD to avoid complications from self absorption. We maintained asphaltene concentrations at or below 0.025 g/liter for analysis. All rotational correlation times were determined at room temperature 19°C, and in toluene with a viscosity of 0.59 cP. Two dyes, obtained from Aldrich Chemicals, were also used in this study, octaethyl porphyrin (OEP) and a solar dye, N,N'-Ditridecyl-3,4,9,10-perylene-tetracarboxylic diimide.

In order to determine the rotational correlation time of the anisotropy decay, a difference curve $D(t)$ and a sum curve $S(t)$ according to Eq. 1 and 2 were created and fitted by a least squares method. The sum curve corresponds to the fluorescence decay alone. For the fluorescence intensity decay (sum curve) a double exponential decay was assumed. Since the anisotropy decay is much faster than the fluorescence decay for our cases, then the difference curve is governed by the anisotropy decay. Consequently, the difference curve was fitted in accordance to the theory to a single exponential decay. A mean lifetime of the fluorescence intensity decay was calculated and the rotational correlation time was obtained by combining the mean fluorescence intensity lifetime of the sum curve with the fluorescence intensity lifetime of the difference curve according to Eq. 3.

III. THEORY

We use the anisotropy decay treatment¹³ which approximates molecules as spheres. This model is widely used to analyze experimental data in part because inclusion of moderate molecular asymmetries does not affect calculated parameters too much.

The following definitions are used:

$$D(t) = I_v(t) - I_h(t) \quad (1)$$

$$S(t) = I_v(t) + 2I_h(t) \quad (2)$$

and

$$r(t) = \frac{D(t)}{S(t)} \quad (3)$$

where $I_{\parallel}(t)$ and $I_{\perp}(t)$ denote a detection of light linear polarized parallel and perpendicular to the linear polarized excitation and $r(t)$ represents the anisotropy of the fluorescence emission. The anisotropy is given by¹³

$$r(t) = \frac{2}{5} e^{-6Dt} \quad (4)$$

where D is given by

$$6D = \frac{kT}{V\eta} \quad (5)$$

where η is the viscosity of the solvent, which makes it easy to relate the fluorescence anisotropy to the volume of the sphere. The decay time of the anisotropy $\tau_{r,spk}$, the parameter of our experiment, can now be written as

$$\tau_{r,spk}^{-1} = \frac{kT}{V\eta} \quad (6)$$

IV. RESULTS AND DISCUSSION

Figure 1b shows the fluorescence emission spectrum of a dilute solution of UG8 asphaltene obtained with 365 nm excitation. This spectrum represents the overlapping spectra of the many chromophores contained within the asphaltene and indicates the range of aromatic moieties in asphaltenes. The asphaltene fluorescence emission is significant in the range of from 400 nm to 650 nm indicating the number of fused rings in the asphaltene chromophores is on the order to 4 to 10.¹² By selection of excitation and emission wavelength, one can select a subset of chromophores. Long wavelength excitation precludes excitation of small chromophores. Correspondingly, with short wavelength excitation, detection of fluorescence from large chromophores can be precluded by detecting short wavelength emission; large chromophores emit long wavelength fluorescence. The full range of chromophores is probed by tuning the excitation wavelength over the relevant spectral range, while keeping a fixed wavelength difference between excitation and emission.

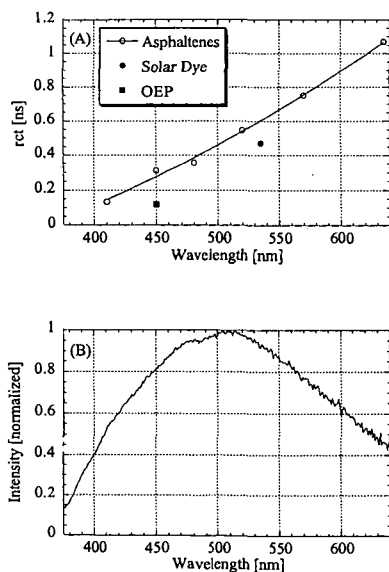


Figure caption 1. a) The rotational correlations of asphaltenes (and two dyes) vs emission wavelength. For each wavelength, the excitation wavelength is about 40 nm to shorter wavelength. b) the emission spectrum of the asphaltenes, showing the relevant spectral range.

Figure 1a shows the rotational correlation time of asphaltenes as a function of the emission wavelength. These emission wavelengths correspond to the largest populations of asphaltene chromophores as seen in Fig. 1b. For each point in Fig. 1a, the excitation wavelengths are ~40 nm to shorter wavelength. In addition, two known chromophores are also plotted in figure 1a to provide a model independent estimate of molecular size and molecular weight. Figure 1a is rich in results. The variation of a factor of 10 for the rotational correlation times for the most prominent asphaltene molecules. Using Eq. 6, one finds that the radius varies by about a factor of two. In table 1, we list molecular rotational correlation times along with the calculated diameters.

Table 1. Fluorescence absorption and emission wavelengths, rotational correlation times and the molecular diameter for asphaltenes and two dyes.

Sample	λ_{ex} (nm)	λ_{em} (nm)	τ_{rc} (ns)	Diameter(Å)
Asphaltenes	365	410	0.1340	12.0
	406	450	0.3115	15.9
	440	480	0.3561	16.6
	480	520	0.5464	19.2
	530	570	0.7518	21.3
	595	635	1.0688	24.0
Solar Dye	480	535	0.4704	18.2
OEP	406	450	0.1194	11.6

Table 1 shows the diameters for the asphaltenes to be in the range of 12 Å to 24 Å. The STM results quoted a mean value of the aromatic component of asphaltenes to be 10 Å in diameter. The fluorescence depolarization technique is sensitive to the size of the entire molecule, while the STM method is sensitive to the size of the aromatic portion only which is roughly 40% of the molecule. Both techniques yield comparable and small sizes for the asphaltene molecules.

Table 1 also lists the diameters for two dyes. Previously, the size of a metallo-OEP was determined by measuring the rotational correlation time using the very different technique, perturbed angular correlation of gamma rays (PAC).¹⁴ (The central metal in the porphyrin has no impact on the diameter of the porphyrin.) In that work, a spherical model was used and a diameter of 11.6 Å was found in excellent agreement with results reported here.

The two disk shaped dyes provide a good estimation of the molecular weight for asphaltenes. The rotational correlation time of the porphyrin OEP is at the lower limit for the asphaltenes. The molecular weight of the porphyrin is 535 amu giving the lower value estimation for the asphaltene molecular weights of 500 amu. The rotational correlation time of the solar dye is located roughly at the mean correlation time of the asphaltenes. The molecular weight of the solar dye is 755 amu giving an estimate of 750 amu for the mean asphaltene molecular weight. Extrapolating the size, molecular weight relation, we estimate the maximum molecular weight of the asphaltenes to be about 1000 amu.

Fig. 1 also shows that there is a monotonic, order-of-magnitude increase in the rotational correlation time across the asphaltene spectral range. That is, there is a strong correlation between the size of the asphaltene chromophore given by the emission wavelength and the size of the molecule, given by the rotational correlation time. This correlation requires that asphaltene molecules have only one or two chromophores per molecule. If an asphaltene molecule possessed say 10 chromophores per molecule, then there would be no correlation between chromophore size and molecular size. A small chromophore attached to a large molecule would exhibit the slow rotational correlation time of the entire, large molecule. The fact that we measure fast rotation for small chromophores and a factor of 10 slower rotation for large chromophores means that these chromophores are an appreciable fraction of the asphaltene molecule. Thus, asphaltene molecules possess one or two chromophores per molecule on average.

V. CONCLUSIONS

The asphaltene rotational correlation times have been measured and corresponding asphaltene molecular diameters are in the range of 12 Å to 24 Å. Using known chromophores, asphaltene molecular weights are estimated to be in the range of 500 to 1000 amu. Furthermore, a strong correlation between chromophore size and asphaltene molecular size indicates that asphaltenes possess 1 or 2 chromophores per molecules, confirming the small molecular weights. Our results

are consistent with previously reported STM results and mass spectroscopy results for petroleum asphaltenes. The confluence of evidence from three very different techniques should end the controversy over the values of asphaltene molecular weights.

VI. REFERENCES

- 1) G. V. Chilingarian, T. F. Yen, Eds., "Bitumens, Asphalts, and Tar Sands," Elsevier Scientific Publishing Co., New York, (1978)
- 2) J.G. Speight, "The Chemistry and Technology of Petroleum," Marcel Dekker, New York, (1980)
- 3) B.P. Tissot, D.H. Welte, "Petroleum Formation and Occurrence," Springer-Verlag, Berlin, (1984)
- 4) J.W. Bunger, N.C. Li, Eds., "Chemistry of Asphaltenes," American Chemical Society, Washington D.C., (1984)
- 5) E.Y. Sheu, O.C. Mullins, Eds., "Asphaltenes, Fundamentals and Applications," Plenum Press, New York, (1995)
- 6) O.C. Mullins, E.Y. Sheu, Eds. "Structures and Dynamics of Asphaltenes," Plenum Press, New York, (1998)
- 7) M.M. Boduszynski, in ref. 4.
- 8) M.M. Boduszynski, *Energy & Fuels*, 2, 597, (1988)
- 9) J.T. Miller, R.B. Fisher, P. Thiyagarajan, R.E. Winans, J.E. Hunt, *Energy & Fuels*, 12, 1290, (1998)
- 10) G.W. Zajac, N.K. Sethi, J.T. Joseph, *Scan. Micros.* 8, 463 (1994)
- 11) R. Scotti, L. Montanari, Ch 3 in ref. 6.
- 12) O.C. Mullins, Ch 2 in ref. 6.
- 13) T. Tao, *Biopolymers*, 8, 607, (1962)
- 14) O.C. Mullins, M. Kaplan, *J. Chem. Phys.* 79, 4475, (1983)

USE OF LASER TECHNIQUES FOR THE STUDY OF ASPHALTENE AGGREGATION AND ADSORPTION.

Sócrates Acevedo^{*1}, María A. Ranaudo¹, Jimmy Castillo², Manuel Caetano² and Alberto Fernández². Labs of Físico Química de Hidrocarburos¹ and Espectroscopia Laser², Escuela de Química, Facultad de Ciencias, 47102, Caracas, 1041 Venezuela.

Keywords: Asphaltenes, Adsorption, Laser

Introduction.

The adsorption of asphaltenes on mineral surfaces is an important phenomena related to many process in crude oil processing such as changes in humectability of oil well, asphaltene precipitation during production, transportation and storage, pore well clogging, catalysis fouling, etc. This has promoted some studies of asphaltene adsorption in the past^{1,2}. Most of these studies, performed with very diluted solutions, afforded L-type isotherms, suggesting the saturation of the interface without further adsorption of sample. However, as shown below, using several laser techniques, we found that adsorption of asphaltenes on silica and glass surfaces could lead to step-wise adsorption and to the formation of thick multilayers which in some cases amount to grams of sample per gram of adsorbent. In this communication we review our previous work in this area and some new results are presented.

Methods.

Furrial crude oil (20° API, and 10% asphaltene) was used. This crude is from Monagas State in the east part of Venezuela and was selected due to the severe asphaltene precipitation problems it presents. Asphaltenes were obtained by precipitation, by the addition of 40 volumes of n-heptane to the crude oil as described elsewhere³. Commercial samples of silica gel for chromatography were used as the adsorbent. Using the dye method (methylene blue-water), an area of about 35 m²/g was obtained for this solid when an area of 120 Å² per molecule was used for the dye⁴. For kinetic runs, small silica plates (2.5x1 cm², 24 mg of silica) were introduced in small glass vials containing 8 mL of asphaltene-toluene solution. These vials were well stoppered to avoid solvent evaporation. Changes in absorbance with time was continuously monitored by passing a He-Ne laser beam (632.8 nm) through the vials and the intensity registered by using a photodiode. In one experiment (asphaltene concentration equal to 200 mgL⁻¹) the solution was stirred by using a small magnetic stirrer. Since no difference in rate was observed with and without stirring all experiment were carried out without stirring. A desorption experiment was performed as follows: Asphaltenes were adsorbed on a silica plate from a 200 mgL⁻¹ solution as described above. After 72 h, the quantity of sample adsorbed was equivalent to 133 mgL⁻¹. The plate was withdrawn, dried and embedded in pure toluene. The absorbance increase was monitored as usual and after 50 h no further change was observed. The amount desorbed was equivalent to 4 mgL⁻¹.

Isotherms were measured using the photothermal surface deformation (PSD) method described earlier³. Briefly, in this method the amount of solute adsorbed on the surface is determined directly. That is, by using a procedure similar to the one described for the kinetic runs (see above) the sample was adsorbed on the silica plate. After the required time, the plate was withdrawn, dried and set for analysis. This was performed by using two lasers, one for pumping and the other as the probe. The pumping beam heat the sample and produces a dilatation that is proportional to the sample mass. This is measured by the probe beam. Signal calibration was performed by comparing with the adsorption measured by transmittance measured as described in the kinetic runs.

In another experiment a silica plate was contacted with a toluene solution of asphaltene (5000 mgL⁻¹) during 24 h in the same way as described above for the kinetic studies. After this time, the plate was withdrawn from this solution, allowed to dry and the sample adsorbed was determined by weight difference. After this, the same plate was contacted with a fresh solution of the same concentration and the procedure was repeated for one day periods during 21 days.

Number average molecular weight (M_n) and molecular weight distribution (MWD) were measured by GPC in THF as described earlier⁵. The samples were analyzed as follows: Toluene solution of asphaltenes were contacted with silica for periods of 1, 4, 8 and 24 hours. After these times, an aliquot was withdrawn, the toluene was evaporated, the residue dissolved in THF and the above M_n and MWD of Furrial asphaltenes were determined in

each case.

When required the area per asphaltene molecule A_a was estimated from equation 1:

$$A_a = 0.166(MA_s/v) \quad 1$$

Here A_s is the area of the silica in m^2/g , v the sample adsorbed is in mg/g , A_a is in Å^2 per molecule and M is the molecular weight.

Results.

On Table I the values for the apparent first order constants k , obtained for the studied solutions are shown. These were obtained by fitting the results to a first order kinetics. The fittings were quite good for the $5\text{-}50 \text{ mgL}^{-1}$ runs. However, for the 200 and 400 mgL^{-1} runs the results suggested that the readings at long times should correspond to a slower rate (see Figure 1). Results from the desorption experiment (see above) showed that desorption from the surface could be neglected in the concentration range examined. The adsorption isotherms obtained are shown in the Figure 2. Note that for 18 and 48 h, the isotherms are L-type whereas the one measured at 96 h shows a tendency towards H-type. In other words, the isotherm slope increases with time and moves to smaller c_s values in the more diluted region. Using the procedure described above, no significant changes in M_n or MWD were detected as a function of the contact time between the asphaltene solution and the silica. M_n values remained constant around 1000 and the MWD measured was in the range from 12000 to 200 in all cases.

In order to have an approximated idea of the amount of asphaltenes that could be adsorbed when the surface is in permanent contact with a liquid with a constant asphaltene concentration, such as the the surfaces in the crude oil well, the experiment above, where the surface is contacted with fresh toluene solutions after 24 h periods was carried out. After 21 days we found that the equivalent of 10g of asphaltene adsorbed on one gram of silica.

Discussion.

Since adsorption rates were not changed significantly by stirring (see above), diffusion to the outer surface of the solid is not rate determining. Also neither average molecular weight nor molecular weight distribution were affected by adsorption (see Methods), suggesting that diffusion into solid pores is not kinetically important. Thus it appears that diffusion along the surface to find a site for adsorption is rate determining, since desorption in this concentration range is unimportant. Using a Langmuir treatment for the dye we found that only 14.4 mg/g of this compound were needed to saturate the silica surface. By using any reasonable value of A_a for asphaltene lying on the surface, one should expect saturation values much smaller than this. However, according to Figure 2, these "saturation" values are higher than 20 mg/g and show a slow increase with time. These results and the first order found, suggest that when asphaltenes are adsorbed they create new adsorption sites where other asphaltene molecules could be adsorbed. In this way the sample could pile up at different places in the surface and by the time the silica surface is completely covered an asphaltene multilayer is already present. This would explain the somewhat slower adsorption rate found at long times with the more concentrated solutions (see above and Figure 1). Also, adsorption of small aggregates, such as dimmers, trimmers, etc is likely in this concentration range. Using a thermal lens technique it was suggested that aggregation of asphaltenes in toluene could begin at very low concentrations, probably around $50 \text{ mgL}^{-1,6}$.

When the adsorption of toluene solutions of asphaltene on glass plates was studied by the above PSD technique in a wider concentration range ($0\text{-}6000 \text{ mgL}^{-1}$) step-wise adsorption isotherms were found for several asphaltene samples (Furrial, Hamaca, Jobo)³. The occurrence of such steps as a result of the adsorption of large aggregates is an interesting possibility. In any case, thick multilayers were apparent from these adsorption measurements.

According to the results above, under appropriated conditions, very large quantities of asphaltenes could be adsorbed on silica (up to 10 g/g or more). This suggest that adsorption alone could easily leads to plugging of pore wells and other problems related to solid formation during oil production.

Conclusions.

Use of lasers, either in the usual transmittance mode or in the PSD mode allows the quantitative study of asphaltene adsorption. Also, reasonable inferences about aggregate formation in solution could be made from these studies. The first order adsorption rates measured in this work were found consistent with multilayer formation and aggregate

adsorption. The L-type isotherm found after 18 h is probably due to saturation of the surface by a multilayer of asphaltene formed either as usual, or by the adsorption of aggregates. Change of these isotherms with time after long periods are due to the adsorption of asphaltene or asphaltene aggregates on the multilayer. Since adsorption alone could lead to plugging of pores and the formation of organic solid deposits, treatment with surfactants and solvents should consider, as a very important consideration, the displacement of asphaltenes from the surface.

Acknowledgments.

Financial support from CONICIT (Grant N° G97000722) and CDCH (Grants 03.12.4897/98, 03.12.3872/98, 03.12.4031/97, 03.12.4087/98) is gratefully acknowledged.

References.

1. S. H. Collins and J. C. Melrose, Soc. pet. Eng. SPE11800, 249 (1983).
2. González, G., and Middea, A. Colloids and Surfaces, 33, (1988), 217.
3. Acevedo, S., Castillo, J., Fernández, A., Goncalves, S., and Ranaudo, M. A., Energy and Fuels, 12, (1997), 386.
4. Giles, H. Ch. In: "Anionic Surfactant. Physical Chemistry of Surfactant Action". (E. H. Lucassen - Reynders, Ed). Surfactant Science Series. V 11. Marcel Dekker, Inc. 1981, Chap. 4.
5. Acevedo, S., Escobar, G., Gutiérrez, L. B., and D'Aquino, J., Fuel, 71, (1992), 1077.
6. Acevedo, S., Ranaudo, M. A., Pereira, J. C., Castillo, J., Fernández, A., Pérez, P., and Caetano, M., Fuel, 1999, to be published.

Table I. Apparent first order rate constant k , for the adsorption of Toluene Solution of Furril Asphaltenes on Silica^a.

Initial concentration (mg L ⁻¹)	$k \times 10^3$ (min ⁻¹) ^a	R ^{2,b}
5	1.09 ± 0.8	0.991
20	1.24 ± 0.3	0.993
50	1.12 ± 0.3	0.996
200 ^c	1.62 ± 0.3	0.992
400 ^c	0.79 ± 0.3	0.994

a: At Room temperature. b: Correlation coefficient for first order fitting. C: see text.

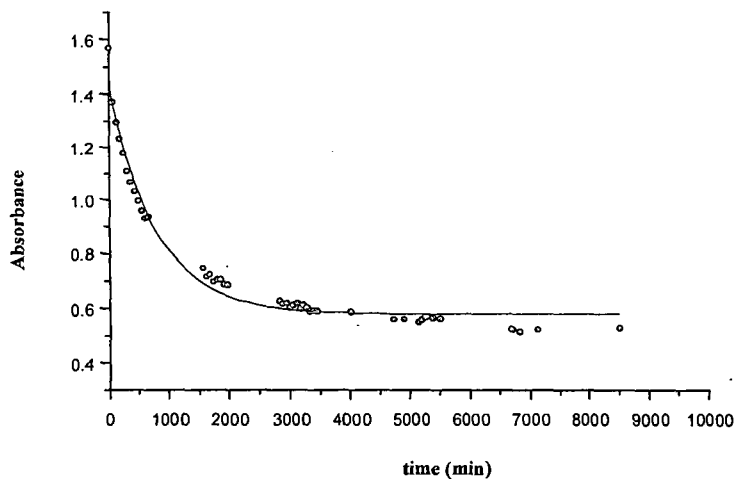


Figure 1. Adsorption kinetics for a toluene solution of Furril asphaltenes (200 mg L⁻¹) obtained on silica at room temperature. Points are experimental and the curve is the fitting to a first order.

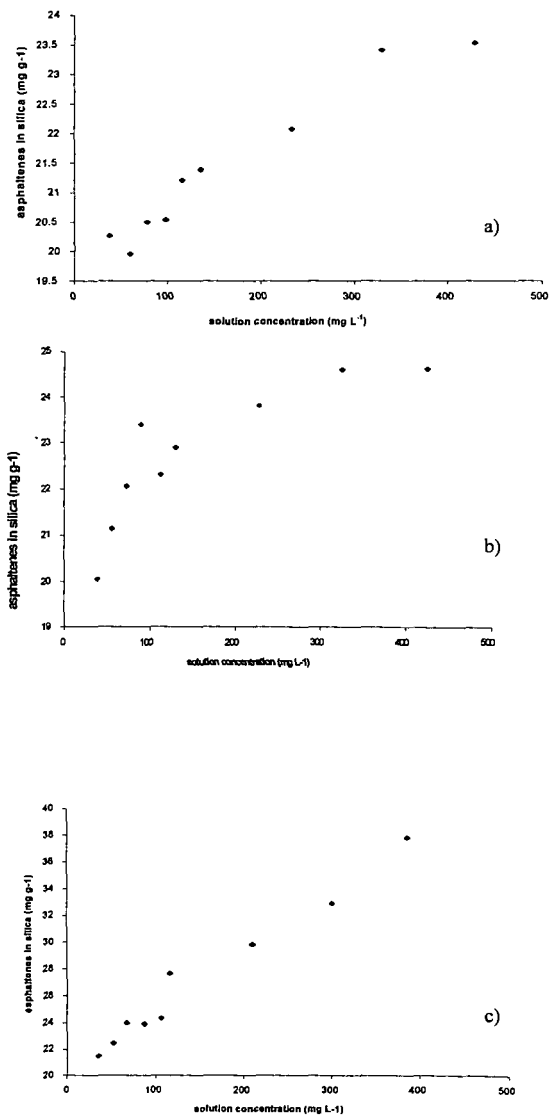


Figure 2. Adsorption isotherm of toluene solutions of Furrrial asphaltenes on silica measured by PSD at room temperature. a) after 18 hours, b) after 48 hours, c) after 96 hours.

STUDY ON THE MICELLE SIZE OF ASPHALTENES IN VACUUM RESIDUE BY DIELECTRIC LOSS

M. Fujii, T. Yoneda, and Y. Sanada*
Advanced Catalysts Research Laboratory
Petroleum Energy Center, Japan
KSP D-1237, 3-2-1, Sakato, Takatsu-ku,
Kawasaki, Kanagawa 213-0012, Japan

* Honor Professor of Hokkaido University
16-1-1, Hiragishi-ichijyo, Toyohira-ku
Sapporo, Hokkaido 062, Japan

KEYWORDS: asphaltene, micelle size, dielectric loss

INTRODUCTION

Asphaltene contained in heavy oils, such as crude oil or vacuum residue is obtained usually as the precipitates when adding alkane to heavy oil. It is defined as n-heptane insoluble-toluene soluble, for example. As asphaltenes are mainly composed of poly-condensed aromatics, they intend to form micelles in the oils by interacting each other, and their stacking governs physical and chemical properties of asphaltene rich heavy oils. A number of analyses have been made by using various kinds of measurements and micellar structural models have been proposed [1,2]. The size of micelle has been studied by using many techniques, such as X-ray diffraction (XRD), dielectric relaxation, rheological measurements, small angle neutron scattering (SANS) technique, X-ray absorption near edge structure (XANES) [3,4]. XRD was done for asphaltene powder, and the others were in various solvents. Therefore, it would not be clear the substantial size of micelles in the real heavy oil. During the course of characterization of asphaltene derived from Arabian heavy vacuum residue (AH-VR), we have found that the mass distribution was in the range from $m/z=200$ to 6000, having a broad peak near 1500 with a shoulder peak near 400, by means of laser desorption mass spectroscopy (LDMS) [5]. In this study, we have attempted to measure the dielectric response for AH-VR by an impedance analyzer, and found the loss peak due to asphaltene component. From the results about the effect on the concentration of asphaltene and resin in VR, the mechanism of micelle formation and the size of micelles are discussed.

EXPERIMENTAL

Samples used were AH-VR and VR fractions (b.p. of 793°K) of the hydrotreated oil from AH atmospheric residue (616°K). Asphaltene was prepared from VR with addition of n-heptane (solvent and VR ratio was 1g / 30ml). Maltene (n-heptane soluble) was separated to three fractions (i.e. saturate, aromatic and resin) by column chromatography. Hydrotreatment was performed in a fixed bed continuous flow reactor system, in which hydrodemetallization (HDM) and hydrodesulfurization (HDS) catalysts were installed respectively. The reactor system and reaction conditions were the same described previously except catalyst and LHSV of 0.75 hr⁻¹ [5].

Dielectric loss was measured with a Hewlett-Packard Impedance Analyzer (HP4194A), connecting with Liquid Test Fixture (HP16452A) at 403K. Electrodes with diameter of 38 mm each have been kept space of 1 mm. The working frequency range was from 100 Hz to 15 MHz. Viscosity measurement was made using a TOKIMEC B type viscometer.

RESULTS AND DISCUSSION

In a condenser of parallel plates, the dielectric loss (ϵ'') is represented as follows:

$$\epsilon'' = 1/2 \pi f C v R p \quad (1)$$

where f is the frequency, Cv the capacity in vacuum ($= \epsilon_0 A/d$), Rp the impedance, d the distance between electrode plates, ϵ_0 the dielectric constant of vacuum, and A the area of electrode [6]. As the conductivity (ρ) is equal to d/RpA , eq.(1) becomes:

$$\epsilon'' = \rho / 2 \pi f \epsilon_0 \quad (2)$$

In our results, the values of ρ at range from 10^2 to 10^3 Hz were rather small than those of higher frequency. So, we evaluated the difference dielectric loss ($\Delta \epsilon''$) calculated the following equation:

$$\Delta \epsilon'' = (\rho - \rho_{100}) / 2 \pi f \epsilon_0 \quad (3)$$

where ρ_{100} is the ρ at 100 Hz.

The dielectric loss spectra for AH-VR and fractions derived from it are shown in Figure 1. For AH-VR two peaks were observed at the low frequency side (7.94×10^2 Hz) and the high side (3.98×10^6 Hz), which were appeared due to the existence of the dipole. As the high frequency peak was also observed for maltene, the low frequency peak was contributed from asphaltene. The loss spectra for saturate and aromatic were also shown in Figure 1 (The spectrum for resin was not obtained because of its poor fusibility). Dielectric loss curve for the saturate was almost flat, while the one for aromatic showed a clear peak at about 3.98×10^6 Hz. The dielectric loss curve for resin would not behave any particular peaks. This is due to that the resin fraction is defined as the difference of maltene and the sum of saturate + aromatic. Dielectric loss spectrum for the resin, which has more or less polarity, was broad without any particular peaks. The relation between a dielectric relaxation frequency and a rotation radius is known as Stokes-Einstein equation:

$$f = k_B T / 4 \pi \eta R_d^3 \quad (4)$$

where k_B is the Boltzmann constant, T the temperature, η the effective viscosity, and R_d the dipole moment weighted particle radius [7]. According to eq.(4), the dipole radius of asphaltene was calculated, that is 10.4 nm.

In order to built up the molecular structure of the asphaltene; we have provided the following characterization parameters: Mw (by LDMS)=2040, carbon aromaticity, f_a (by $^1\text{H-NMR}$)=0.52. Structural parameters of the asphaltene molecules were calculated by a computer aided structure analysis method [8], and average structure model was drawn, where we were taking consideration the fact that the LDMS result suggested cata type of aromatic condensed ring in shape [5]. The longitudinal size of the asphaltene molecule was about 6 nm, which was about a half of the micelle radius obtained above. This is reasonable value from the mechanism of stacking of asphaltene molecules, because they interact each other by their polarity of aromatic sheets and/or metallic ions.

Figure 2 shows the dielectric loss curves for the mixtures of asphaltene with maltene. When the asphaltene content increased from 15.3 wt% (corresponding to the composition of VR) to 20 wt%, the loss peak became larger and shifted to the lower frequency side. On the other hand, the peak became smaller and shifted to the higher side for the mixture with 5 wt% of asphaltene. It was noticeable that the peak shape was rather flat in the case of 10 wt%, which might show the uncontinuous change in size. These evidences imply that the shape of dielectric loss spectra depend upon the content of asphaltene. It has been investigated the surface and interfacial tensions system for asphaltenes in aromatic solvents and indicated possible asphaltene aggregation as well as the probable existence of critical micelle concentration [2,9]. From the frequency at the maximum intensity of dielectric loss, we can calculate the micelle size in medium. The micelle radius for 5 wt% of asphaltene content is 8.4 nm, 9.7 nm for 10 wt%, 10.4 nm for 15.3 wt% (as shown above) and 10.4 nm for 20 wt%, respectively. It is suggested a critical micelle formation point at the given asphaltene concentration, which is below 5 wt% in our case.

The spectra changes of resin content in VR matrix are shown in Figure 3. The

frequency at the maximum loss were almost unchanged at the range from 23 wt% (corresponding to VR) to 0 wt% of resin content in matrix as well as the viscosity of the same specimens. The facts suggest the size of micelles might be independent on resin content. The intensity changes would be caused by the change of relative content.

Further, we have obtained dielectric property for VR fractions derived from hydrotreated oils with HDM and HDS catalysts. Characterization data were illustrated in Table 1, where asphaltene content decreased from 15.3 wt% in the original VR to 7.6 and 5.7 wt%, respectively. Although molecular weight distribution by LDMS for HDM and HDS shifted slightly to lower side, averages molecular weight was almost unchanged. Chemical structure expressed with *fa* altered some extent with the hydrotreatment. In fact, structural parameters, such as the number of aromatic carbon, *Ca*, and the number of aromatic ring, *Ra*, were decreased by the hydrotreatment; *Ca*: 109 to 79 for HDM and 85 for HDS, *Ra*: 28 to 22 for HDM and 25 for HDS, respectively. Figure 4 shows the dielectric loss spectra for those VRs. The intensities for both samples decreased to the same extent and the shape was almost the same too. It is not clear why the shape of dielectric loss spectra did not change nevertheless decreasing the asphaltene content. From the results that metal content decreased from 121 ppm in the original VR to 66 and 31 ppm by HDM and HDS, respectively, it seems that the aromatic structure would be more effective on the intensity than metal. The loss spectra for these VRs became flat and the peaks were resultantly collapsing with the hydrotreatment, which was almost similar to that of 10 wt% of asphaltene as already illustrated in Figure 2. The micelle radii were calculated from the shoulder peak frequencies for reference, 9.3 nm of HDM and 10 nm of HDS, respectively. It would be suggested that the critical micelle formation point is deeply dependent upon the structural changes.

CONCLUSIONS

The micelle size of the asphaltene in Arabian heavy vacuum residue was investigated from the dielectric loss measurements at 403K. It was observed that the loss spectrum of asphaltene in AH-VR was in the wide range from 1×10^2 to 1.5×10^7 Hz having two peaks, and that the former was at low frequency and the latter was at high frequency. We found that the low frequency peak was contributed from asphaltene by comparing with that of maltene. The micelle size in VR was determined from the frequency at the maximum intensity of the loss spectra and the viscosity, using Einstein-Stokes equation, 10.4 nm in radius. This value was about two times of the length of the average molecular structure drawn from its characterization.

From the results of loss spectra changes with asphaltene and resin contents in maltene, and those for VR derived from the hydrotreated oils, it was found that the intensity of loss spectra was affected by not only asphaltene but also metal contents. And, it was also suggested that the aromatic structure would be more effective than metal.

Then, we discussed about the size of micelles determined from the loss spectra to make sure the mechanism of micelle formation. It was suggested that the micelle size might be depend upon the asphaltene content and the size of condensed aromatic rings of asphaltene, not upon the resin content, which implied the critical micelle formation point.

ACKNOWLEDGMENTS

This work has been carried out as a research project of the Petroleum Energy Center with the subsidy of the Ministry of International Trade and Industry.

LITERATURE CITED

- (1) Speight, J. G., *The Chemistry and Technology of Petroleum*, Marcel Dekker Inc.
- (2) Yen, T. F. and Chilingarian, G. V., *asphaltenes and asphalt*, 1, Elsevier Science
- (3) Fujii, M., Sanada, Y., Yoneda, T., and Sato, M., Prep. Div. Fuel Chem., ACS, **43**, (3), 735(1998)
- (4) Sheu, E. Y. and Mullins, O. C., *Asphaltenes Fundamentals and Applications*, Plenum Publishing
- (5) Yen, T. F., Erdman, J. G. and Pollack, S. S., Anal. Chem., **33**, 1587(1961)
- (6) Nihonkagakukai edition, *Jikkenkagakukouza*, **2**, Maruzen co.
- (7) Sheu, E. Y., Storm, D. A. and Shields, M. B., Energy & Fuels, **8**, 552(1994)
- (8) Katayama, Y., Hosoi, T., Takeya, G., Nihonkagakukaishi, (1), 127(1975)
- (9) Mohamed, R. S. and Ramos, A. C. S., Energy & Fuels, **13**, 323(1999)

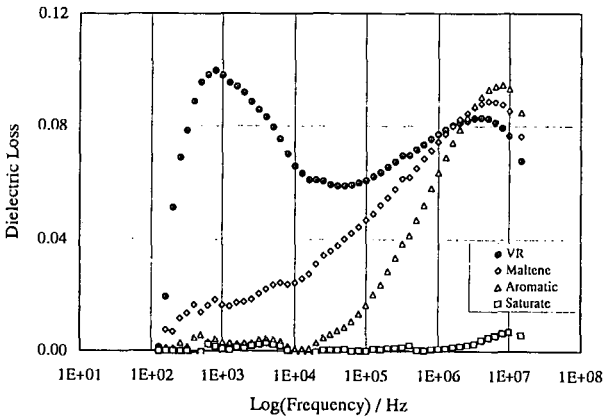


Figure 1. Dielectric loss spectra for AH-VR and fractions derived from it

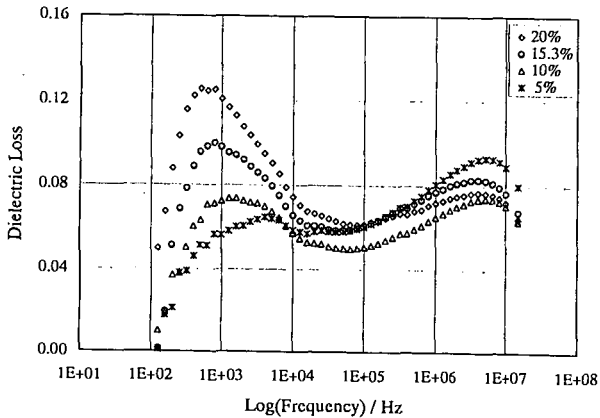


Figure 2. Dielectric loss spectra for mixture of asphaltene and maltene

Table 1. Properties of asphaltenes

Sample	Asph. Content	Density	H/C	Mw	fa	Ca	Ra
	wt%	g/cm ³	-	LDMS	1H-NMR		
AH-VR	15.3	1.165	1.05	2040	0.52	109	28
HDM	7.6	1.180	1.07	2140	0.48	79	22
HDS	5.7	1.141	1.04	2130	0.54	85	25

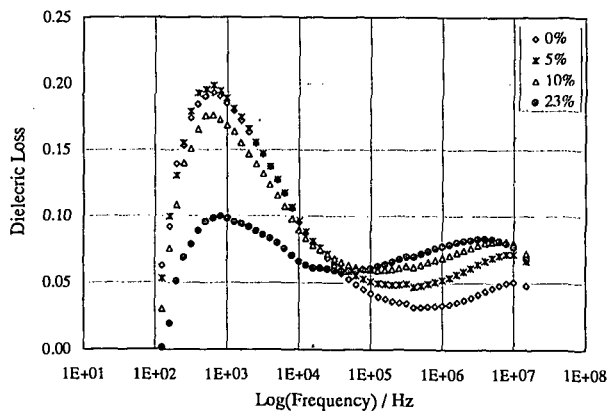


Figure 3. Dielectric loss spectra for mixture of resin and matrix

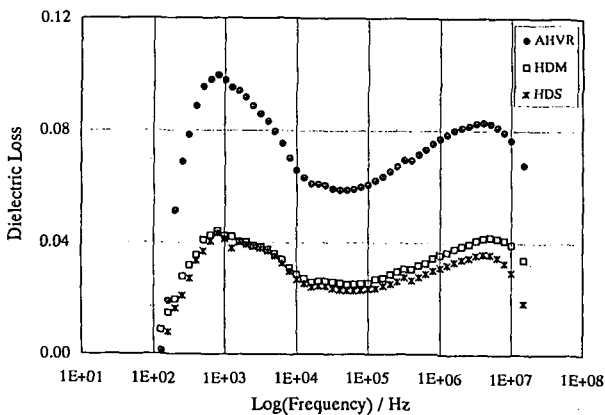


Figure 4. Dielectric loss spectra for VR obtained with hydrotreatment

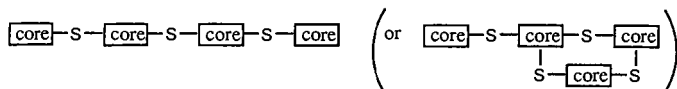
COVALENT STRUCTURE AND MOLECULAR ARCHITECTURE OF ATHABASCA ASPHALTENE

O.P. Strausz, Department of Chemistry, University of Alberta, Edmonton, AB T6G 2G2, Canada; P. Peng, Guangzhou Institute of Geochemistry, Guangzhou 510640, People's Republic of China; J. Murgich, Centro di Quimica, Instituto Venezolano de Investigaciones Cientificas, Apartado 21827, Caracas 1020-A, Venezuela.

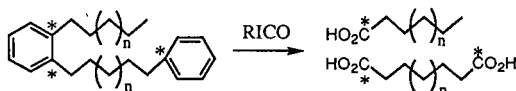
INTRODUCTION

Extensive research in the recent past has led to new insights into the composition,¹ covalent structure² and molecular architecture^{3,4} of Athabasca asphaltene (AA). Employing thermolytic and chemolytic degradations such as the nickel boride (Ni/B) cleavage of the C-S bonds in sulfides, the ruthenium ions-catalyzed oxidation (RICO) of the C_{arom}-C_{arom/aliph} bonds, the basic hydrolytic cleavage of the ≡CO-C(O)-C ester bonds and the BBr₃ cleavage of the ≡C-O-C≡ ether bonds yielded an array of products representing structural elements in the asphaltene molecules. Thus, the principal products from the mild thermolysis were homologous series of thiolanes, thianes, thiophenes, benzothiophenes, dibenzothiophenes, methylbenzenes and fluorenes. All these structures were *n*-alkyl substituted—in the C₁₂-C₂₈ total carbon range—in such a fashion that upon ring cleavages at appropriate places the entire carbon skeleton of the molecules could be stretched out into an *n*-alkane chain, pointing to the *n*-alkanoic origin of these cyclic structures. Significantly, cyclic terpenoid sulfides, abundant in the maltene fraction of the parent bitumen, appear to be lacking in the asphaltene. Additional products identified were: series of partially hydrogenated di-, tri- and tetrabenzothiophenes, two- and three-ring aromatics and hydroaromatics, and one-through three-ring naphthenes, all alkyl substituted with a total carbon number up to ~28, *n*-alkanes, iso- and anteisoalkanes and isoprenoids. Among the polar products the dominant ones were *n*-alkanoic acids, *n*-alcohols and *n*-alkanoic amides (originally hydrogen-bonded acid-amine complexes?), all exhibiting a marked even-to-odd carbon preference. The latter feature is the fingerprint of a relatively recent origin related to secondary microbial degradation of the precursor oil of the present-day bitumen. Small quantities of alkyipyridines and alkyquinolines were also detected.

The Ni/B cleavage of the sulfide bonds in acetone-extracted AA afforded about 2.5% aromatics, 2.5% polars and 0.1% saturates. The saturates comprised entirely biomarkers, *n*-alkanes, di-, tri- and pentacyclic terpenoids including γ -cerane and regular steranes, all corresponding to distribution representing a significantly lower level of thermal maturity than that of the maltene of the parent bitumen. These compounds were originally present in the asphaltene molecule as sulfur-bound appendages and possibly bridges. And, what is from a structural point of view an even more noteworthy phenomenon, is the drastic fourfold drop in the MW of the residual asphaltene after Ni/B reduction, proving a molecular architecture in which four asphaltene core segments are bound together by three (or more) sulfur atoms, e.g.

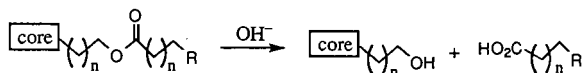


The RICO produced, among other products, series of *n*-alkanoic and α,ω -di-*n*-alkanoic acids, signifying the presence of *n*-alkyl side chains and bridges attached to aromatic carbons.

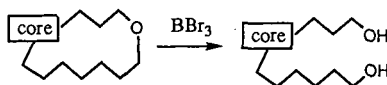


Lastly, cleavage of ester and ether bonds resulted in the formation of *n*-alkanoic acids and *n*-alcohols, again dominated by the even carbon members.

In the present context the important structural elements in the asphaltene molecules are the alkyl (polymethylene) bridges connecting aromatic or naphthenic rings, the alkyl, ether and ester appendages as well as other types of appendages. Long bridges (up to C₂₈) can connect distant carbon sites and create loops and internal cavities. From RICO studies the evidence for the existence of long polymethylene bridges connecting two aromatic carbons and an aromatic carbon with a naphthenic carbon is unambiguous. The Ni/B cleavage of the C-S bonds in sulfides shows that there are small amounts of long alkyl sulfide bridges as well. In the cleavage of C-O bonds it is only the external moiety in the bond that is liberated, e.g.



If the ether or ester represents a bridge anchored at both ends to the core then no GC-detectable products would result from the cleavage reaction, e.g.



The total amounts of acids and alcohols liberated in the C-O cleavage reaction are quite substantial, alcohols ~3.0% and acids ~ 0.5%, and therefore it would be reasonable to assume that there are some ethers and esters present in bridge positions as well as in side-chain appendages. Indirect experimental evidence appears to support this conclusion. The total number of bridges can be estimated to be about eight per asphaltene molecule or about two per core segment. Consequently, internal cavities of varying sizes have to be an integral feature of the molecular structure of asphaltene. This has been discussed previously in connection with a model for asphaltene structure and has been confirmed by molecular mechanics computations on the isolated model.

The present communication deals with some aspects of the adsorption properties of AA and the question related to its pore structure.

RESULTS AND DISCUSSION

Several series of studies have been carried out on the adsorption properties of AA. Here, only some, yielding information on the pore structure and adsorption capacity, will be discussed.

When, in a series of experiments,⁵ the adsorption of C₉-C₃₂ alkanes, squalane and squalene was investigated in CH₂Cl₂ solutions, it was observed that the *n*-alkanes were not adsorbed, squalane was adsorbed moderately and squalene, substantially. Thus, AA in a 10% solution adsorbed 0, 20 and 46% of 10,000-ppm dissolved *n*-alkanes, squalane and squalene. If the adsorption mechanism were purely physical adsorption by van der Waals forces, then *n*-alkanes should adsorb more readily than squalane because the presence of the branched methyl groups in squalane hinders a close contact between the methylene groups of the alkane chain and the adsorbent. Since the experimental finding was the reverse of this intuitive expectation, other factors must be involved. The simplest explanation at hand would be the operation of an adduct mechanism, implicating an appropriate-size pore structure. *n*-Alkanes have a molecular diameter of about 3.0 Å and can be adducted to molecular sieves 5 Å which have an internal pore diameter of 3.0 Å. Molecular sieves 5 Å would not adduct squalane because the effective molecular diameter of squalane exceeds 3 Å. Squalane (along with other isoprenoids) with a molecular diameter of about 7 Å could, however, be clathrated with substrates of appropriate size pore structure, such as thiourea. On the other hand, *n*-alkanes cannot be clathrated with thiourea because the narrow *n*-alkane molecules would not be held firmly enough in the wide pores.

Thus, from the experimental observation that squalane can be adsorbed on AA whereas *n*-alkanes cannot, we conclude that the adsorption is, in effect, an adduction of the squalane molecule into an appropriate-size cavity in the asphaltene structure. The cavity may be present in the covalent molecular structure, in the micelle-loke aggregates or in the form of a combination of the two. The simplest assumption one can make is that the cavity is located in the covalent molecular structure because in the micelle-like aggregate the dynamic equilibrium continuously rearranges the structure, rendering the adduction (clathration) process ineffective.

The high value of the adsorbed squalane can be viewed as the result of the combined effects of adduction and adsorption, the latter being due to the higher dispersion force in the interaction of the olefinic π bond with the aromatic ring systems of the asphaltene.

Another important question in this regard is the capacity, that is, the maximum amount of squalane a unit weight of the asphaltene is capable of adducting. This would provide a measure of the number of cavities (in the appropriate size range) present in the asphaltene. The same question is also relevant to the amount of resins the asphaltene can hold, and whether a precipitated asphaltene (say *n*-C₅-AA with 21.1% adsorbed maltene, resins and low-MW asphaltene fragments) represents a (unimolecularly) saturated state of the asphaltene-adsorbate system or rather a steady-state equipartition distribution of the adsorbate between the oil and the adsorbed phase.

In order to answer this question, an experiment was carried out⁶ in which *n*-C₅-AA was sequentially re-precipitated seven times and the desorbed material combined. A portion of this desorbed material was then dissolved in *n*-pentane and freshly *n*-C₅-precipitated solid asphaltene was added to the *n*-C₅/CH₂Cl₂ (40:1) solution. After standing overnight the asphaltene adsorbed 44% of the desorbed material (corresponding to 8.8% of the asphaltene), clearly manifesting that the precipitated solid asphaltene is capable of adsorbing significantly more resinous material than it contained.

ACKNOWLEDGEMENT

We thank the Natural Sciences and Engineering Research Council of Canada and the Alberta Oil Sands Technology and Research Authority for financial support.

REFERENCES

1. Payzant, J.D.; Montgomery, D.S.; Strausz, O.P. *AOSTRA J. Res.* **1988**, *4*, 117-131; Payzant, J.D.; Lown, E.M.; Strausz, O.P. *Energy & Fuels* **1991**, *5*, 445-453.
2. Mojelsky, T.M.; Montgomery, D.S.; Strausz, O.P. *AOSTRA J. Res.* **1985**, *2*, 131-137.
3. Peng, P.; Morales-Izquierdo, A.; Hogg, A.; Strausz, O.P. *Energy & Fuels* **1997**, *11*, 1171-1187.
4. Strausz, O.P.; Mojelsky, T.W.; Faraji, F.; Lown, E.M. *Energy & Fuels* **1999**, *13*, 207-227.
5. Strausz, O.P.; Ignasiak, T.M.; Kotlyar, L.; Montgomery, D.S. to be published.
6. Strausz, O.P.; Torres, M. to be published.

THE STABILITY OF THE ASPHALTENE AND RESIN AGGREGATES AND THEIR CHEMICAL REACTIVITY

J. Murgich, R. Isea, J. Abanero, and O. P. Strausz*

Centro de Química, IVIC, Apartado 21827,

Caracas 1020A, Venezuela;

*Department of Chemistry, University of Alberta,

Edmonton, Canada T6G 2G2

KEYWORDS asphaltenes, micelles, chemical reactivity

INTRODUCTION

The structure of the known asphaltenes can be divided into two main types: one

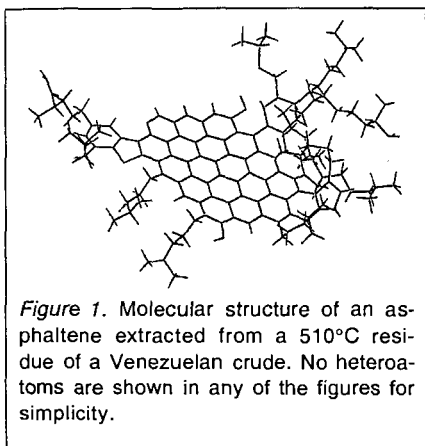


Figure 1. Molecular structure of an asphaltene extracted from a 510°C residue of a Venezuelan crude. No heteroatoms are shown in any of the figures for simplicity.

formed by molecules with a large aromatic "continent" with many rings plus alkyl branches (see Fig. 1) (1) and another composed by smaller aromatic islands connected by alkyl bridges ("archipelago" type) (2) (Fig. 2). These different 3D shapes play an important role in the reactivity of the different atoms of these molecules and in the formation and stability of the molecular aggregates or micelles that are responsible for its solubility in crude oil and residue. An analysis of the three dimensional shape of the available asphaltene molecules and of the factors involved in the stability of aggregates

formed with resins will help in the understanding of their reactivity in crude oils or residues.

THEORY

Crude oil is a complex molecular fluid that has been classified as a colloidal

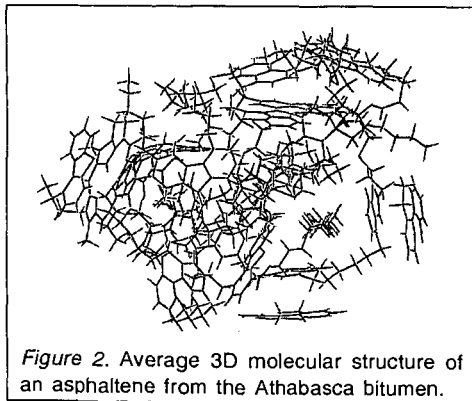


Figure 2. Average 3D molecular structure of an asphaltene from the Athabasca bitumen.

dispersion of asphaltenes in a nonaqueous solvent (3). The micelles in oil are formed by asphaltenes peptized mainly by resin molecules. Similar micelles were found in many residues of different crude oils (3b). As in all complex molecular liquids, the noncovalent interactions (van der Waals, Coulomb, and repulsive ones) (4) are responsible for the molecular recognition process that exists between the heavy

components of crude oils and residues. The resulting recognition between these molecules are very important in determining the structure and the lifetime of their aggregates (5).

MOLECULAR SHAPES AND CHEMICAL REACTIVITY

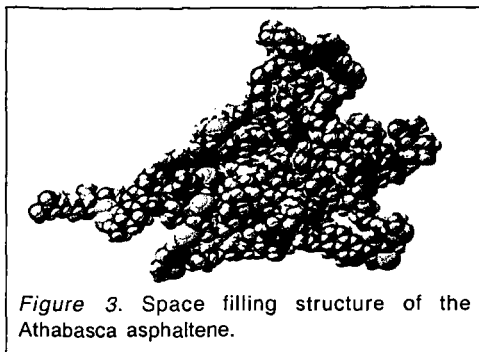


Figure 3. Space filling structure of the Athabasca asphaltene.

The acetone fraction of the asphaltenes of the Athabasca sands has been studied (6) and a 3D structure was proposed recently using molecular dynamics calculations (1) (Fig. 2). The resulting average structure showed a noticeable similarity with that proposed for an asphaltene obtained from a Boscan crude (7). On the other hand, molecules with a central

condensed aromatic core with alkyl branches were found in an asphaltene isolated from a 510 °C residue of a Venezuelan crude (Fig. 1) (1), and for several others extracted from different oils (3a).

From Figs. 2 and 3, one can see that the asphaltene from Athabasca has a very complex three dimensional form that includes cavities and tunnels of different shapes and sizes. The alkyl bridges act as elastic links between the more rigid aromatic regions that form the molecule. The final structure reflects this difference and shows a compromise between the bond and angle requirements of these two main regions. The Athabasca (also Boscan) asphaltene molecule contains a significant number of atoms that are inside these cavities or are located in places where the steric interference is high. Consequently, these sites are not always available for reactions with other molecules. This means that the number of different types of atoms obtained from elemental analysis for this kind of asphaltenes is always larger than the number that is actually available for chemical reactions. This is important in the study of the removal of atoms such as S or N because not all of them will be available for the required reactions. Clearly, not only is important to know the heteroatom content but it is also convenient to have information about its distribution for its efficient removal.

In macrocycles and other concave structures, the reactivity of atomic groups residing in the interior of molecular cavities differs from that of the same groups located on external sites (8). Significant changes were found in the acidity and other proprieties of internal and external groups in a variety of macrocycles and enzymes (8). The existence of internal cavities in asphaltenes of the archipelago type suggests that the reactivity of its atoms will depend on their relative position within these molecules and the size and shape of the internal cavities.

In the structure of lowest energy shown in Fig.2, the asphaltene molecule showed some alkyl bridges with strained bonds, C atoms with perturbed tetrahedral angles and also departures from planarity in some of its aromatic regions. The departures from the normal bond values influences the reactivity of these macromolecules. Strained bonds are weaker than normal ones and, consequently, chemically more reactive (9). Then, they are more easily broken in these asphaltenes than the unstrained ones, thus adding another factor to the complex reactivity of these molecules. In the case of asphaltenes of the continental type (Fig. 1), only the steric interference in crowded atoms will affect their reactivity as no internal cavities are present in these molecules. Consequently, the reactivity of these asphaltenes is reflected in its elemental analysis better than in the case of the archipelago type.

The formation of micelles that are peptized by resins further complicates the chemistry of the asphaltenes in residues and crude oils. Micelles are dynamic units, constantly forming and dissociating (5). For typical surfactants in water, the micelles are generated on a time-scale in the microsecond to millisecond range (5). The chemical complexity of crude oils and its residues implies the existence of many heavy molecules with different 3D shapes. These shapes influence the type, number and lifetime of the micelles of asphaltenes and resins formed in these fluids. It is expected that a polydisperse system composed by a large variety of micelles will be formed with the asphaltene and resin molecules (3b). It is difficult to estimate their lifetimes but one may reasonably assume that they are at least similar to that of the surfactants in water. The existence of these molecular aggregates adds a new dimension to the chemistry of the asphaltenes. These large molecules will not longer be available for reactions as readily as in the case of being a monomer in solution of a simple liquid. If the asphaltene solubility is low, the concentration of free molecules will be also quite small so most of them will be part of some micelle. This will have an impact in the catalytic conversion of this part of the crudes and residues because the diffusion of such micelles are much slower than for the free molecules. The resins that are located in the periphery of the micelles introduces also an additional obstacle to the direct contact of the asphaltenes with the catalysts. The strength of the asphaltene-resin interactions will determine the importance of this contribution to the availability of the asphaltenes for re-action.

The asphaltene of the continental type interacts strongly with other molecules containing planar aromatic regions (2) (Fig. 4). The large contact area produces a favorable contribution to the enthalpy of complexation of this type of asphaltenes and resins (1). The contact in the archipelago type is much smaller

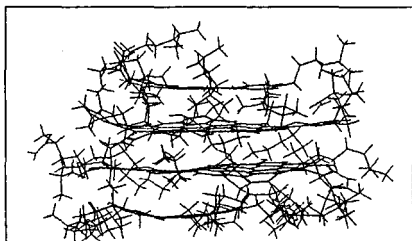


Figure 4. Lateral view of the micelle formed with two internal asphaltene molecules of Fig. 1 and two external resins molecules found in the same residue.

as seen at the bottom right of Fig. 2, where a resin is noncovalently attached to this type of asphaltene. The smaller contact area indicates the formation of weaker aggregates if all the other enthalpic and entropic factors are equal (1). This difference shows the importance of the aromatic regions in the stability of the micelles of asphaltenes and resins.

The chemical changes occurring during the cracking process modify the structure of asphaltenes and resins. As in other colloidal systems, these changes produce variations in the micelles present in the residue (5). It is important to monitor these changes and control them with conveniently design additives. They can be designed taking into account the studies of the interaction between different asphaltene and resins present in micelles of typical residues. These additives can be such that they will be able to change the properties of the resulting residue through association with the micelles and the free asphaltenes. In this way, the conversion of asphaltenes to lighter fractions can be noticeably improved.

ACKNOWLEDGMENT

This work was partially supported by the Natural Sciences and Engineering Research Council of Canada.

REFERENCES

- 1) Murgich, J.; Abanero, J.A.; and Strausz, O.P. *Energy Fuels*, **13**, 278-286 (1999)

- 2) Murgich, J., Rodríguez, J., and Aray, Y., *Energy Fuels*, **10**, 68-76 (1996)
- 3a) Speight, J. G. *The Chemistry and Technology of Petroleum*, 2nd. ed., Marcel Dekker, New York, (1991) and b) Syuniaev, Z.I.; Safieva, R.Z. and Syuniaev, R.Z., *Neftyanie Dispersnye Sistemy*, Kislorda, Moscow, 1997
- 4) Israelachvili, J., *Intermolecular and Surface Forces*, 2nd. ed., Academic, New York, 1991.
- 5) Evans, F.D., and Wennerström, *The Colloidal Domain*, VCH Publishers, New York, 1994.
- 6) Strausz, O. P., Mojelsky, T. W. and Lown, E. M. *Fuel*, **71**, 1355-1362, (1992),
- 7) Kowalewski, I., Vandenbroucke M., Huc, A.Y., Taylor, M.J., and Fauton, J.L., *Energy Fuels*, **10**, 97-107 (1996)
- 8) Lüning, U.; *Adv. Phys. Org. Chem.*, **30**, 63-116 (1995)
- 9) Isaacs, N.S.; *Physical Organic Chemistry*, Longman, Harlow, Essex, 1987

STOCHASTIC MODELING OF PETROLEUM RESID - THE USE OF REACTIVITY INFORMATION IN STRUCTURE DETERMINATION

Achin Vasudeva, Ankush Kumar
Department of Chemical Engineering
University of Delaware, Newark, DE 19716

Michael T. Klein
College of Engineering
Rutgers, The State University of New Jersey
Piscataway, New Jersey 08854-8058

KEYWORDS : resid, stochastic, reaction

INTRODUCTION

Structural characterization of petroleum resid has gained importance in the petroleum industry in recent years owing to the increasing abundance of such material in the petroleum produced worldwide. It is estimated that at least 85% of the world proven reserves of petroleum contain large amounts of "heavy" material boiling above 650°F. On the other hand, according to recent reports, about 50% of the petroleum products consumed in the United States at the present time are gasoline and an additional 40% are other distillate fuels boiling below about 650°F [1]. These trends have focused attention on the efficient upgrading of petroleum resids to light distillates. In order to meet the challenge of optimal upgrading of heavy petroleum fractions, a detailed understanding of the resid structure is required.

The traditional approach for modeling such complex systems has been to use lumped models where molecular species are grouped according to some physical property, such as boiling point or solubility [2]. However, lumped models are clearly incapable of providing molecular information about the feedstock since, by lumping molecules according to some physical characteristic, the molecular detail is lost. With recent government regulations having established concentration limits for specific molecules in a feedstock, an example being benzene, a known carcinogen, molecularly explicit models are required that can predict the concentrations of individual species. Lumping strategies can also lead to difficulties in developing an accurate model. For instance, a C₁₀ paraffin and a C₁₀ aromatic (alkyl benzene) would be lumped together in the same boiling point range and the lumped model would represent them by the same pseudo component. Clearly, however, an alkyl benzene would react quite differently from a paraffin.

The limitations of lumped models motivate the development of molecule-based models. The development of such molecularly explicit models has been made possible by the explosion in available computational resources. To develop molecule-based models, the initial conditions need to incorporate molecular level details. For models dealing with a feedstock as complex as a petroleum resid, which has tens of thousands of molecules, tracking each species is impractical considering the prohibitively large solution times associated with solving such a reaction model. A stochastic description of the complex feedstock provides a path forward. Such a model retains the molecular detail of the feedstock and at the same time can be reduced to generate a small set of representative molecules (of the order of ~ 50-100) to be used in the reaction model.

STOCHASTIC DESCRIPTION OF PETROLEUM RESID

The construction algorithm for petroleum resid is presented in Figure 1. For each molecule, the molecular type (e.g., paraffin, naphthenic, aromatic/resin, or asphaltene) is determined first. The stochastic description of a feedstock involves viewing each molecule as a collection of molecular attributes. Once the molecular type has been identified, the value of each attribute needed to specify the molecule is determined. For instance, an aromatic molecule would be specified by the number of aromatic rings, the number of naphthenic and thiophenic rings attached to it, the number of side chains, the length of side chains and the number of side chain sulfur atoms.

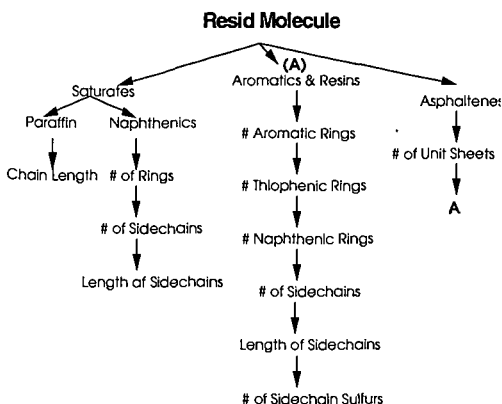


Fig. 1 Construction algorithm for petroleum resid

Each molecular attribute is characterized by a probability distribution function (pdf) which provides the quantitative probability of finding the value or less of a given attribute. The applicability of probability distribution functions to describe complex mixtures in general and petroleum fractions in particular has been well documented in the literature [7,9,11,14,17]. Monte Carlo sampling of the set of pdf's (one set for each feed) provides a large ensemble of molecules (of the order of 10^5). The properties of this set of molecules generated are compared to experimentally obtained analytical data to obtain an optimal set of pdf parameters, which define the feedstock. The pdf parameters are optimized using the following objective function:

$$\begin{aligned}
 \chi^2 = & \left(\frac{MW_{exp} - MW_{pred}}{0.05 * MW_{exp}} \right)^2 + \left(\frac{HtoC_{exp} - HtoC_{pred}}{0.02 * HtoC_{pred}} \right)^2 + \\
 & + \left(\frac{Halp_{exp} - Halp_{pred}}{0.02} \right)^2 + \left(\frac{Harom_{exp} - Harom_{pred}}{0.01} \right)^2 \\
 & + \left(\frac{1}{\#Comps} \right) \sum_{i=1}^{\#Comps} \left(\frac{SARAW_{i,exp} + SARAW_{i,pred}}{0.03} \right)^2 \\
 & + \left(\frac{1}{\#Fracs} \right) \sum_{i=1}^{\#Fracs} \left(\frac{SIMDIS_{i,exp} - SIMDIS_{i,pred}}{0.01} \right)^2
 \end{aligned} \tag{1}$$

The numerator in each term of the above equation is the difference between the experimentally determined property and the predicted property, and the denominator is a weighting factor equal to one experimental standard deviation. A simulated annealing global optimization technique is employed to minimize the objective function and generate an optimal set of pdf parameters.

In general, the only information available about petroleum resids are some average properties like molecular weight (Vapor Pressure Osmometry), elemental analysis, boiling point distribution (SIMDIS) and NMR (1H and ^{13}C) data. Analytical techniques like GC/MS which yield molecular level details also provide only broad lumps due to the extreme complexity of the feedstock. This limited amount of structural information often renders the optimal set of pdf parameters non-unique, thus preventing the development of an accurate stochastic description of the resid. To tackle the issue of non-uniqueness, further structural information is required. One possible source of such information is a detailed product distribution from the controlled reaction of the resid.

The approach adopted in this study has been to crack the resid in the presence of hydrogen under conditions where the reaction pathways and associated rate constants can be estimated with reasonable accuracy. The light fractions obtained as a result of the controlled reaction are subject to detailed compositional analyses (GC/MS, High Detail Hydrocarbon Analysis) to obtain a molecularly explicit description of the product. This information is incorporated into the objective function as a term representing the difference between experimental and predicted weight fractions of all the species in the product. The objective function is thus modified as follows:

$$\chi^2 = \left(\frac{MW_{exp} - MW_{pred}}{0.05 * MW_{exp}} \right)^2 + \left(\frac{HtoC_{exp} - HtoC_{pred}}{0.02 * HtoC_{pred}} \right)^2 + \left(\frac{Halpha_{exp} - Halpha_{pred}}{0.02} \right)^2 + \left(\frac{Harom_{exp} - Harom_{pred}}{0.01} \right)^2 + \left(\frac{1}{\#Comps} \right) \sum_{i=1}^{\#Comps} \left(\frac{SARAW_{i,exp} + SARAW_{i,pred}}{0.03} \right)^2 + \left(\frac{1}{\#Frac} \right) \sum_{i=1}^{\#Frac} \left(\frac{SIMDIS_{i,exp} - SIMDIS_{i,pred}}{0.01} \right)^2 + \left(\frac{1}{\#Species} \right) \sum_{i=0}^T \sum_{j=1}^{\#Species} \left(\frac{Wfrac_{i,exp} - Wfrac_{i,pred}}{0.01} \right)^2 \quad (2)$$

Minimization of the modified objective function thus yields an improved stochastic description of the feedstock.

In cases where such complex feedstocks are to be part of a molecularly explicit reaction model, a much more compact molecular description of the feedstock is desirable. This is because handling the thousands of molecules generated by Monte Carlo sampling and their associated reactions and rate constants can result in enormous solution times using present day computers. This molecular lumping is achieved by means of a quadrature technique, wherein ordered sampling of attribute values based on equiprobable regions (to allow sampling over the entire range of attribute values) results in the finite set of representative molecules (of the order of ~10-100 molecules) to be used in the reaction model. The entire modeling approach is thus outlined in Fig.2.

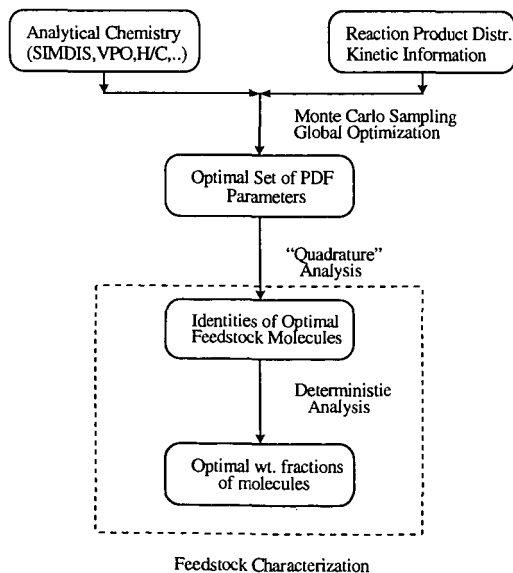


Fig. 2. Modeling approach for stochastic description of petroleum resid

EXPERIMENTAL

The resid was cracked in the presence of excess hydrogen in a flow reactor setup. The catalyst precursor employed was molybdenum naphthenate containing 6% by wt. Mo (obtained from The Shephard Oil Company). Molybdenum naphthenate was sulfided in situ by sulfur present in the petroleum resid to generate the active catalytic species, MoS_2 . The particular choice of dispersed catalyst ensured sufficient conversion of resid to light products while at the same time inhibiting coke production [6,8,15]. A catalyst concentration of 3000 ppm (by weight of Mo in resid) was used. The resid was dissolved in toluene in the ratio of 1:3.5 by weight (resid : toluene). Toluene was the choice of solvent because of its excellent solvation properties (for the resid under investigation) and its inertness under reaction conditions. The hydrogen pressure in the reactor was maintained at 1100 psig and the reaction was carried out at 470°C. The liquid flow rate was about 0.28 ml/min while the hydrogen flow rate was controlled at 150 std ml/min. The residence time of the liquid in the reactor was about 15 minutes.

The gas product was analyzed online in an HP 5890 GC equipped with a 100 m HP-1 capillary column (ID : 0.25 mm, film thickness : 0.5 μm) coupled with an FID for identification of hydrocarbons and a 1 m HayeSep C packed column coupled with a TCD for detection of polar gases such as ammonia and hydrogen sulfide. The liquid product was collected and subjected to HDHA (High Detail Hydrocarbon Analysis) and GC/MS analysis to yield the product distribution.

REACTION MODEL

The driving force for cracking of petroleum resid in the presence of excess hydrogen employing molybdenum naphthenate as the catalyst precursor is thermal activation. At a mechanistic level, the catalyst has no effect on C-C bond cracking so that the initial population of free radicals is determined by the severity of conditions. The next step in the reaction sequence is the saturation of the reactive fragments, which is promoted by the catalyst. The efficient uptake of hydrogen facilitated by the catalyst ensures that the reactive fragments do not undergo fast undesirable reactions, such as condensation reactions, which give rise to the appearance of mesophase and then to coke deposition. Instead, the catalyst controls the rate of free radical propagation that, via β -scission reaction, favors the process of resid conversion to lighter products [4,5].

A pathways level model describing the resid cracking reaction has been employed in this study. At the pathways level, the main reactions are considered to be breaking of intersheet linkages for asphaltene molecules and side chain cracking reactions including dealkylation for aromatic and naphthenic molecules. Hydrogenation of ring molecules and subsequent ring opening, although not significant, are also considered. The above reactions are used to generate a reaction network consisting of about 250 molecular species. The rate constants for all the species and their associated reactions have been estimated from previous studies conducted with model compounds under similar reaction conditions [12,13]. For example, rate constants for alkyl aromatics undergoing side chain cracking are calculated from the reaction of pentadecyl benzene (PDB) using first order approximations as :

$$k_i = k_{\text{PDB}} (i/15)^{0.5} \quad (3)$$

where i is the number of carbon atoms in the side chain of the alkyl aromatic molecule. The breaking of intersheet linkages in asphaltene molecules has also been modeled as side chain cracking of alkyl aromatic species. Similarly, the rate constants for reactions of alkyl hydroaromatic and alkyl naphthenic species have been estimated from available data on ethyl tetralin and tridecyl cyclohexane respectively.

Monte Carlo sampling of the pdf parameters describing the structural attributes of resid molecules generates a large ensemble of molecules which provide the initial condition for the reaction model. Solution of the reaction model results in predicted product concentrations which are compared to experimentally obtained data and the difference forms part of the objective function, which is minimized. Reactivity information is thus utilized to develop an improved stochastic description of the petroleum resid.

REFERENCES

1. Altgelt, K. H., and Boduszynski, M. M., *Composition and Analysis of Heavy Petroleum Fractions*, Marcel Dekker Inc., New York, pp 1-7 (1994).
2. Beaton, W. I., and Bertolacini, R. J., *Catalysis Reviews - Science and Engineering*, **33**, 281-317 (1991).
3. Campbell, D. M., *Stochastic Modeling of Structure and Reaction in Hydrocarbon Conversion*, Ph.D. Dissertation, University of Delaware (1998).
4. Cebolla, V. L., Membrado, L., Vela, J., Bacaud, R., and Rouleau, L., *Energy & Fuels*, **9**, 901-905 (1995).
5. Del Bianco, A., Panarati, N., Di Carlo, S., Beltrame, P. L., and Carniti, P., *Energy & Fuels*, **8**, 593-597 (1994).
6. Fixari, B., Peureux, S., Elmouchnino, J., Le Perchec, P., Vrinat, M., and Morel, F., *Energy & Fuels*, **8**, 588-592 (1994).
7. Flory, P. J., *J. Am. Chem. Soc.*, **58**, 1877 (1936).
8. Kim, H., and Curtis, C. W., *Energy & Fuels*, **4**, 206-214 (1990).
9. Libanati, C., Monte Carlo Simulation of Complex Reactive Macromolecular Systems, Ph.D. Dissertation, University of Delaware (1992).
10. Logwinuk, A. K., and Caldwell, D. L., *Chem. Econ. Eng. Rev.*, **15**, 31 (1983).
11. Pederson, K. S., Bilie, A. L., and Meisingset, K. K., *Ind. Eng. Chem. Res.*, **31**, 1378-1384 (1992).
12. Savage, P. E., *Chemical and Mathematical Modeling of Asphaltene Reaction Pathways*, Ph.D. Dissertation, University of Delaware (1986).
13. Savage, P. E., and Klein, M.T., *Ind. Eng. Chem. Res.*, **26**, 488-494 (1987).
14. Shibata, S. K., Sandler, S. I., and Behrens, R. A., *Chem. Eng. Sci.*, **42**, 1977-1988 (1987).
15. Ting, P., Curtis, C. W., and Cronauer, D. C., *Energy & Fuels*, **6**, 511-518 (1992).
16. Trauth, D. M., *Structure of Complex Mixtures through Characterization, Reaction, and Modeling*, Ph.D. Dissertation, University of Delaware (1990).
17. Whitson, C. H., *Soc. Pet. Eng. J.*, 683 (1990).

STRUCTURE AND REACTIVITY OF THE ASPHALTENE FRACTION OF AN ARABIAN LIGHT/MEDIUM CRUDE MIXTURE

Masakatsu Nomura^a, Koh Kiden^a, Satoru Murata^a, Yan Su^a, Levent Artok^b,
and Yasuhiro Miyatani^b

^a Department of Molecular Chemistry, Graduate School of Engineering,
Osaka University, 2-1 Yamada-oka, Suita, Osaka, 565-0871, JAPAN

^b Department of Chemistry, Çukurova University, Adana 01330, TURKEY

Keywords: Asphaltene, Structure, Cracking reaction

INTRODUCTION

In the petroleum industry, further utilization of distillation end points (i.e. residua) is of high interest because petroleum refineries will have to deal with much heavier crude in the future decades. Petroleum asphaltenes, which are operationally defined as pentane- or heptane-insoluble and toluene-soluble organic materials of crude oil or the bottoms from a vacuum still, are the heaviest fraction of the crude oil, and their amounts and structures are known to be source dependent. In upgrading processes of residua, asphaltenes are responsible in sludge formation due to their flocculation, which reduces the flow and plugs down stream separators, exchangers, and towers. They show bad behavior in poisoning and reducing the activity of hydrocracking catalysts with its high heteroatom content, trace metals, and high tendency in coke formation. In order to overcome their problematic issues, the role of asphaltenic materials in the upgrading processes should also be interpreted at the level of molecule. Under these circumstances, the better comprehension of asphaltene structure is essential. Although enormous amount of effort has been paid to the structural elucidation of asphaltenes for several decades, their precise molecular description does not exist yet. On the basis of detailed NMR work along with complementary information from various analytical techniques employed, many researchers have concluded that asphaltenes are the mixture of polydispersed-condensed polyaromatic units, with heteroatoms contents, bearing alicyclic sites, and substituted and connected with each other via aliphatic chains. In their researches, asphaltenes were precipitated either from the crude sample or residue. The latter type asphaltene structurally may be different from the former type because at distillation temperatures, in general 300-500°C, some extent of cracking and condensation reactions may take place simultaneously. There are a number of studies which have postulated chemical models for asphaltenes, the most recent ones being based on the ¹H/¹³C NMR data and elemental composition. The models, in general, consist of one or two units of polyaromatic units in varying condensation degree combined with alicyclic sites and connected by aliphatic chains, most of the aliphatic chains being attached to the aromatic carbons[1-7]. Some researchers have used degradative methods such as pyrolysis and oxidation methods to gain more precise insight into the molecular characteristics of asphaltenes. The former method involves formation of smaller fragments and accompanies their identification, the identified components being considered as covalently bonded moieties of asphaltene molecules[8]. Strausz *et al.* were the first group applied the ruthenium-ions catalyzed oxidation (RICO) reaction to asphaltenes to recognize aliphatic types[9]. They processed the invaluable information from the RICO reaction along with those from NMR and pyrolysis studies to comprehend the structure of Alberta oil sand asphaltenes and consequently proposed a very different model structure: instead of a single condensed aromatic system with a large number of rings, a set of smaller aromatic units, heteroaromatics and naphthenic units with aliphatic substituents linked by aliphatic bridges comprised the structure. Particularly, the presence of relatively polymeric naphthenic and aliphatic sites in this molecule is a striking feature. The structure of heavy fraction of crude oil and their conversion to value products have also been of our interest.

In this paper, we have processed the information from the NMR work of the asphaltene sample together with data from the RICO reaction of the asphaltene to elucidate the distribution of the aliphatic carbons more precisely. The detailed analytical information over this sample is summarized within a model structure. As to the reactivity of the asphaltene, its hydrocracking reaction using metal loaded Y-type zeolite catalyst was elucidated, the results being compared with the case of the other lighter fractions.

EXPERIMENTAL SECTION

Samples.

The propane insoluble fraction of the vacuum residue of Arabian crude mixture (80% light and 20% medium) was provided from Nippon Oil Ltd. Co. The asphaltene sample used in this study was the insoluble fraction (21wt% yield, based on propane insoluble) from the pentane Soxhlet extraction of the provided sample. The elemental composition of the asphaltene sample is 83.7% C, 7.5% H, 0.84% N, 6.8% S, 0.012% Ni, 0.038% V, on dry basis and has an H/C atomic ratio of about 1.08.

Analysis of the asphaltene sample.

The RICO reaction was performed by stirring the mixture of the asphaltene sample (1 g), H₂O (30 ml), CCl₄ (20 ml), CH₃CN (20 ml), NaO₂ (15 g), and RuCl₃·nH₂O (40 mg) at 40°C for 24 h. During the reaction, N₂ gas was flowed and the resulting CO₂ was purged through CaCl₂ and ascarite containing tubes. The amount of CO₂ formed was determined from the weight increase of ascarite. The details of the workup procedure have been given elsewhere[10]. NMR analyses were conducted by a JEOL JNM-GSX-400 spectrometer operating at 400 MHz for ¹H NMR and 100 MHz for ¹³C NMR measurements. The NMR samples were prepared by mixing approximately 100 mg of the sample with 1 ml of CDCl₃; tetramethylsilane (TMS) was used as an internal standard. The quantitative ¹³C NMR measurements were acquired by adding a relaxation agent, chromium

trisacetylacetonate (Cr(acac)₃, 0.2 M) in inverse gated decoupling system with a pulse delay of 5 s, acquisition time of 1.088 s and pulse width of 3.3 μ s. The distortionless enhancement by polarization transfer (DEPT) spectra were collected for flip-angles of 45°, 90°, and 135°. The acquisition time was the same as those for the quantitative carbon runs. A pulse delay of 2 s and a carbon-proton coupling constant of 125 Hz were used. The carbon 90° pulse was 10 μ s, while proton 90° pulse was 26.3 μ s. The GPC tests of the THF or CHCl₃ solutions of the asphaltene (0.5 mg/ml and 1.4 mg/ml, respectively) were performed by a Shimadzu system with 1 ml/min flow rate of THF or CHCl₃ carrier solvents, respectively, at a UV wavelength of 270 nm. The columns used in these tests were Shodex KF-802 and Shodex AC-802 for THF and CHCl₃ carrier solvents, respectively. Standard polystyrene samples were used for the calibration of relationships between molecular weight and retention time. MALDI-TOF/MS (Matrix assisted laser desorption ionization-time of flight/mass spectrometry) spectra were obtained by a Voyager RP mass spectrometer of Perspective Biosystems Co. The linear TOF mode was used with an accelerating voltage of 30 kV in positive ion. One μ l of THF solution of the sample with 2.5 μ g/ml concentration was applied to target and let it evaporate at atmospheric condition.

Hydrocracking reaction of the asphaltene sample.

A mixture of heavy oil (1.0 g) and metal-loaded zeolite (0.5 g) was placed in a 70 ml SUS316 autoclave, which was pressurized up to 6.9 MPa with cold hydrogen, and heated up to a desired temperature range (400°C) at a heating rate of 8K/min. Before collection of the gaseous products, these were passed through aqueous iodine solution (1 mol/l, 20 ml) to recover hydrogen sulfide produced. Gaseous hydrocarbon products were analyzed quantitatively by a gas chromatograph. The iodine solution was diluted to 200 ml by deionized water, 20 ml of which was submitted to titration with sodium thiosulfate solution (0.1 mol/l), using aqueous starch solution as an indicator. After the collection of gaseous products, the autoclave was opened, the inside of which was then washed with tetrahydrofuran (THF) to recover liquid and solid products. After the filtration of the resulting mixture to remove coke and catalyst, the products were separated into three fractions, gasoline + THF (the fraction distilled off by a rotary evaporator at 65°C, atm. 5 mmHg), gas oil (the fraction distilled off by a glass tube oven at 150°C, atm. 5 mmHg, corresponds to the fraction with bp < 310°C), and residue (THF soluble and undistilled fraction). Due to the severe difficulty in weighing of THF plus gasoline fraction in an accurate way the yield of gasoline fraction was calculated based on subtraction of the yield of the other fractions (gas, light oil, residue, hydrogen sulfide, and coke) from total of 100%. Amounts of coke were estimated based on the weight and elemental analysis of THF insoluble portion.

RESULTS AND DISCUSSION

Structural analysis of the asphaltene

RICO reaction afforded the acid products from the aliphatic portion of the sample. The amount of lower carboxylic acids (C₂-C₅) was 3.9 mol/100molC in asphaltene, corresponding to ~5.5 aliphatic carbon/100C. Figure 1 shows the distribution of aliphatic monoacids up to C₂₈ including C₂-C₅ acids. The amount of longer *n*-alkanoic acids showed a smooth decrease as the carbon number increased. Therefore, the most of the alkyl groups attached to the aryl carbon or the monomethylene bridge carbon are in the range of C₁-C₇. We recovered the diacids ranging from C₄ to C₂₀ from aqueous and dichloromethane (DCM) soluble phases of the product. Their distribution was shown in Figure 2. These acids represent alkyl bridge structures connecting two aryl units and α,ω -triaryl substituted bridges, however, short chain acids (C₄-C₆) may also arise from oxidation of various hydroaromatic structures. Several amounts of ethanedioic acids were detected, this acid representing biaryl linkages in the sample. Although this acid implies the significance of biaryl linkages, its amount can not represent the amount of such type of bond due to its relative instability. Propanedioic acid could not be observed, because it can not survive the RICO reaction. Therefore, no direct evidence could be obtained from the reaction products. We also recovered the aliphatic polycarboxylic acids which were formed from three or more aryl-substituted alkyl bridges or alicyclic parts of partially saturated condensed structures. Other polymeric aliphatic fraction could not be analyzed by GC, but was analyzed by NMR in detail. The weight of this fraction was >90% of the DCM extract. The weight and elemental composition of DCM soluble fraction indicates that the amount of carbon atom in this fraction corresponds to 24.6 C per 100 C atoms in asphaltene. GPC analysis of this fraction after methylation (methyl esterification of acids) shows a number-averaged MW of 821 Da. Figure 3 shows the ¹³C NMR spectrum of DCM soluble fraction before methylation. This fraction had <4% aromatic, 87.9% aliphatic, 6% carboxylic and 3.1% carbonyl carbon. The results indicated that the dominant part of this fraction is comprised of polymeric aliphatic structures. The fact that this fraction had an aliphatic hydrogen to aliphatic carbon ratio of 1.72, calculated on the basis of ¹H/¹³C NMR and elemental analysis data, confirms the presence of alicyclic sites. The aliphatic region of the ¹³C NMR spectrum (Figure 3) consists of sharp bands on a broad hump between 10 and 50 ppm, much of this broad hump being ascribed to naphthenic carbon. DEPT analysis of this fraction was also very helpful to assume the structure of this fraction. Aromatic acids were recovered from the aqueous phase of the products workup. Such acids correspond to the presence of condensed aromatic moieties.

The GPC test for the whole asphaltene sample show a range starting well below 200 Da extending over 100 000 Da, while MALDI-TOF/MS indicates the ions higher than 200 Da. This discrepancy confirmed the existence of adsorption phenomenon in the case of GPC procedure. On the other hand, MALDI-TOF/MS test led ionization above 200 m/z extending over 3000 m/z, giving maximum abundance about 450 m/z. Nevertheless, inefficient ionization for polydispersed materials are known to be an impediment of this method to lead underestimation of the higher mass components[1]. Thus, caution must be exercised when interpreting average molecular weight distribution values from MALDI, especially for highly polydispersed complex molecules. We understand that no conclusive-absolute molecular weight could be estimated based on the techniques presented above, however, it seems that GPC method with THF eluent provides more

applicable information compared to others employed in our study: the number averaged molecular weight was estimated as 801 Da.

The structural information was drawn from the combination use of ^1H and ^{13}C NMR data and elemental data. Figure 4 shows the ^{13}C NMR spectrum of the asphaltene sample, having the general features in accordance with previous work. The aromatic region consists of a broad featureless absorption, whereas the aliphatic region contains discrete sharp peak overlapping a broad hump. These sharp peaks are commonly attributed to the chain carbon and methyl substituents on aromatics, alkyl chains, and naphthenic units. Also here, DEPT analysis provides helpful information to differentiation of CH_3 , CH_2 , and CH carbons.

We applied a methodology in construction of a model structure for the asphaltene tentatively in a manner similar to that of bituminous coal[12]. The types of aromatic main units were deduced from the results obtained by the pyrolysis(py)/GC and RICO reaction. The XPS study revealed the sulfur structures as sulfide, thiophenic and sulfoxide. The type and distribution of aliphatic chain structure, functionality, and naphthenic structure were postulated based on the RICO, py/GC, and NMR data. We should emphasize that the asphaltene is consisted of mixture of hundreds of organic molecules rather than a single macromolecule structure. We tried to draw several molecules in the proposed chemical structural model for asphaltene, and four molecules of different structures were contained in the proposed model (Figure 5).

Hydrocracking reactions of the asphaltene

Figure 6 compares the hydrocracking results of the propane-insoluble heavy oil and its deasphalted (pentane-soluble) fractions at the temperature range of 350-400°C with the presence of Pd-Ni loaded Y type zeolite catalyst. As it can clearly be seen deasphalted heavy oil sample showed higher reactivity toward hydrocracking reaction. The removal of asphaltene increased the total liquid and gaseous products (bp. <310°C) roughly by the factor of 2 at 350°C, from 30% to 53% at 375°C, and 42% to 65% at 400°C. Even if we consider the conversion values of the propane-insoluble sample on asphaltene free basis, i.e. it is assumed that asphaltene does not convert to low boiling yields, but contributes to the residue fraction, the resulting values, except for the highest temperature, are far less than those of the deasphalted sample. Asphaltene free calculations of total hydrocracked products were 24, 44 and 64 % with respective increase of the reaction temperature. The comparison of these values with those from deasphalted sample suggests that the effect of the removal of asphaltene on the hydrocracking of the heavy oil became less with increasing the reaction temperature. The effect of asphaltene removal was more remarkable on HC gaseous product formation at all temperatures, their increase varying by the factor of 2-3 even at higher temperature, this indicating the effect of asphaltene removal on hydrocracking activity even at 400°C. These results reveal that asphaltene greatly retards hydrocracking reactions upon probably reducing the activity of the catalyst, especially at the lower temperatures.

The polymerized fraction or coke formations seem to be not likely reason for the detrimental effect of the asphaltene since both the whole and deasphalted residue approximately yielded similar amount of these fractions. Our laboratory recently showed that Pd-Ni-Y catalyst is very active in hydrocracking and hydrodesulfurization reactions[13]. We have also showed that the molecule should diffuse into the cage so that sufficient reactions take place[14,15]. The asphaltene molecules with large molecular segments probably reduce the effective diffusion of molecules which are capable to enter through the pores, by plugging the entrance points. At higher temperatures, probably, the adsorption phenomenon becomes less favorable, due to the reduced adsorption strength and the more effective solubility of the asphaltene molecules within the reaction medium, thus resulting in overall increased effective diffusibility of the units with appropriate sizes.

SUMMARY

This work summarized the structural characterization of the vacuum residue asphaltene based on the mainly spectroscopic and pyrolytic methods, and discussed the results with combination use of those from the RICO reaction. Then, a structural model for the asphaltene was presented. The reactivity of the asphaltene was also discussed from the catalytic hydrocracking reaction of it in a batch reactor using metal-loaded Y-type zeolite catalyst.

ACKNOWLEDGMENT

This work was carried out as a research project of The Japan Petroleum Institute commissioned by The Petroleum Energy Center with the subsidy of The Ministry of International Trade and Industry.

REFERENCES

1. Hirsch, E.; Altgelt, K. H. *Anal. Chem.* **1970**, *42*, 1330.
2. Takegami, Y.; Watanabe, Y.; Suzuki, T.; Mitsudo, T.-aki; Itoh, M. *Fuel* **1980**, *59*, 253.
3. Suzuki, T.; Itoh, M.; Takegami, Y.; Watanabe, Y. *Fuel* **1982**, *61*, 402.
4. Christopher, J.; Sarpal, A. S.; Kapur, G. S.; Krishna, A.; Tyagi, B. R.; Jain, M. C.; Jain, S. K.; Bhatnagar, A. K. *Fuel* **1996**, *75*, 999.
5. Storm, D. A.; Edwards, J. C.; DeCanio, S. J.; Sheu, E. Y. *Energy Fuels* **1994**, *8*, 561.
6. Ali, L. H.; Al-Ghanman, K. A.; Al-Rawi, J. M. *Fuel* **1990**, *69*, 519.
7. Rafenomanantsoa, A.; Nicole, D.; Rubini, P.; Lauer, J.-C. *Energy Fuels* **1994**, *8*, 618.
8. Ritchie, R. G. S.; Roche, R. S.; Steedman, W. *Fuel* **1979**, *58*, 523.
9. Strausz, O. P.; Mojelsky, T. W.; Lown, E. M. *Fuel* **1992**, *71*, 1355, and references therein.
10. Artok, L.; Murata, S.; Nomura, M. Satoh, T. *Energy Fuels*, **1998**, *12*, 391.
11. Burlingame, A. L.; Boyd, R. K.; Gaskell, S. J. *Anal. Chem.* **1998**, *70*, 647R, and references therein.
12. Nomura, M., Artok, L., Murata, S., Yamamoto, A., Hama, H., Gao, H., Kidena K., *Energy Fuels*, **1998**, *12*, 512.

13. Wada, T.; Kaneda, K.; Murata, S.; Nomura, S. *Catalysis Today* **1996**, *31*, 113.
 14. Matsui, H.; Akagi, K.; Murata, S.; Nomura, M. *Energy Fuels* **1995**, *9*, 435.
 15. Nomura, M.; Akagi, K.; Murata, S.; Matsui, H. *Catalysis Today* **1996**, *29*, 235.

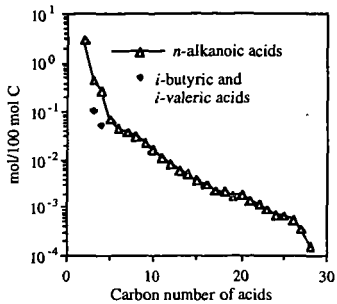


Figure 1. Distribution of aliphatic monoacids from RICO reaction.

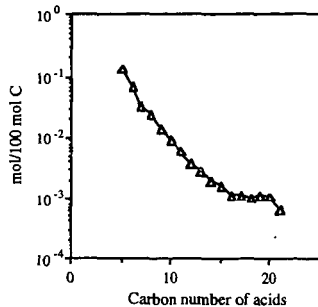


Figure 2. Distribution of aliphatic diacids from RICO reaction.

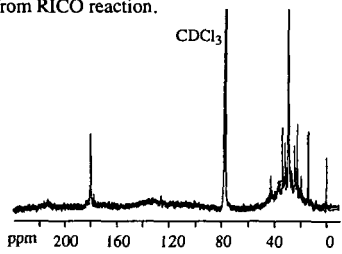


Figure 3. ^{13}C NMR spectrum of the dichloromethane soluble fraction of RICO product.

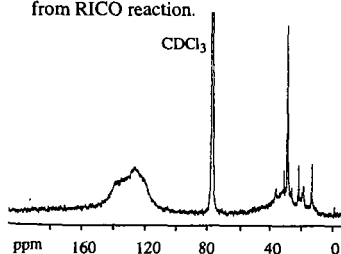


Figure 4. ^{13}C NMR spectrum of the asphaltene.

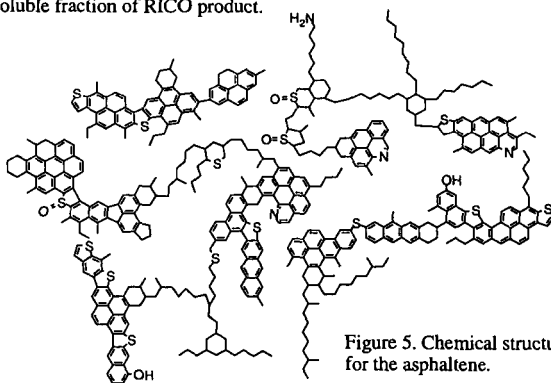


Figure 5. Chemical structural model for the asphaltene.

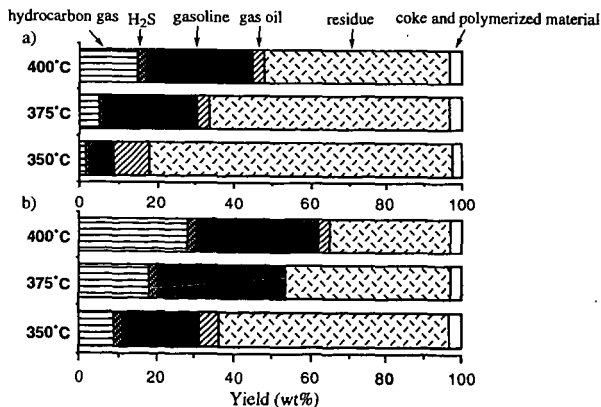


Figure 6. The comparison of hydrocracking conversion results on (a) C_3 -heavy oil sample and (b) C_5 -soluble portion of the C_3 -heavy oil sample.

CHARACTERIZATION AND ADSORPTION TREATMENT OF VACUUM RESIDUE FRACTIONS WITH CARBONS

Kinya Sakanishi, Toru Manabe, Izumi Watanabe, and Isao Mochida

Institute of Advanced Material Study, Kyushu University
Kasuga, Fukuoka 816-8580, Japan

Keywords: Vacuum residue fractions, step scan liquid mode XRD, adsorption treatments

ABSTRACT

The adsorption treatment of VR by using variable amounts of carbon particles was performed with stirring at 60 °C for 1 h. After the treatment, the adsorbent was first washed with n-hexane and then thoroughly washed with THF(tetrahydrofuran) under the ultrasonic irradiation to recover the soluble fractions of hexane soluble(HS) and hexane insoluble but THF soluble(HI-THFS) from the adsorbent. The THF insoluble(THFI) yield increased with the added amount of Ketjen Black(KB). The HI but THF soluble fraction decreased with the increased amount of THFI fraction. About 3 wt% of KB addition based on VR appeared enough for the selective removal of the heavier fraction without increasing the HI-THFS fractions. The slow step scan XRD revealed that the untreated KB showed a very slight peak around 26°. The adsorbed THFI exhibited a broad peak around 26°, while the relatively sharp peak of the original asphaltene around 26° decreased with the addition of KB, indicating selective adsorption of the heavier fraction in the asphaltene. Based on the above results, it is suggested that a certain amount of KB addition may selectively separate the heavier fraction, where the more polar and metal-containing compounds are concentrated, from the VR. Such an adsorption treatment using carbon nanoparticles is expected to remove the catalyst poisons such as the heavier asphaltene and metallic compounds prior to the catalytic upgrading hydrotreatments.

INTRODUCTION

It is desirable to remove metallic compounds in petroleum residues before catalytic hydrocracking and hydrodesulfurization reactions in refineries, because they cause severe catalyst deactivation.¹⁻³ They are usually concentrated in the asphaltene fraction which is known to be comprised of micellar aggregates.⁴ The micellar structure is believed to be formed through intermolecular aromatic plane stacking, hydrogen bonds, and charge transfer interactions. Such a micelle structure of the asphaltene interferes with its conversion into smaller molecules as it promotes the production of sludge and coke precursors over the catalyst through retrogressive reactions of dealkylation and dehydrogenative condensations, especially under the severe conditions used to achieve high conversions via hydrocracking.⁵⁻⁸

The metallic compounds in the asphaltene and/or polar fractions are deposited onto the catalyst along with a considerable amount of carbon precursors, and deactivate the hydrogenation activity. These deposits also enhance dehydrogenation reactions and coke formation in the hydrotreating processes. Hence, the deoagulation of the asphaltene fraction is very important for its depolymerization so as to allow the demetallation to proceed with minimal carbon deposition. There have been many reports on attempted ways to handle the asphaltene, such as extractive removal, solvation, and hydrogenation.⁹

In the present study, the aggregate structure of a vacuum residue and its fractions is investigated by step scan XRD at variable temperatures with or without solvent, in order to clarify the changes in

their micellular structure during the heating or the solvation. In addition, adsorptive concentration of the heavy asphaltene fraction from the vacuum residue by using carbon particles is also applied for the removal of catalyst poisons in the following catalytic upgrading processes.

EXPERIMENTAL

An Arabian mix crude vacuum residue (VR) was used in the present experiments. VR was fractionated by hexane extraction. In the present study, the hexane insoluble(HI) and soluble (HS) fractions were defined as asphaltene and maltene, respectively. The HS was further fractionated into three components of saturates(Sa), aromatics(Ar), and polars(Po) by a conventional alumina column chromatography. The elemental analyses of the fractions before and after the hexane fractionation are summarized in Table 1. Some properties of carbon supports used in the present study are summarized in Table 2.

The adsorption treatment of VR(20 g) by using variable amounts of carbon adsorbent(0 - 4.0 g) was performed with stirring at 60 °C for 1 h. After the treatment, the adsorbent was first washed with n-hexane and then thoroughly washed with THF(tetrahydrofuran) under the ultrasonic irradiation to recover the soluble fractions of hexane soluble(HS) and hexane insoluble but THF soluble(HI-THFS) from the adsorbent. The yield of the THF insoluble residue was calculated based on the weight of the dried adsorbent.

The step scan XRD(a high resolution liquid mode by Rigaku-2000) of VR fractions was measured by the scan speed of 0.4 sec/0.01 ° at variable temperatures of 30 to 300 °C with or without solvent of toluene of variable amounts.

RESULTS AND DISCUSSION

Composition and Structure of VR Fractions

The VR was consisted of 7.4 % HI and 92.6 % of HS, the latter of which was further fractionated into 16.3 % of Sa, 50.2 % of Ar, and 26.1 % of Po. The heteroatom-containing compounds including metallic compounds were concentrated in the HI as summarized in Table 1.

The XRD patterns of VR fractions are shown in Figure 1. The original VR showed a broad peak around 20 ° with a rather sharp shoulder peaks around 22 ° and 24 °. The HI showed a relatively sharp peak around 26 ° with a slight peak of 20 °, reflecting their larger aromatic rings and their stacking aggregate structure. Ar and Sa showed a rather sharp peak around 20 °, indicating entanglement of their longer alkyl chains of variety and polymethylene entanglement. The Po fraction showed a similar peak around 26 ° to that of the HI with a higher peak around 20 °, suggesting the similar structure to the asphaltene but with a smaller aromatic ring and molecular weight, and longer alkyl chains as reported in a previous paper.⁹

The Effect of the Heating and Solvent on the Aggregate Structure of the Asphaltene

Figure 2 shows the XRD patterns of VR during the heating from 30 to 300 °C. The sharp peaks around 22 and 24 ° disappeared by the heating to 100 °C, and the broad peak around 20 ° was shifted to the smaller angle direction during the heating up to 300 °C, suggesting that the aliphatic chain entanglement may be liberated by the heating. The shoulder peak around 26 ° derived from the asphaltene fraction also disappeared by the heating up to 200 °C. Figure 3 shows the XRD pattern of HI during the heating to 300 °C. The peak around 26 ° was not changed by the heating to 200 °C, while the further heating to 300 °C weakened the peak very much, but it was still survived at a high temperature 300 °C in the case of the asphaltene fraction alone.

10 to 30 % addition of toluene to VR decreased the peaks around 22 ° and 24 ° with the broadening of the peak around 20 °. These peaks were almost completely removed by the addition of 50 % toluene. On the other hand, the addition of toluene to the HI broadened the whole peak with decreasing markedly the peak of 26 °. The larger amount of toluene addition over 75 % appeared necessary for the complete removal of the peak around 26 ° derived from aromatic plane stacking.

Adsorption Treatment of VR by Carbon Supports

Figure 4 shows the yields in the adsorption treatment of VR by KB at 60 °C. The THF insoluble (THFI) yield increased with the added amount of KB, and 2.0 g of KB addition removed almost completely the HI fraction from VR as THFI. The HI but THF soluble fraction decreased with the increased amount of THFI fraction. 0.6 to 1.0 g of KB addition appeared enough for the selective removal of the heavier fraction without increasing the HI-THFS fractions. Figure 5 illustrates the XRD profiles of the THFI before and after the adsorption treatment by KB. The untreated KB showed a very slight peak around 26°. The adsorbed THFI exhibited a broad peak around 26°, while the relatively sharp peak of the original asphaltene around 26° decreased with the addition of KB, indicating selective adsorption of the heavier fraction in the asphaltene.

Figure 6 illustrates the comparison of the adsorption treatments of VR with variable carbon adsorbents. The heavier fraction in VR was selectively adsorbed on carbon blacks and mesoporous carbons, but never adsorbed onto the microporous activated carbon fibers such as OG-7A and 15A.

Table 2 also summarizes the adsorbed amount of THF insoluble (THFI) with the metal concentrations analyzed by XRF measurements. MA 600 adsorbed the very small amount of THFI (0.37 wt%) with the higher concentrations of V (489 ppm) and Ni (187 ppm), although its surface area was as low as 150 m²/g. Carbon blacks of KB-600JD and BP2000 were also effective for the removal of the concentrated heavy fraction from VR, although the adsorbed amount of THFI was relatively higher than the other carbon adsorbents. A efficient recovery procedure of the heavier fraction from carbon black particles of high surface area should be designed for the application of such adsorbent to the upgrading of VR.

Based on the present study, mesoporous carbon particles can be a candidate for the selective removal of metal-containing heavy asphaltene fraction from VR and the regenerative recovery without too strong adsorption of the polar and heavier fraction.

ACKNOWLEDGMENT

This work has been carried out as a research project of The Japan Petroleum Institute commissioned by the Petroleum Energy Center with the subsidy of the Ministry of International Trade and Industry.

REFERENCES

1. Speight, J.G. *"The Desulfurization of Heavy Oils and Residua"*, Dekker, New York, 1981.
2. Nelson, W.L. *Oil & Gas J.* 1976, 74, 72.
3. H.R.Siewert, H.R.; Koenig, A.H.; Ring, T.A. *Hydrocarbon Process.* 1985, 64, 61.
4. Yen, T.F.; Erdman, J.G.; Pollack, S.S. *Anal.Chem.* 1961, 33, 1587.
5. Howell, R.L.; Hung, C.W.; Gibson, K.R.; Chen, H.C. *Oil & Gas J.* 1985, 83, 121.
6. Mochida, I.; Zhao, X.Z.; Sakanishi, K.; Yamamoto, S.; Takashima, H.; Uemura, S. *Ind. Eng. Chem. Res.*, 1989, 28, 418.
7. Mochida, I.; Zhao, X.Z.; Sakanishi, K. *Ind.Eng.Che.Res.*, 1990, 29 334.
8. Sakanishi, K.; Zhao, X.Z.; Mochida, I. *J. Petrol. Inst. Jpn.* 1992, 35, 203.
9. Sakanishi, K.; Yamashita, N.; Whitehurst, D.D.; Mochida, I. *Catal. Today*, 1998, 43, 241.

Table 1 Elemental Analysis of Arabian mixed crude vacuum residue

Sample	Content [wt%]	wt%				H/C	N/C	Vanadium (ppm)
		C	H	N	Others			
Original VR	100.0	84.4	10.4	0.39	4.9	1.48	0.003	87
HS	92.6	84.5	10.4	0.34	4.4	1.53	0.002	90
Sa	16.3	85.6	13.3	0.04	0.74	1.85	0.000	-
Ar	50.1	84.3	10.2	0.30	5.4	1.45	0.002	-
Po	36.1	82.6	8.6	0.23	8.1	1.24	0.009	-
HI	7.4	84.1	7.4	0.23	7.6	1.06	0.006	998

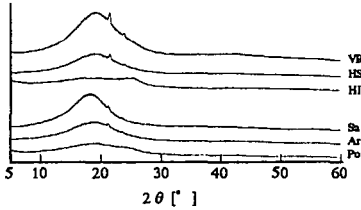


Figure 1 XRD of each Fraction in VR (Step Scan 4sec/0.01°)

Table 2 Some properties of carbon adsorbents and their adsorption performance of VR

	S.A. [m ² /g]	ave. radius (Å)	adsorbed as THF-I [wt %]	V of adsorbed fraction [ppm]	N of adsorbed fraction [ppm]
KB 600JD	1270	-	1.42	301	128
MA600	150	-	0.37	489	187
BP2000	1475	-	2.00	256	132
OG-7A	957	8.36	0.00	-	-
OG-15A	1776	9.76	0.00	-	-
OG-20A	1930	9.83	0.10	61	192
MP-60	1276	16.50	0.78	188	70
MP-90	1371	21.10	1.62	200	69

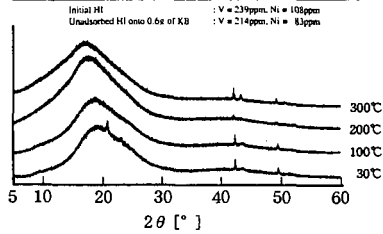


Figure 2 XRD of Heated VR (Measuring Temp. 30 to 300°C, Step Scan 4sec/0.01°)

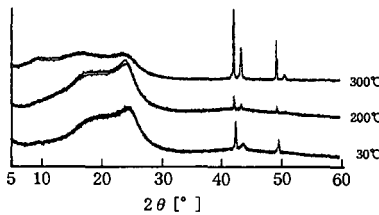


Figure 3 XRD of Heated HI (Measuring Temp. 30 to 300°C, Step Scan 4sec/0.01°)

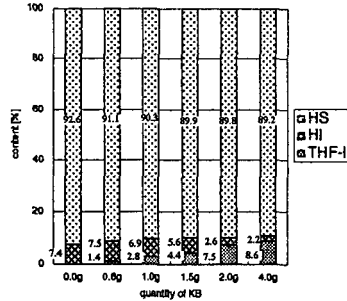


Figure 4 Adsorption of VR into KB (VR/KB = 20.0g/Xg, Mixing Time = 1h, Temp = 60°C)

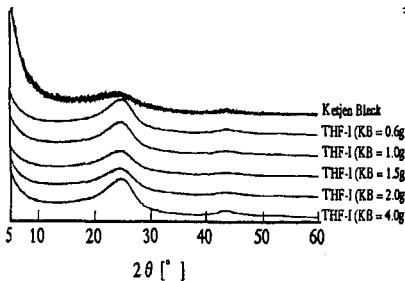
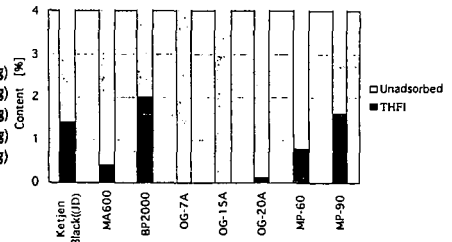


Figure 5 XRD of THF-I adsorbed on KB (VR/KB = 20.0g/Xg, Mixing Time = 1h, Temp = 60°C, Step Scan 4sec/0.01°)



(VR= 20.0g, Carbon = 0.6g, Mixing Time 1h, Temp 60°C)

Figure 6 Adsorption treatment of VR with variable carbons

SULFUR CHARACTERIZATION IN ASPHALTENE, RESIN, AND OIL FRACTIONS OF TWO CRUDE OILS

Sudipa Mitra-Kirtley, Oliver C. Mullins, Corie Y. Ralston, and Courtney Pareis

Rose-Hulman Institute of Technology, IN 47803 (SMK, CP)
Schlumberger Doll Research, Old Quarry Road, Ridgefield, CT 06877 (OCM)
Albert Einstein University, New York, NY 10461 (CYR)

Sulfur chemical species have been determined for asphaltene, resin, and oil fractions of two crude oils by using X-ray absorption near-edge structure (XANES) spectroscopy. The prevalent sulfur species are thiophene, sulfide, and sulfoxide. The asphaltene fraction of one of the oils, CAL, is known to have a very high sulfoxide content. The asphaltene fractions of both the crude oils were analyzed several years ago, and had generated similar sulfur fractions as the present study. This shows that the oxidation of the sulfides in CAL occurred within the earth formation, and not by air oxidation after the production of the crude oil. This also confirms the robustness of the analysis method. Results from this study also show that large sulfoxide fractions are obtained for *all* components of CAL, even in the (typically) non-polar oil fractions. The second crude oil is lower in oxygen, and shows similar composition in *all* three fractions.

Key Words: Sulfur, XANES, Asphaltenes

INTRODUCTION

Crude oils are described as consisting of three fractions—asphaltenes, resins, and oils; these fractions are determined by solubility classification.¹⁻³ One definition is that the oil fractions are the pentane-soluble portion of crude oils, resins are pentane-insoluble and heptane-soluble portions and asphaltenes are heptane-insoluble portions of crude oil. The solubility classification of these crude oil components correlates strongly with chemical properties of the derived components. For instance, asphaltenes from different crude oils are remarkably similar in their chemical properties. Asphaltenes interfere with producing, transporting, and refining of crude oils, and the resins stabilize the suspension of asphaltenes in crude oils; they are, therefore, both prominent in crude oil utilization. Asphaltenes and resins contain higher fractions of heteroatoms, compared to the oil fraction. Consequently, heteroatoms, particularly their polar moieties, partly determine the chemical properties of these crude oil fractions, and, to the extent that solubility is influenced, partly define these fractions. For example, chromatographic studies have shown that certain alkyl sulfides are present in the resin fraction, while the corresponding sulfoxides are present in the asphaltene fraction. The much greater polarity of the sulfoxide group moves the oxidized component from the resin to the asphaltene fraction. The object of this paper is to investigate the relative abundances of the different sulfur chemical forms, especially the polar groups, in the different fractions. The asphaltenes had been studied by the same method about a decade ago, and the present study verified the reproducibility of the results.

XANES spectroscopy has been successfully employed to probe the chemical nature of sulfur in different fossil-fuel components³⁻¹⁰ such as asphaltenes^{3,5,6}, crude oils^{3,7}, and coals^{3,8,9}. Generally, each different chemical form of sulfur gives rise to its own characteristic single, large peak (1s-3p electronic transition). The resonance peaks of sulfide and thiophene are resolvable but are close, introducing some errors in their fractions. The sulfoxide peak, however, is well resolved from all others, and has less associated errors. In asphaltenes, sulfur occurs as mostly thiophenic (aromatic) and sulfidic (saturated) forms. Sulfoxide is the oxidized form of sulfur found in asphaltenes, and usually appears to have resulted from oxidation of sulfide present in crude oils. In some asphaltenes, thiophenic sulfur dominates, while in others, thiophenic and sulfidic forms are comparable. More thermally matured crude oils have prominent thiophenic fractions in the asphaltene fractions. In coal sulfur exists in both organic and inorganic forms. Many coals contain pyrite, and the lowest rank coals may contain sulfate. The organic forms of sulfur in coals are in thiophenic and sulfidic forms, similar to asphaltenes except that coals lack sulfoxides. Nitrogen has also been explored in XANES studies on asphaltenes and other carbonaceous materials.³ These studies have shown that in asphaltenes nitrogen occurs almost entirely in aromatic forms,

in pyrrolic and pyridinic structures.

In this study, we present results of sulfur XANES spectroscopy on asphaltenes, resins, and oil fractions obtained from two crude oils. One of the two asphaltenes is known to be high in sulfoxide, the other low, thus the two crude oils constitute a good test case for the deposition of polar sulfur chemical groups in different crude oil fractions. The asphaltene fractions from both the crude oils had been analyzed by XANES method several years ago, and one of the issues this paper addresses is to verify the robustness of the analysis method, as well as to investigate if there is any considerable air oxidation. In both the studies, XANES sulfur spectra were analyzed with the use of reference spectra of model compounds in the usual fashion.³ The principal finding here is that the three components of the crude oils have similar fractions of sulfoxide. The very polar sulfoxide group does not alter solubility sufficiently to transfer all sulfoxide-containing molecules to the heavy ends.

EXPERIMENTAL

Sulfur K-edge XAFS spectra were collected at beam-line X-19A at the National Synchrotron Light Source (NSLS) at Brookhaven National Laboratory. A double-crystal monochromator of Si (111) crystals was used for dispersion. In order to minimize effects from higher order harmonics, about 80% detuning were used. The X-ray beam exited the UHV through a beryllium window immediately adjacent to the sample chamber, which was filled with helium in order to ensure minimum X-ray absorption by the atmosphere. The data were collected in the fluorescence mode with the use of a Stern-Heald detector and Mylar films were used in the sample chambers to hold the sample.

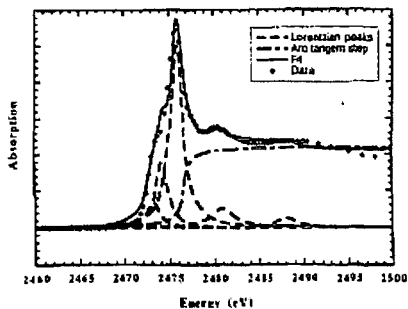
The sulfur model compound samples were first diluted in boric acid, finely ground, and then smeared on sulfur-free Mylar film, which was placed in the beam path. The fossil fuel samples were either ground and mounted on the film, or diluted in CCl_4 and evaporated to dryness on a film that was then placed in the beam path.

All the sulfur models were obtained from Aldrich Chemical Company; they were dibenzyl sulfide, dibenzothiophene, thianaphene, dibenzyl sulfoxide, iron (II) sulfide, potassium sulfate, and sodium thiosulfate. The fossil-fuel samples were the asphaltene, resin, and on fractions obtained from CAL and KUW2 (UG8) crude oils.

Virgin stock-tank crude oils CAL and KUW2 were used for analysis. Samples were prepared as follows: a solution was prepared with 40 cc of pentane per gram of crude oil. The solution was stirred for 24 h and filtered. The filtered soil was washed with pentane until the pentane wash was colorless. Pentane was removed from the filtrate by evaporation to yield the on fraction. The separated solid was dissolved in a small volume of toluene; heptane was then added in the volume ratio of 40: 1. After being stirred for 24 h, the asphaltenes were filtered, and the heptane solution was taken to dryness to obtain the resins. We note that in the non-unique definitions of crude oil components, one could label all pentane-insoluble as asphaltenes. According to this classification, our three fractions would be the heavier asphaltene fraction (heptane-insoluble), the lighter asphaltene fraction (pentane-insoluble and heptane-soluble) and the maltenes. This classification was noted to help comparisons with other work.

A least-squares fitting program was used to quantitatively analyze the sulfur spectra. The spectra were analyzed by methods previously described⁸. The spectra of models and the fossil fuels were first normalized with respect to the step heights and then fitted to a sum of several Lorentzian peaks and an arctangent step. The Lorentzian peaks correspond to resonant electronic transitions,

Figure 1



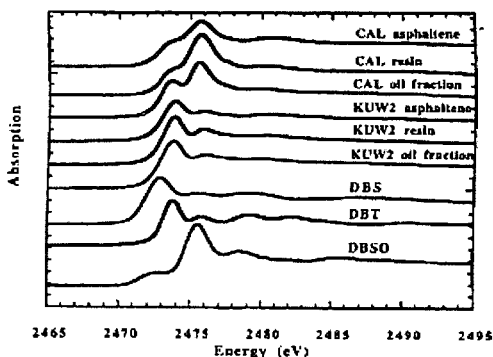
whereas the step accounts for electronic transition to the continuum. The curves from the model compounds were used as basis vectors to fit the curves of the crude oil components. Concentration corrections were applied to the model spectra. Figure 1 illustrates the fitting procedure of a typical sulfur XANES

spectrum, here a spectrum for CAL resin. The fitting procedure was performed on a Macintosh computer using the curve-fit routine of KaleidaGraph software. Using this procedure, all the XANES spectra of the models and the crude oil fractions were fitted. The spectra of the crude oil fractions were then represented as a linear sum of the spectra of model compounds in order to generate sulfur fractions. The error for the sulfide and thiophene fractions is about 10% due to the close proximity of their peaks and the error is smaller for the sulfoxide and higher oxide fractions, which all have isolated peaks.

RESULTS AND DISCUSSION

Figure 2 is a plot of the sulfur XANES of the asphaltene, as well as resin and oil fractions

Figure 2



obtained from CAL and KUW2 crude oils. All these spectra have been normalized to the same step height. In addition, Fig. 2 shows the spectra of dibenzyl sulfide, dibenzothiophene, and dibenzyl sulfoxide, the three relevant model compounds. The model compounds show the dramatic effect that oxygen has on the energy of the 1s-3p resonance; higher oxidation states of sulfur yield higher transition energies. The

thiophene and sulfide both have a formal oxidation state of zero, but the thiophene is at a slightly higher energy. This is probably due to effects of aromatic electron delocalization.³ Some electron density in the sulfur lone-pair p_z orbital is delocalized in the ring, thereby reducing electron density on the sulfur site. This effect is very large on nitrogen in the more aromatic pyrrole rings.³

The most striking difference between the two suites of oil component data is seen in the relative intensities of the oxidized (sulfoxide) and reduced sulfur resonance's. For *all* components of the CAL crude oil, the sulfoxide peak dominates. In *all* KUW2 fractions, the sulfoxide is a minor component and reduced sulfur species dominate. The spectra immediately show that sulfoxide is present in approximately the same amounts in all the three components for each crude oil and is not limited to the more polar resin and the asphaltene fractions.

Table I. Relative abundances of sulfur forms in the asphaltene, resin, and oil fractions of CAL, and KUW2 (UG8).

	Sulfide	Thiophene	Sulfoxide	Sulfone	Sulfate
CAL Asph	15	29	50	5	1
CAL Resin	11	27	59	1	1
CAL Oil	24	27	46	1	1
KUW2 Asph	40	55	2	1	1
KUW2 Resin	40	52	5	1	1
KUW2 Oil	45	47	5	1	1

The relative abundance's of the different sulfur forms of the asphaltenes, resins and oil fractions obtained from CAL and KUW2 crude oils is tabulated in Table I. These samples are not expected to have any sulfone or sulfate, and, within error, which is estimated to be within 10%, none was found. All the fractions of CAL and KUW2 show considerable fractions of organic

sulfide and thiophene. In addition, all fractions of CAL contain high and comparable quantities of sulfoxide. Asphaltenes and resins are known to be more polar than the oil fraction; moreover, sulfoxide is very polar. In spite of this observation, the oil fraction of CAL contains a high fraction of oxidized sulfur. Of course, sulfur represents a smaller mass fraction of the oil phase than of the heavier ends. The resin fraction of CAL has a greater sulfoxide fraction than the asphaltene fraction does, perhaps making the resins the most polar fraction for this crude oil. The sulfur compositions of the KUW2 fractions are all low in sulfoxide and are also comparable in their sulfide and thiophene fractions. For both CAL and KUW2, the oil fractions have slightly higher sulfide fractions. Similarly, the carbon in the oil fraction is also less aromatic in the oil fraction than in the heavy ends.¹⁻³

Table II. Results from XANES analysis by Waldo et al.⁷

Asphaltene	Sulfide	Thiophene	Sulfoxide	Sulfone	Sulfate
CAL	16	36	44	3	<1
KUW2	43	52	4	2	<1

Previously, asphaltene fractions from CAL and KUW2 were studied by Waldo et al. by XANES spectroscopy, and yielded similar results, as shown in Table II⁷, in spite of the seven-year difference in the isolation and analysis of the different CAL and KUW2 asphaltene samples. Error analysis performed on the analysis procedure confirms that the above analysis method is robust, and the numbers are within a 10% error margin. The present study also confirms that the most likely source of sulfoxide is oxidation of the sulfide *within* the crude oil,⁶ which is consistent with the well-known lability of some sulfides towards oxidation. A stock tank oil sample was used for the experiments, and not a sealed-bottom-hole sample. Therefore, it is unlikely that the sulfoxide in CAL was generated after production of the crude oil by air oxidation. We have treated all our asphaltene and crude oil samples in a similar manner, yet CAL asphaltene has a sulfoxide fraction four times greater than any other we examined,⁶ while the KUW2 asphaltene has little sulfoxide. Furthermore, the CAL resin and the CAL oil phase contain large sulfoxide fractions, while the corresponding KUW2 fractions show little sulfoxide in spite of identical treatment of these crude oil samples. Thus, we believe that the extreme oxidation of the sulfides in CAL occurred within the earth formation, perhaps due to contact with meteoric water. The small thiophene fraction in CAL is consistent with low maturity, the shallow depth of burial allowing for exposure to meteoric water.

CONCLUSIONS

Sulfur XANES analysis shows that the sulfoxide-to-sulfur ratios are comparable in all fractions of a given crude oil. Sensitivity analysis confirms the robustness of the XANES analysis method, previous results were similar, in spite of the seven-year difference in the isolation and analysis of the different CAL and KUW2 asphaltene samples. This study also supports the contention that the oxidation process took place *in situ*; thus, the sulfur speciation of different virgin asphaltenes and crude oils can be very different in nature, with sulfoxide fractions varying from 0 to 50%. Such large variations in the chemistry of different petroleum asphaltenes are unusual. These results should be considered when comparing asphaltene results from different studies and samples, because sulfoxides are very polar and thereby partly determine the asphaltene fraction.

ACKNOWLEDGMENT

The XANES experiments were carried out at the National Synchrotron Light Source at Brookhaven National Laboratory, which is supported by the US. Department of Energy.

REFERENCES

1. *Bitumens, Asphalts and Tar Sands*, G.V. Chilingarian and T.E. Yen, Eds. (Elsevier, New York, 1978).
2. J. G. Speight, *The Chemistry and Technology of Petroleum* (Marcel Dekker, New York, 1980).
3. O. C. Mullins, in *Asphaltenes: Fundamentals and Applications*, E. Y. Sheu and O. C. Mullins, Eds. (Plenum Press, New York, 1995).

4. O. P. Strausz, The Fine Particle Soc. Meeting, Chicago, Illinois (1995); Also see J. D. Payzant, T. W. Mojelsky, and O. P. Strausz, *Energy & Fuels*, **3**, 449 (1989).
5. G. N. George and M. L. Gorbaty, *J. Am. Chem. Soc.* **111**, 3182 (1989). 6. G. S. Waldo, O. C. Mullins, J. E. Penner-Hahn, and S. P. Cramer, *Fuel* **71**, 53 (1992).
7. G. S. Waldo, R. M. K. Carlson, J. M. Moldowan, K. E. Peters, J. E. Penner-Hahn, *Geochim. Cosmochim. Acta* **55**, 802 (1991).
8. G. P. Huffman, S. Mitra, F. E. Huggins, N. Shah, S. Vaidya, and F. Lu, *Energy & Fuels* **5**, 574 (1991).
9. M. L. Gorbaty, G. N. George, and S. R. Kelemen, *Fuel* **69**, 945 (1990).
10. S. Mitra-Kirtley, O. C. Mullins, J. van Elp, S. J. George, J. Chen, and S. P. Cramer, *J. Am. Chem. Soc.* **115**, 1, 252 (1993).

FRACTIONATION AND MOLECULAR ANALYSIS OF A VACUUM RESIDUE ASPHALTENES

Ming-Gang Yang¹ and Semih Eser^{1, 2}

1. Lab. for Hydrocarbon Proc. Chem, The Energy Institute, Penn State Univ., 209 Acad. Proj. Bldg.

2. Dept. of Energy and Geo-Environmental Eng., Penn State Univ., 154 Hoster Building,
University Park, PA 16802

KEYWORDS: Petroleum asphaltenes, Pyrolysis-GC/MS, NMR, LDIMS

INTRODUCTION

Petroleum asphaltenes are defined as the n-pentane or n-heptane insoluble but toluene soluble fraction of crude oils or petroleum residua. This operational definition is a consequence of the extremely complex structure of asphaltenes which consist of thousands of compounds containing highly aromatic cores, long chain aliphatic groups, heteroatoms (sulfur, nitrogen, and oxygen) as well as trace quantities of heavy metals (vanadium and nickel). Therefore, it is extremely difficult to elucidate the molecular structure of petroleum asphaltenes.

A number of studies have been carried out including asphaltene pyrolysis^{1, 2}, chemical reduction³ and oxidation (RICO)⁴ with catalysts using many analytical techniques⁵⁻⁹ such as GC-MS, MALDI, LDIMS, HRMS, ¹H/¹³C NMR, FT-IR, UV-vis spectra, EXAFS, SEC, ESR, XRD, SANS, etc., to investigate the asphaltene structure at the molecular level. The results from these studies have brought to light a wealth of valuable information on asphaltenes. Recent structural models suggest that asphaltene molecules be composed of an aromatic core with six condensed aromatic rings on average that is substituted by n-alkyl groups averaging C₈ in length¹⁰. In addition, bridging polymethylene groups may be present which connect the aromatic core to smaller aromatic and thiophenic rings. In general, about 25% of the sulfur is thermally labile alkyl and cyclic sulfides, while the remaining sulfur is present in the aromatic core along with the majority of the N and O heteroatoms^{11, 12}. The distribution and structure of the heteroatoms in the aromatic core is largely unknown. The molecular weight of individual asphaltene molecules averages less than 1000 amu, but the asphaltene molecules interact strongly in solution, forming colloidal aggregates with very high apparent molecular weights¹³.

In this study, a petroleum residue asphaltenes were separated into six subfractions based on their solubility in binary solutions of n-pentane and toluene at different proportions. The separated subfractions were analyzed by laser desorption ionization mass spectrometry (LDIMS), ¹H/¹³C NMR, and pyrolysis gas chromatography/mass spectrometry (Py-GC/MS).

EXPERIMENTAL

The n-pentane (HPLC grade, 99.8 %) and toluene (HPLC grade, 100 %) were supplied by Fisher Chemicals, and J.T. Baker Inc. respectively. Chloroform-d (99.8 atom% D) and Chrom(III)-acetylacetonate (97 % UV) used in ¹H/¹³C NMR analysis were supplied by Aldrich Chemical Company, Inc., and Fluxa Chemika. A commercial petroleum vacuum residue sample was used as a source of asphaltenes.

The vacuum residue sample was separated into maltenes (n-pentane soluble) and asphaltenes (n-pentane insoluble) by adding n-pentane in a volume/weight ratio of n-pentane to residue of 60:1 (mL/g) followed by filtration. A sample of 1 g asphaltenes was dissolved in 27 mL toluene, and 33 mL n-pentane was added into the solution by stirring with a magnetic bar at ambient temperature. After adding n-pentane, the ratio of the total volume of the two solvents to asphaltenes was 60:1 mL/g with an n-pentane to toluene ratio of 55/45 in volume. The solution was covered and stirred overnight for precipitation of insolubles. After filtration, the insoluble fraction was collected and dried in an oven at 75 °C and 0.1MPa vacuum overnight to obtain the first subfraction (Sample AS6). The n-pentane and toluene in the filtrate were evaporated in a rotary evaporator to collect the remaining asphaltenes that were dried in an oven at 75 °C and 0.1MPa vacuum overnight. The dried sample was dissolved in toluene again, and following the procedure described above, sample AS5 was precipitated in a solution with an n-pentane to toluene ratio of 65/35 in volume. Similarly, samples AS4 (n-pentane to toluene = 75/25), AS3 (85/15) and AS2 (95/5) were precipitated in binary solutions with the increasing proportion of n-pentane. The last fraction, AS1, (dissolved in the solution of n-pentane to toluene = 95/5) was obtained by evaporating the solvents. The asphaltene fractionation scheme is shown in Figure 1.

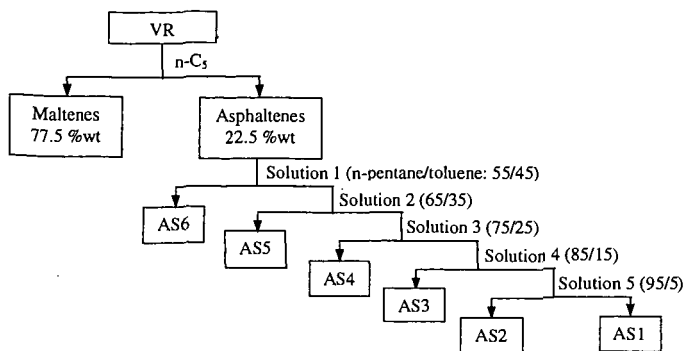


Figure 1. Flow chart for fractionation of petroleum vacuum residue asphaltenes.

The LDIMS spectra were acquired on a PerSeptive Biosystems Voyager-DE STR mass spectrometer using 337 nm light from a pulsed nitrogen laser for ionization. High-resolution spectra ($M/\Delta M \sim 10000$ at m/z 500) were obtained using the reflector mode. Samples were prepared by dissolving approximately 50 micrograms of material in 200 microliters of tetrahydrofuran. The sample solution of 0.5 microliters was deposited on the gold-plated target, and the solvent allowed to evaporate under ambient laboratory conditions. Samples were introduced into the mass spectrometer and analyzed as soon as possible to minimize evaporation of more volatile components. Ionization was conducted using laser fluency slightly above the threshold for ionization (laser power ~ 106 W/cm²), and a total of 256 laser shots acquired over numerous sites within each sample were averaged.

The NMR spectra were obtained using a BRUKER AMX360 NMR instrument operating at 360 MHz for ¹H NMR, and 89 MHz for ¹³C NMR measurements. The NMR samples were prepared by dissolving about 100 mg asphaltenes into 1 mL chloroform-d solvent. Tetramethylsilane (TMS) was used as an internal standard mixed with chloroform-d solvent as received. A relaxation agent, chrom(III)-acetylacetonate, was added into the sample solution (0.03M) to get quantitative ¹³C NMR measurements

For Pyrolysis-GC/MS experiments, samples (about 6 mg) were first loaded in an unsealed quartz tube. Then, the tube was inserted into a filament coil that is placed in the probe gun. The gun tube was inserted into an interface where the sample was pyrolyzed. Pyrolysis temperature, time, and the interface temperature were controlled by Pyroprobe 1000. Pyrolysis conditions were 800 °C, 10 seconds, and a heating rate of 5 °C/ms. The interface temperature was set 290 °C. Pyrolysis products were collected in a capillary column at liquid nitrogen temperature and then separated in a temperature programmed DB-17 capillary column by HEWLETT 5890 II GC, and characterized by HEWLETT 5971A MS.

RESULTS AND DISCUSSION

The petroleum vacuum residue contained 77.5 wt% maltenes and 22.5 wt% asphaltenes (n-pentane insoluble). Table 1 shows the yields of asphaltene subfractions separated following the scheme shown in Figure 1.

Table 1. Yields of solvent subfractions of asphaltenes.

Subfraction	AS1	AS2	AS3	AS4	AS5	AS6	Loss
Distribution / wt%	25.5	5.3	18.0	22.9	21.0	4.2	3.1

The results in Table 1 show that the vacuum residue asphaltenes could be further fractionated using the binary mixtures of n-pentane and toluene with different composition. The yields of subfractions AS2 and AS6 were much lower than those of the other subfractions.

Laser desorption ionization mass spectrometry (LDIMS) results in little fragmentation of the constituent molecules. Therefore, it is a useful technique to determine the molecular weight distribution in complex mixtures. The mass distributions of samples AS2, AS4 and AS6 are shown in Figure 2. Each asphaltene subfraction displayed a different molecular weight distribution. The distribution became wide and the number average molecular weight increased in mass/charge ratio from AS2 (250-600) to AS4 (300-800), and to AS6 (350-1100). The maximum abundance of

molecular constituents for the three samples, AS2, AS4, and AS6 is at 300, 350 and 500 m/z, respectively.

The ^1H NMR spectra have been divided into four regions consisting of γ -methyl hydrogens (H_γ) between 0 and 1 ppm; hydrogens from β -methyls, methines, and methylenes β or further to the aromatics (H_β) between 1 and 2 ppm; hydrogens from all aliphatic sites attached to aryl carbon (H_α) between 2 and 5 ppm; and aromatic hydrogens (H_{ar}) between 6 and 9 ppm. The ^{13}C NMR spectra have been divided into two integration domains which are aliphatic carbons (C_{al}) between 10 and 65 ppm, and aromatic carbons (C_{ar}) between 100 and 170 ppm. The hydrogen and carbon molar distributions derived from $^1\text{H}/^{13}\text{C}$ NMR spectra are listed in Table 2.

Table 2. Relative molar distribution of hydrogen and carbon in asphaltene subfractions

	AS2	AS3	AS4	AS5	AS6
H_α	0.17	0.33	0.12	0.21	0.37
H_β	0.63	0.43	0.62	0.57	0.49
H_γ	0.08	0.05	0.04	0.04	0.03
H_{ar}	0.12	0.19	0.22	0.18	0.11
C_{al}	0.60	0.54	0.53	0.52	0.51
C_{ar}	0.40	0.46	0.47	0.48	0.49

The carbon aromaticities of all the subfractions are similar to one another with a slightly lower aromaticity of AS2 compared to the other samples. There are, however, significant differences in the distribution of hydrogen between the subfractions. The relatively low hydrogen aromaticities of AS2 and AS6 can be attributed to more extensive alkyl substitution, and more condensed structures of aromatic ring systems, respectively. Differences in aliphatic hydrogen distribution between AS2 and AS6 also indicate variations in the nature of the alkyl groups. From the distribution of aliphatic hydrogen groups, similarities are noted between AS2 and AS4, and between AS3 and AS6. The fraction AS5 falls into an intermediate position between the two groups, particularly in H_α and H_β contents.

The average structural parameters do not give much information regarding the type and distribution of molecular constituents and their organization within the molecules. Pyrolysis GC/MS may provide some useful data on thermally labile molecular units and how they are connected. Asphaltenes during Py-GC/MS experiment were converted into three fractions: volatiles, nonvolatile heavy oils or tar, and remainder coke (tetrahydrofuran insoluble). The yield of each fraction was dependent on the pyrolysis conditions and the sample used. The sample AS2, for example, gave volatile fraction yield of 11.8 wt% at 600 °C, while at 800 °C, the yield increased to 45.2 wt%. The yields of volatile fractions from samples AS1 to 6 at 800 °C are listed in Table 3. The samples AS1 and AS6 showed higher yields of volatile fraction than samples AS3 and AS5.

Table 3. Yields of volatile fraction in asphaltene pyrolysis at 800 °C.

Sample	AS1	AS2	AS3	AS4	AS5	AS6
Yield / wt%	54.7	45.2	33.1	41.5	37.1	48.8

A Py-GC/MS total ion chromatogram for AS1 is shown in Figure 3. The volatile products consist mainly of alkanes (C_8 to C_{35}), 1-alkene (C_5 to C_{35}), alkylbenzenes (alkyl: C_1 to C_5), alkylnaphthalenes (alkyl: C_1 to C_3) and sulfur compounds (alkyl substituted thiophene, benzothiophene, dibenzothiophene and naphthothiophene). A small amount of isoalkanes and cycloalkanes (alkyl C_5 and C_6 ring) was also identified in the volatile products. Although the asphaltene subfractions AS1 to 6 gave different yields of volatile products, their composition appeared to be similar.

CONCLUSIONS

Asphaltenes derived from petroleum vacuum residua can be further separated into several subfractions based on their solubility in binary mixtures of n-pentane and toluene with different composition. Each subfraction still contains a large number of individual compounds. Distinct differences were observed between subfractions in average molecular weights, molecular weight distribution, aromaticity, and distribution of aliphatic hydrogen.

ACKNOWLEDGMENTS

We thank Dr. A. Daniel Jones (Director, Penn State Intercollegiate Center for Mass Spectrometry) for providing the data on Laser Desorption Mass Spectrometry analysis of the asphaltene subfractions.

REFERENCES

1. Ritchie, R.G.S.; Roche, R.S.; Steedman, W. *Fuel* **1979**, 58, 523.
2. Calemma, V.; Rausa, R.; D'Antona, P.; Montanari, L. *Energy & Fuels* **1998**, 12, 422.
3. Peng, P.; Morales-I, A.; Lown, E. M.; Strausz, O. P. *Energy & Fuels* **1999**, 13, 248.
4. Su, Y.; Artok, L.; Murata, S.; Nomura, M. *Energy & Fuels* **1998**, 12, 1265.
5. Montanari, L.; Scotti, R. In *Structures and Dynamics of Asphaltenes*, Edited by Oliver C. Mullins and Eric Y. Sheu, Plenum Press, New York. **1998**, p 79-113.
6. Miller, J. T.; Fisher, R. B.; Thiyagarajan, P.; Winans, R. E.; Hunt, J. E. *Energy & Fuels* **1998**, 12, 1290.
7. Wilt, B. K.; Welch, W. T.; Rankin, J. G. *Energy & Fuels* **1998**, 12, 1008.
8. Ralston, C. Y.; Mitra-K., S.; Mullins, O. C. *Energy & Fuels* **1996**, 10, 623.
9. Shirokoff, J. W.; Siddiqui, M. N.; Ali, M. F. *Energy & Fuels* **1997**, 11, 561.
10. Strausz, O. P.; Lown, E. M. *Fuel Sci. Technol. Int.* **1991**, 9, 269.
11. Savage, P. E.; Klein, M. T. *Ind. Eng. Chem. Proc. Des. Dev.* **1985**, 24, 1169.
12. Mullins, O. P. In *ASPHALTENES-Fundamentals and Applications*, Edited by Eric Y. Sheu and Oliver C. Mullins, Plenum Press, New York. **1995**, p 53-96.
13. Boduszynski, M. M. *Energy & Fuels* **1988**, 2, 597.

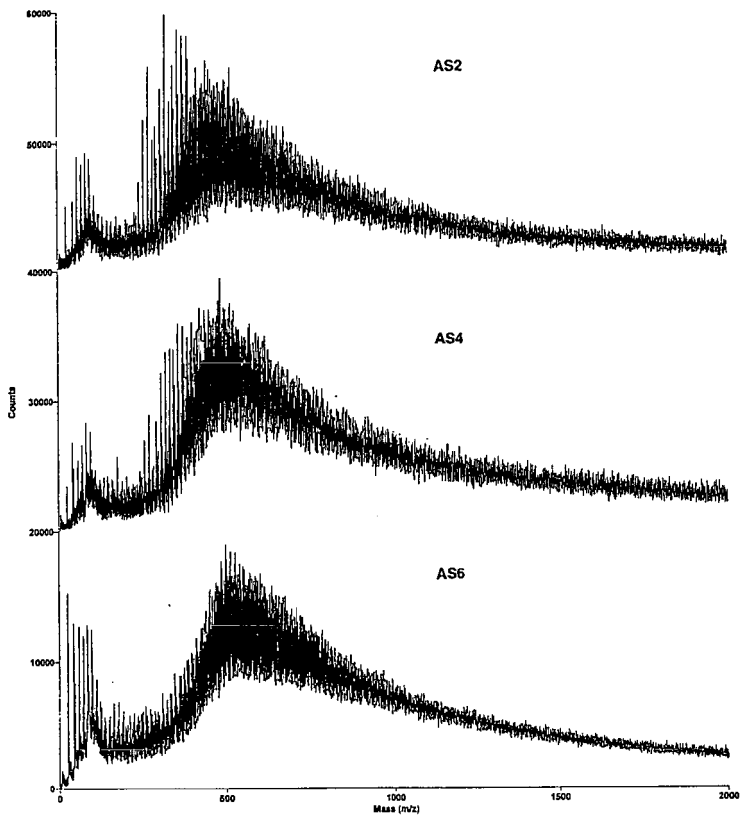


Figure 2. LDIMS spectra of three asphaltene subfractions.

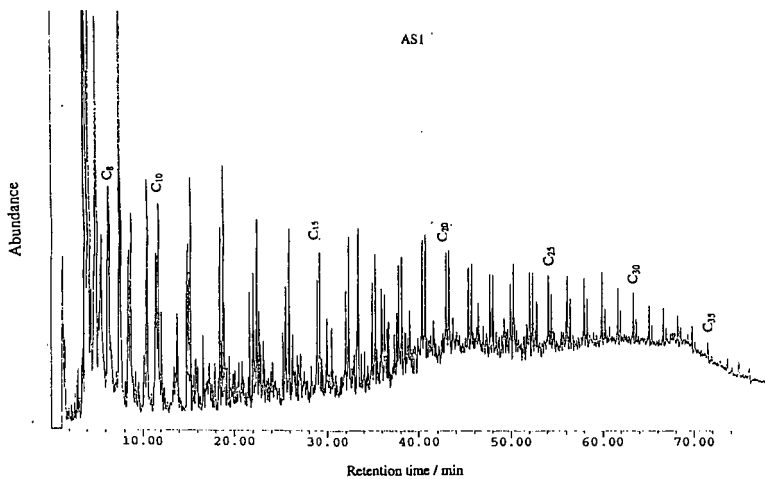


Figure 3. Py-GCMS total ion chromatogram for asphaltene subfraction AS1.

COLLOIDAL NATURES OF TWO TYPICAL CHINESE VACUUM RESIDUA I: COLLOIDAL STRUCTURES IN TERMS OF SFEF FRACTIONS

Li Shenghua¹ Fu Honglan² Liu Chenguang³ Liang Wenjie³

¹Department of Precision Instrument, Tsinghua University, Beijing 100084

²Department of Biology, Peking University, Beijing 100871

³Department of Petroleum Refining, University of Petroleum, Shandong 257062

ABSTRACT: The physical structures of vacuum residua are of industrial potentiality in applications such as prevention of heavy organics deposition in petroleum production and phase separation of coke precursors in petroleum refining. Disclosure of the physical structures of two representative Chinese vacuum residua, Daqing and Shengli vacuum residuum, and their SFEF (supercritical fluid extraction and fractionation) fractions on the colloidal scale by FFRTEM (Freezing Fracture Replication Transmission Electronic Microscopy) indicate that all of them assume colloidal structures with different structural details dependent heavily upon their compositions or origins.

KEYWORDS: colloidal structures, vacuum residua, SFEF fractions

INTRODUCTION

Although more and more information has been accumulated about the natures of the physical structures of VR(VR), very limited images of the physical structures of the original VR are now available with the exception of some apriori knowledge about the colloidal aspects of VR with the support of indirect experiments and field experiences^[1,2]. It is currently recognized that the physical structures of VR assume locally ordered structures on the molecular scale and heterogeneous micell structures on the colloidal scale^[1]. Presently, it seems that the core of all the left issues concerning the colloidal characters of VR is not only to ascertain, with direct evidences, their apparent colloidal features but also to uncover their building units (components or fractions) as well as formation mechanisms.

The authors have attempted with Freezing Fracture Replication Transmission Electronic Microscopy (FFRTEM) to disclose the physical structures of Daqing, Shengli and Gudao VR on the colloidal scale and to evaluate the contributions of the SARA pseudo-pure-components to the colloidal configurations^[3]. Conclusions drawn state that VR are of sol structures; asphaltenes and heavy resins construct the dispersed phases and the other fractions form the dispersing media. Useful as the deductions from FFRTEM are, they need further confirmation as there leaves some room for improvement in sample separation and structure identification employed by the authors.

Firstly, the conventional separation procedure of SARA compositions of VR may incur breakdown or distortion of the real physical structures of original VR. With the supercritical fluid extraction and fractionation (SFEF) technique, however, the possible influences on the real physical structures of original VR could be controlled to the minimum for the solubility classes from the SFEF technique can best keep the continuity of both the compositional and the structural distributions of VR; and secondly, though the FFRTEM technique is able to display in a qualitative manner the colloidal nature of VR and the shape and size of the dispersed phases, it presents no information on the chemical compositions of both the dispersed and the dispersing phases without assistance from the sample separation technique. In fact, when solubility class compositions are employed to characterize the colloidal structures of VR, the validity and conciseness of the FFRTEM technique itself to determine the solubility class compositions of both the dispersed and the dispersing phases depend heavily on the fineness of the VR fractionation.

Still, the established FFRTEM technique was adopted in this study to unfold the colloidal structures of two typical Chinese VR and their SFEF fractions. In such a way, more valid and more direct evidences, instead of the apriori and indirect knowledge, could be accumulated to lend some support to the construction details of the colloidal VR.

MATERIALS AND METHODS

Separation of vacuum residua into SFEF fractions

A Supercritical Fluid Extraction and Fractionation (SFEF) technique^[4], which was developed by the State Key Laboratory of Heavy Oil Processing, University of Petroleum, China, was

utilized to separate nondestructively Daqing and Shengli VR into the proper number of subfractions. In the operation, n-pentane was used as the extractant with flow rate of 100mL /min; the initial pressure of 4.0MPa was set and the final pressure was controlled to be 12.0MPa with a linear pressure increase being kept at 1.0MPa/hr; the temperatures at the bottom of the extraction batch and at the top of the fractionation column were respectively 240°C and 250°C.

With the technique, either narrow or wide fractions could be obtained by extracting varied quantity of lighter constituents out of VR. All the fractions left after extraction are the de-oil asphaltenes (DOA). The more the lighter constituents are extracted, the heavier the DOAs are. For example, in view of wider SFEF fractions adopted in this research, they become heavier and heavier from 30%DOA to 40%DOA to 50%DOA to 60%DOA. The original VR are the lightest as compared with their DOAs.

Elemental and SARA compositions of the studied vacuum residua and their SFEF fractions

Daqing vacuum residue (DVR) and Shengli vacuum residue (SVR), derived from two representative Chinese crude oils, were employed. Their main elements and SARA compositions were analyzed as listed in Table 1 and Table 2.

Table 1 Element and SARA compositions of Daqing vacuum residue and its SFEF fractions

	DVR	30%DOA	40%DOA	50%DOA	60%DOA
C, %	86.23	86.71	86.65	86.74	86.68
H, %	12.86	12.52	12.37	12.16	11.94
S, %	0.145	0.17	0.20	0.21	0.22
N, %	0.44	0.43	0.52	0.60	0.66
Saturates, %	41.9	22.3	19.2	14.1	9.15
Aromatics, %	32.7	38.0	38.5	39.3	39.3
Resins, %	25.4	39.6	42.5	46.6	51.2
Asphaltenes, %	0	0.15	0.19	0.20	0.28

Table 2 Element and SARA compositions of Shengli vacuum residue and its SFEF fractions

	SVR	30%DOA	40%DOA	50%DOA	60%DOA
C, %wt	85.88	85.29	85.42	85.30	84.82
H, %wt	11.34	10.99	10.62	10.39	10.04
S, %wt	3.01	3.88	4.05	4.44	4.32
N, %wt	0.95	1.18	1.26	1.37	1.44
Saturates, %wt	16.1	3.58	1.30	0.31	0.53
Aromatics, %wt	30.6	27.9	23.3	15.6	11.4
Resins, %wt	51.1	66.0	72.5	79.7	81.3
Asphaltenes, %wt	2.2	2.46	2.86	4.38	6.77

Microscopic technique for finer structure identification

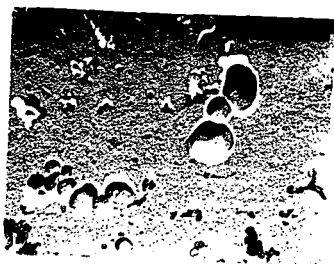
There are many direct or indirect approaches available to characterize colloidal dispersions and Transmission Electronic Microscopy (TEM) is among those direct viewing techniques most widely employed. Considering that TEM has peculiar requirements on the physical states (e.g. thickness) and properties (e.g. volatility) of the observed samples, the sample freezing and one-time replication technique was adopted in this study to prepare the TEM observed samples of VR and their SFEF fractions. Operational procedure of the freezing fracture replication TEM, abbreviated as FFRTEM, was detailed in Ref.[3].

RESULTS AND DISCUSSION

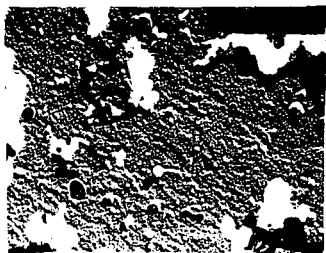
FFRTEM icons of vacuum residua and their SFEF fractions

In Figures 1 through 2 are displayed the FFRTEM photos of the two VR studied and their

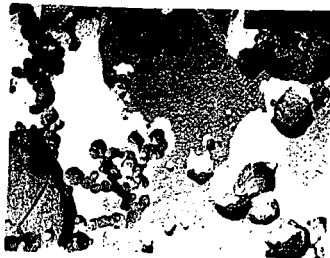
SFEF fractions. The fundamental colloidal attributes presented by these photos are clearly seen in terms of the size and size distribution and morphology of the dispersed phases, as well as the colloidal types of which they are.



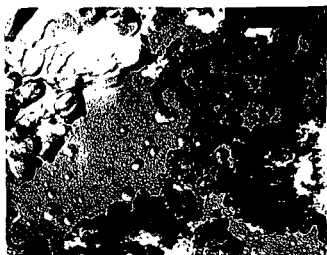
(a) original vacuum residue (61,000 times)



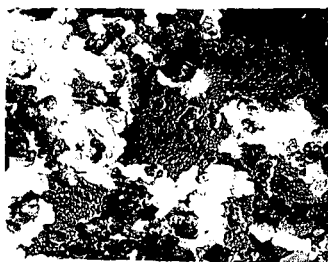
(b) 30% DOA (61,000 times)



(c) 40% DOA (61,000 times)

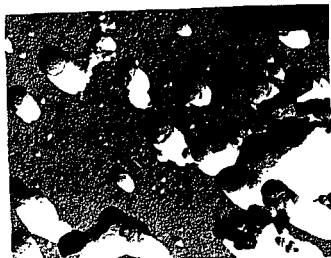


(d) 50% DOA (61,000 times)



(e) 60% DOA (33,000 times)

Figure 1 FFRTEM icons of Daqing vacuum residue and its SFEF fractions



(a) original vacuum residue (61,000 times)

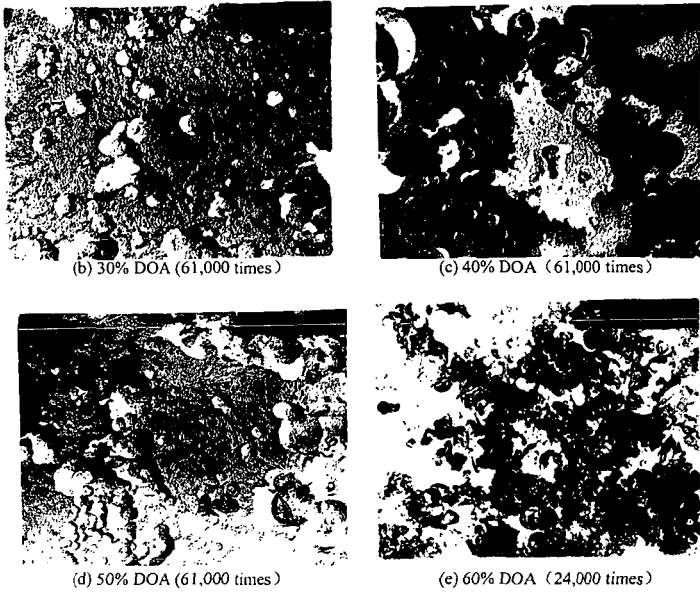


Figure 2 FFRTEM icons of Shengli vacuum residue and its SFEF fractions

Colloidal attributes of vacuum residua and their SFEF fractions

Conventionally, the so-called colloidal particles refer to the molecular aggregates with at least one dimension ranging between 1nm and $1\mu\text{m}$, and considerable interfacial layers exist among the dispersed phases of the colloidal particles and the surrounding dispersing medium^[5]. In the two VR and their SFEF fractions, though there occurs a wide size distribution of the dispersed particles, their dimensions are evidently in the spectrum of colloidal particles, and what is more, rather distinct interfaces can be viewed between the dispersed phases and their surrounding phase. It is therefore concluded that both Daqing and Shengli vacuum residue as well as their SFEF fractions are all colloidal dispersion systems.

Morphology of dispersed phases in vacuum residua and their SFEF fractions

The geometrical shapes of the colloidally dispersed phases are among the most distinguished parameters characterizing colloidal dispersing systems. It is evident from the FFRTEM photos in Figures 1 through 2 that the colloidal particles in the two VR and their SFEF fractions assume spherical and non-spherical shapes with the spherical or sphere-agglomerated dispersed particles in an overwhelming majority. On the other hand, the abundance of the spherical particles relative to the non-spherical particles exhibits rather differently in the original VR and their SFEF fractions. Concretely, almost all the dispersed particles in the two VR and their 30%DOA, 40%DOA and 50%DOA assume spheres or spherical stacking configurations; while in the 60%DOA of the two VR, there exist not only spherical dispersed particles but some tabulate dispersed phases of larger sizes as well. Such observations were further confirmed by the TEM photos displayed in Figure 3.

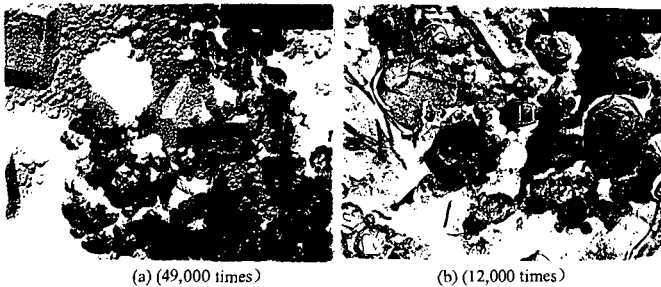


Figure 3 FFRTEM icons of 60%DOA of Daqing(a) and Shengli(b) vacuum residue

It is generally considered that, in the aggregated colloidal systems, the dispersed micell assume spherical shapes when the concentration of the surfactant remains low, e.g. not higher than CMC; when the surfactant is in such a high concentration that its content exceeds as ten times CMC as high or reaches more than 10%, the dispersed phases might as well adopt unsymmetrical configurations or layered stackings^[1]. Since the asphaltenes and the resins in the VR and their SFEF are of the general characteristics of conventional surfactants both in structures and in behaviors, it is not so difficult to qualitatively clarify, in accordance with colloidal solution theories of surfactants, the variations of the geometrical shapes of the dispersed phases in the VR and their SFEF fractions as they become heavier and heavier.

Multidispersity of colloidal vacuum residua and their SFEF fractions

The multidispersion characteristics of the colloidal systems of the VR and their SFEF fractions are embodied in many aspects such as the morphology, average sizes and size distributions of the dispersed phases. Because of the non-homogeneity of the dispersed phases in size and geometrical shapes in the VR and their SFEF fractions, they are all multi-dispersing systems. On the other hand, as the SFEF fractions of the VR become heavier and heavier, the average size and quantity of the dispersed phases will undergo noticeable variations. Generally, more and more dispersed phases will come into being as the SFEF fractions of the VR go heavier.

Both the morphology and the multidispersity of the dispersed phases in the VR and their SFEF fractions imply that these dispersed phases are made from innumerable non-identical constituents or molecules of VR. Such a fact provides one more proof of the multidispersity of the colloidal VR and their SFEF fractions.

Colloidal types of vacuum residua and their solubility classes

Generally, the colloidal structures of the VR and their SFEF fractions become more advanced in the heavier fractions than in the lighter ones. In average, there appear more cross-linked dispersed phases in Shengli vacuum residue and its SFEF fractions than in those of its Daqing counterparts. In terms of the colloidal types, the original vacuum residua and their 30%DOA are more sol structures, while their 50%DOA and 60%DOA appear more gel structures. The structure of the 40%DOA goes in-between, that is, 40%DOA assumes sol-gel structures.

CONCLUSIONS

(1) The combinatorial SFEF-FFRTEM technique is among the most useful approaches to reveal the colloidal structures and attributes of VR and their SFEF fractions in a qualitative way.

(2) Both Daqing and Shengli vacuum residue as well as their SFEF are of colloidal structures with the basic colloidal attributes dependent upon their fractional compositions.

(3) The fact that the original VR and their SFEF fractions exhibit different colloidal structures and attributes implies that they may find different applications due to their unique physical structures and chemical compositions; or different thermodynamic or dynamic behaviors displayed by the original VR and their SFEF fractions may originate from the subtle differences of their physical and/or chemical structures.

ACKNOWLEDGMENTS

The authors are greatly indebted to the financial support of the project by China Postdoctoral Science Fund.

REFERENCES

- [1] S. H. Li, *Physical structures and thermodynamics of petroleum vacuum residua and their applications*. The Postdoctoral Research Report. June 1998.
- [2] J. G. Speight, *J. Petrol. Sci. Eng.*, 1999, 22(1-3):3-15
- [3] S. H. Li, C. G. Liu, G. H. Que et al. *Fuel*. 1996, 75(8):1025-1029
- [4] *New Evaluation Methods for Vacuum Residua and Evaluations of Some Chinese Vacuum Residua*. A Research Report. The State Key Laboratory of Heavy Oil Processing, University of Petroleum, China. March 1997.
- [5] Z. K. Zhou. *Fundamentals of Colloid Chemistry*. Peking University Press. 1987

COLLOIDAL NATURES OF TWO TYPICAL CHINESE VACUUM RESIDUA II: REVISIT AND CHARACTERIZATION OF COLLOIDAL STRUCTURES

Li Shenghua¹ Fu Honglan² Liu Chenguang³ Liang Wenjie³ Zhang Zhong⁴

¹Department of Precision Instrument, Tsinghua University, Beijing 100084

²Department of Biology, Peking University, Beijing 100871

³Department of Petroleum Refining, University of Petroleum, Shandong 257062

⁴Research Institute of Criminalistics, Chongqing 400016

ABSTRACT: Evidences both from TEM observation of Daqing and Shengli vacuum residue and their DOAs prepared by ultra-microtomy and from environmental SEM observation of the untreated Daqing and Shengli vacuum residue and their de-oil asphaltenes confirmed that all of them are of colloidal configurations. It has been generally concluded that, of the microscopic observation tools and the sample treatment techniques employed in the current study of the physical structures of VR, the freezing fracture replication TEM is the best approach in terms of its efficaciousness of displaying the fundamental features of colloidal VR. The independent and combinatorial distribution characteristics of the resins and the asphaltenes are the pivotal parameters in determining the general colloidal features of VR and their de-oil asphaltenes.

KEYWORDS: colloidal structures, vacuum residua, SFEF fractions, SARA fractions

INTRODUCTION

Identification of the colloidal structures of vacuum residua (VR) and their solubility classes is just one aspect concerned by the *Petroleum Physics* studies^[1]. As well documented in previous reports and in the first part of this article^[2,3], the combined SFEF-FFRTEM technique is a sound way in the revelation and characterization of the physical structures of VR on the colloidal scale. For better recognition of the technique, further proofs are strongly required from cross validation experiments in which factors affecting the colloidal structure identification could be manipulated. Among those contributing much to the physical structures of VR, the influence of temperature of the bulk VR on their physical structures accounts for the most besides chemical compositions.

In the procedure of the FFRTEM technique, one issue at point is that the observed samples are to be prepared by freezing replication: the sample is firstly frozen in the liquid nitrogen of -196°C and then replication of the fractured cross-sections of the samples by carbon-coating is conducted in the environment of ca.-120°C. The doubt is that such a process might bring some unrecoverable changes to the physical structures of the bulk VR, which finally results in false deductions about the features and properties of the physical structures of VR. TEM observation of very thin VR samples prepared by ultra-microtomy minimizes the thermal effects on the physical structures of VR. However, it is not clear enough whether the solidification of VR by the solidifying agents in the technique will exert any influences upon their physical structures.

All in all, the VR have to go through a long procedure of physical and/or chemical treatments before they could finally be observed under TEM whether they are prepared by the freezing fracture replication or the ultra-microtomy. In order to take the real images of the untreated VR, Environmental Scanning Electronic Microscopy (ESEM) was attempted to unfold in different manners the physical structures of VR and their formation in terms of solubility classes.

In this part of the paper, not only TEM observations of samples prepared by ultra-microtomy but also their ESEM observations without any physical or chemical treatments were conducted so as to derive more direct evidences, and to lend support to the construction details of the colloidal VR. For deeper understanding of the colloidal VR structures, an attempt will be made to correlate their colloidal features, such as colloidal types and attributes, multidispersity and morphology of dispersed phases, to the SARA pseudo-pure-components.

EXPERIMENTAL

Employment of sample imbedding and ultra-microtomy for TEM observation were made in the present endeavor which serves two purposes: one is to ascertain the comparability of freezing fracture replication in the validity of revelation of the physical structures of VR, and the other is to compare the reliability of different techniques in the reflection of the true physical structures of VR. The introduction of ESEM for the demonstration of the physical structures of VR and their DOAs is another attempt to supply additional proofs to the colloidal identity of VR.

RESULTS AND DISCUSSION

Ultra-microtomy TEM icons of vacuum residua and their SFEF fractions

In Figure 1 is exhibited the TEM photos of Shengli vacuum residue and its DOAs, with the observed samples prepared by ultra-microtomy. As both the solidifying agent and the procedure, such as sample solidifying and the ultra-microtomy, do not interfere with the structural properties of the samples, so the TEM microphotos present images of the vacuum residue and its DOAs without noticeable distortions to the true physical structures.

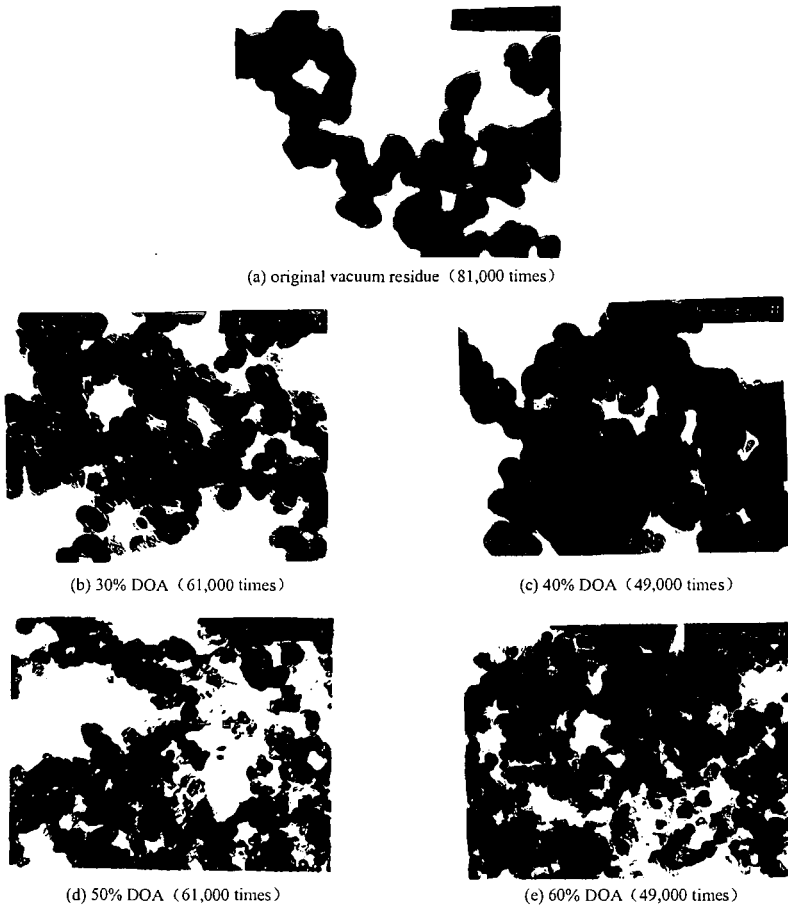


Figure 1 TEM icons of Shengli vacuum residue and its SFEF fractions by ultra-microtomy

It is understandable that, since it is difficult to keep complete consistency of the samples and their viewing areas under microscopes, only the general colloidal features of VR and their DOAs could be compared, such as the morphology of the dispersed phases and the colloidal types. As seen, both the FFRTEM photos and the photos in Figure 1 could reflect, in almost the same patterns and similar textures, the colloidal features of the studied vacuum residue and its DOAs.

ESEM icons of vacuum residua and their SFEF fractions

The most useful advantage of ESEM is that not any pretreatment is required for the samples. Thus, it presents true physical structures of samples in a nondestructive manner. However, the ESEM images are not demonstrating the structure details of the bulk phase of samples.

Figure 2 exhibits the ESEM icons of Shengli vacuum residue and its solubility classes. It is obvious that both TEM and SEM can, in combination with appropriate sample preparation procedures, be employed to ascertain and identify the colloidal characteristics of VR and their solubility classes. Therefore it is advisable to select suitable sample preparation techniques and

finer observation tools to compare and contrast the general colloidal features of various VR or their solubility classes. However, it should be reminded that each combination has its own preferable application circumstances. Generally, the FFRTEM technique is the best candidate for studying the physical structures of VR and their solubility classes on the colloidal level while the ESEM technique is preferred when major concerns are about the elemental compositions of the dispersed and dispersing phases. The ultra-microtomy, while useful in exhibiting the colloidal features of VR in combination with common TEM technique, is more appropriate to disclose the pseudo-orderliness of the bulk VR in combination with high resolution TEM technique. Details of the latter two techniques and their usefulness in providing more detailed physical and/or chemical information of the physical structures of VR will be reported later.

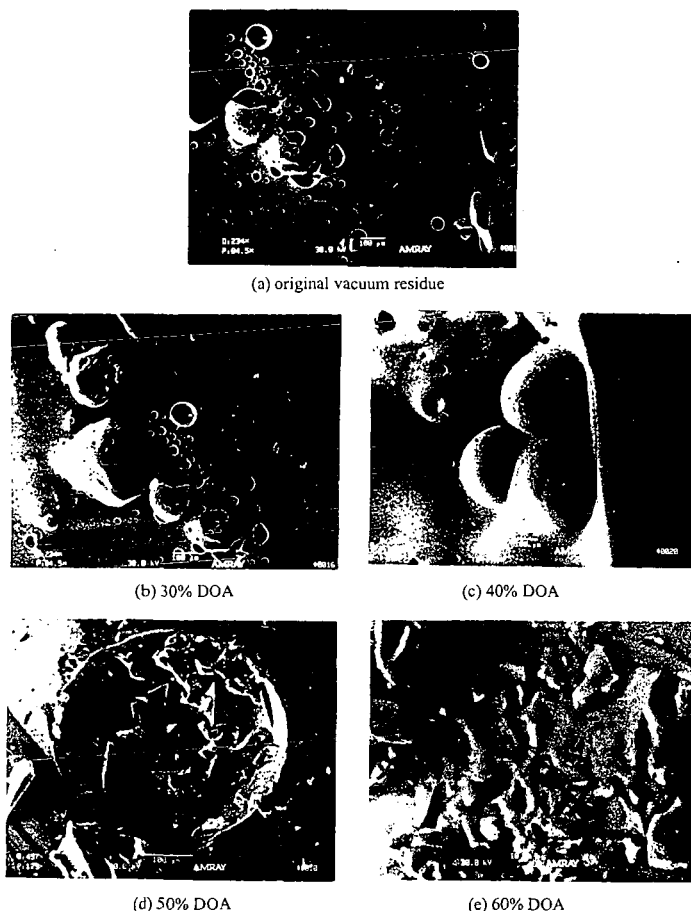


Figure 2 ESEM icons of Shengli vacuum residue and its solubility classes

Characterization of colloidal structures of vacuum residua in terms of SARA compositions

Of all the compositional and structural parameters of VR, their SARA compositions, i.e., saturates, aromatics, resins and asphaltenes, are among the most potential ones capable of characterizing the identity of VR. So it is natural to employ these four pseudo-pure-components of VR to correlate the possible relations which might occur between the general colloidal features of VR and their compositions.

It was confirmed that it was the n-pentane insoluble asphaltenes, which is tantamount to the n-heptane insoluble asphaltenes plus the heavy resins, which construct the micell in the colloidal systems of VR^[5]. Considering the difficulty with which to determine the content of the heavy resins of VR, the content of the total resins is taken, in combination with the content of the asphaltenes (the n-heptane insolubles and toluene solubles), to have an approximate appraisal of the colloidal features of VR and their DOAs, i.e., it is both the asphaltenes and the total resins,

the two kinds of surfactant-like constituents, which are supposed to participate the formation of the micell in the VR. As a matter of fact, since the determination of the SARA compositions of VR has come into the widest use in common petroleum chemistry laboratories, so it is of great significance to employ the SARA compositions of VR to characterize their colloidal structures and general properties. With these in mind, some rough understandings of the relations between the colloidal features of the VR and the quantities of the asphaltenes and/or the resins could be derived by three parameters as defined and specified below.

(1) $W_{Asp} + W_{Re}$: The total amount of asphaltenes and resins is an index which could be used to approximately estimate the quantity of the dispersed phases and their geometrical shapes, as well as their colloidal types. Generally, with the increase of $W_{Asp} + W_{Re}$, more dispersed phases will be formed with their morphologies changing, in the main, from spherical to tabulate, and the bulk structures of the VR and their DOAs transform from sol to sol-gel or gel.

(2) W_{Asp}, W_{Re} : These two independent parameters, in addition to their significance of $W_{Asp} + W_{Re}$, concern the sizes and size distributions of the dispersed phases in VR and their DOAs. Due to the variations in molecular sizes and elemental compositions, the average size of the micell formed by the resins is smaller than that of the micell of the asphaltenes.

(3) W_{Re}/W_{Asp} : The quantity ratio of the resins and the asphaltenes is an indicator for rough evaluation of the aggregation states of the dispersed phases. As the micell of the resins are looser and the micell of the asphaltenes are tighter in terms of the compactness of their molecularly aggregated configurations, so the lower the W_{Re}/W_{Asp} , the tighter the mixed resin-asphaltene micell, which leads to the worse compatibility of these micell with the surrounding dispersing media and less stable colloidal VR and their DOAs.

With the three parameters outlined above, the independent and combinatorial distribution characteristics of the resins and the asphaltenes in the VR and their DOAs are plotted, as shown in Figures 3 through 4. It is obvious that, as the VR and their DOAs become heavier and heavier, both the independent parameter (W_{Re}, W_{Asp}) and the combinatorial parameters ($W_{Re} + W_{Asp}, W_{Re}/W_{Asp}$) vary in rather systematic ways: W_{Re}, W_{Asp} and $W_{Re} + W_{Asp}$ increase and W_{Re}/W_{Asp} decreases as the VR and their DOAs go from lighter to heavier. As the colloidal types and stability of VR and their DOAs are of potential significance in industrial practices, it is instructive to have knowledge of the colloidal types and stability of VR and their DOAs in terms of the independent and combinatorial parameters based on the SARA compositions.

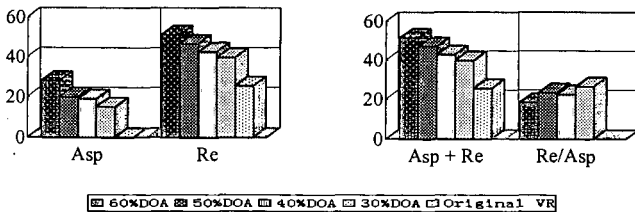


Figure 3 Independent and combinatorial distributions of resins and asphaltenes of Daqing vacuum residue (Data of the asphaltenes in the first graph are plotted in 100 times of their true values, while data of the Re/Asp in the second graph at a tenth of their true values)

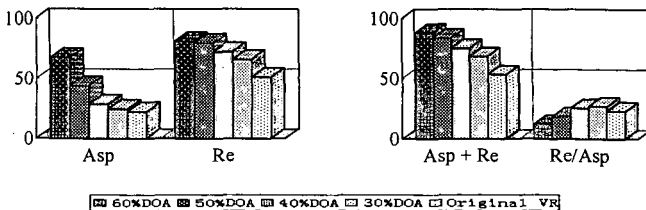


Figure 4 Independent and combinatorial distributions of resins and asphaltenes of Shengli vacuum residue (Data of the asphaltenes in the first graph are plotted in 10 times of their true values)

(1) With the VR and their DOAs becoming heavier, their W_{Re}, W_{Asp} and $W_{Re} + W_{Asp}$ all keep increasing. As both the resins and the asphaltenes are of the characters of surface active molecules, so the average size of the dispersed phases in the VR and their DOAs becomes larger and their quantity becomes more as the VR and their DOAs goes from lighter to heavier. Roughly, for Daqing vacuum residue and its DOAs, the colloidal systems with $W_{Re} + W_{Asp} < 40\%$

are in sol states and the colloidal systems with $W_{Re} + W_{Asp} > 50\%$ are in gel states, while for the colloidal systems with $W_{Re} + W_{Asp}$ going in-between, they are of the sol-gel states. For Shengli vacuum residue and its DOAs, the approximate values of $W_{Re} + W_{Asp}$ corresponding respectively to the sol, sol-gel and gel state are less than 60%, in the range of 60~70% and higher than 70%. The reason why Daqing vacuum residue and its DOAs become the gel states at lower Asp + Re than its Shengli counterparts could be contributed to the fact that, in Daqing vacuum residue and its DOAs, the micell are mainly composed of the resins and the micell of the resins are of loosely aggregated molecular assembles. These simple analyses not only corroborate again that the dispersed phases in the VR consist of both the resins and the asphaltenes species but also suggest that the relevance of the colloidal types of VR to their critical values of $W_{Re} + W_{Asp}$ may be attributed the molecular properties of the resins and the asphaltenes of the specific vacuum residua. It is evident, therefore, that more precise relationship between the colloidal types of VR and such parameters as W_{Re} , W_{Asp} and $W_{Re} + W_{Asp}$ could be well defined if the narrower fractions of VR are employed to conduct their colloidal studies and the heavier resins are quantitated.

It is of industrial implication for the colloidal types of VR to be related to W_{Res} , W_{Asp} and/or $W_{Re} + W_{Asp}$. In the thermal or catalytic conversion of vacuum residua, both W_{Asp} and $W_{Re} + W_{Asp}$ keep increasing; once they reach some critical values, the reaction system comes into the sol-gel state, signifying that the reaction system arrives at the critical state in which the second liquid phase of condensed asphaltenes is about to occur⁴¹. As in the thermal conversion of vacuum residua, the appearance of the second liquid phases is immediately followed by the commencement of coke formation, it is therefore of great industrial significance to predict the induction period of coke formation by the real-time monitoring of the variations of W_{Asp} and $W_{Re} + W_{Asp}$ or by the establishment of their dynamic equations.

(2) With the VR and their DOAs becoming heavier, their $W_{Re} + W_{Asp}$ continues to decrease and accordingly, their colloidal stability keeps decreasing. Since the sol-gel system corresponds to the critical state between stable and unstable colloidal VR, it is estimated from Figures 3 through 4 that the critical W_{Re}/W_{Asp} ratio for keeping stability of colloidal VR is ca. 20~25. Such a fact implies that, for Daqing and Shengli vacuum residue and their DOAs, when the value of W_{Re}/W_{Asp} is lower than 20~25, their colloidal systems are thermodynamically unstable while when the value of W_{Re}/W_{Asp} is greater than 20~25, they remain stable in the sense of thermodynamics.

CONCLUSIONS

(1) With evidences from the FFRTEM, ultra-microtomy TEM and ESEM techniques, it can be well assumed that both Daqing and Shengli vacuum residue as well as their de-oil asphaltenes are all colloidal systems.

(2) Of the three combination techniques for sample preparation and observation, both the FFRTEM and the ultra-microtomy TEM are suitable to study the colloidal structures of VR and their solubility classes in the qualitative way. And just from the viewpoint of the qualitative study of the colloidal structures of VR and their solubility classes, influences from either the freezing in FFRTEM or the solidification in ultra-microtomy TEM could be neglected to some extent.

(3) The colloidal features of VR and their solubility classes could be well characterized by their compositions of the saturates, the aromatics, the resins and the asphaltenes. Particularly, the contents of the resins and the asphaltenes are the two key parameters in the finer characterization of the important colloidal properties of VR, such as the colloidal types of the bulk VR, the morphology and the size and size distribution of the dispersed phases.

ACKNOWLEDGMENTS

The authors are greatly indebted to the financial support of the project by China Postdoctoral Science Fund.

REFERENCES

- [1] S. H. Li, *Physical structures and thermodynamics of petroleum vacuum residua and their applications*. The Postdoctoral Research Report. June 1998.
- [2] S. H. Li, C. G. Liu, G. H. Que et al. *Fuel*, 1996, 75(8):1025-1029
- [3] S. H. Li, W. J. Liang, Y. J. Zhu: *Oil and Gas Processing*, 1994, 4(1):1-9
- [4] S. H. Li, C. G. Liu, G. H. Que et al. *Preprints, Div. Petro. Chem., ACS*, 1995, 40(3):736

PRELIMINARY RESULTS ON THE MOLECULAR STRUCTURES OF THE ATHABASCA AND COLD LAKE ASPHALTENES

Jonathan P. Mathews^a, Semih Eser^a, and Parviz-Rahimi^a*

^a The Energy Institute, College of Earth and Mineral Sciences, The Pennsylvania State University, University Park, PA 16802

* National Center for Upgrading Technology, Suite A202, 1 Oil Patch Drive, Devon, Alberta, Canada, T9G 1A8

Keywords: Asphaltene structure, high-resolution mass spectroscopy

INTRODUCTION

Asphaltene research has recently undergone a significant revitalization to facilitate utilization of heavier crude oils and to develop the massive oil sand reserves in Canada. The average chemical properties of natural asphaltenes tend to fall in a narrow range despite wide variations in their chemical behavior. In other words, the average bulk parameters of asphaltenes do not necessarily provide useful information for upgrading and behavioral studies. The final objective of this study is to generate molecular models for asphaltenes from two different sources, Cold Lake and Athabasca, to understand the differences in their molecular composition. These two asphaltenes give similar average structural parameters, yet behave quite differently (carbonization yields). Analysis by high-resolution laser pyrolysis indicated a distribution of molecular masses (100 to 1,500 AMU). Elemental compositions of these peaks will provide the input for molecular models without the need for extensive "averaging" of bulk parameters, thus, better indicating some of the structural diversity within the asphaltenes.

EXPERIMENTAL

Pentane asphaltenes from Athabasca and Cold Lake bitumens were prepared using 40:1 solvent to sample ratios. Briefly, 10 g bitumen was placed in a flask and 400 mL of n-pentane was added. The flask was placed in an ultrasonic bath for 45 min and left to settle overnight at room temperature. The mixture was then placed in an ultrasonic bath again for 30 min and the asphaltenes were filtered using a medium porosity (10-15 μ m) fritted glass disk. The solid asphaltenes were rinsed with excess pentane until the washing was clear. To ensure that asphaltenes were free from residual maltenes, the collected asphaltenes were mixed with 50 mL of n-pentane, sonicated and filtered as before. Asphaltenes were then dried under vacuum at 45°C for 3 h.

Elemental analysis including C, H, S and N contents were determined using Perkin Elmer 2400 and O was determined using Carlo Erba 1104. Molecular weights of asphaltenes were determined in o-dichlorobenzene at 120°C using VPO.

Coking potential was obtained using a modified Conradson carbon residue test(1) utilizing a TGA instead of the prescribed glass sample vial. The results are not directly comparable to the Conradson method, as secondary cracking and mass transfer will significantly differ and hence underestimate the coke yield potential. Briefly 5 ± 0.5 mg of sample was heated from 30 °C to 400 °C at 15 °C/min under nitrogen. The temperature has held constant for 90 minutes. The weight remaining was attributed to coke and ash. Ash was determined by heating the sample to 600 °C and changing the atmosphere to air, the remaining mass after 10 minutes was attributed to ash.

Mass spectra were acquired on a PerSeptive Biosystems Voyager-DE STR mass spectrometer using 337 nm light from a pulsed nitrogen laser for ionization. High-resolution results were obtained using reflector mode. Samples were prepared by dissolving approximately 50 micrograms of material in 500 ml of THF. Aliquots of 0.5 ml were deposited on the gold-plated target, and the solvent allowed to evaporate under ambient laboratory conditions. Samples were introduced into the mass spectrometer and analyzed as soon as possible to minimize evaporation of more volatile components. Ionization was conducted using laser setting slightly above the threshold for ionization. A total of 256 laser shots acquired over numerous sites within each sample were averaged. Calculated elemental analysis for mass spectral fragments were calculated using the non-weighted averages of 10 major peaks spanning 100 AMU's.

RESULTS AND DISCUSSION

Unfortunately, asphaltene structural research is hampered by the use of the term "asphaltene" to describe such diverse structural entities as naturally occurring asphaltenes (from coal, crude and oil sands), C₅, C₆ and C₇ "cuts" and products from the refining process where the processing conditions are likely to produce larger aromatic "raft" structures. Utilizing high-resolution mass spectroscopy it is possible to determine the elemental composition of the pyrogram peaks. Utilizing this methodology to generate possible fragments allows us to have more realistic components from which construction of models than from "average structures" which do not demonstrate the structural diversity within the asphaltene. This may be important if only certain structures or certain sizes of structures are responsible for the negative (or positive) aspects of the asphaltene.

Based on the elemental analysis and vapor pressure osmometry the average molecular structure should contain C₇₇H₉₆N₁S_{2.6}O₁ (VPO mw = 1,020 AMU) and C₁₇₆H₂₁₅N_{6.5}O_{6.5} (VPO mw = 2,468 AMU) for Cold Lake and Athabasca C₇-asphaltenes, respectively. This is comparable with previous work for the Athabasca asphaltene (mw 2,618(2), and 2,750(3)), and for the Cold Lake asphaltene (mw 2,030(3)). However, there is poor agreement between average molecular weights determined by different techniques: laser desorption mass spectroscopy and by VPO(4). The

indication being that either VPO measurements yield molecular weights of strongly bound associations of smaller asphaltene structures or that laser desorption mass spectroscopy fragments larger structures, or does not analyze large structures. The average molecular weights reported here are consistent with the range found by electron impact high-resolution mass spectroscopy of a Mayan (vacuum resid) asphaltene(4). However, the mass spectra technique is known to underestimate the molecular weight, the issue of contention is, by how much? Identification of small multi ring systems is consistent with the general average structural interpretation away from very large aromatic "rafts" structures to smaller sized entities(5). A range of molecular weights and their relative abundance are shown in Table 1. Both asphaltenes are similar in their maximum abundance's in the 300-600 AMU range (74 and 77% of the relative abundance for Cold Lake and Athabasca, respectively). Cold lake has a contribution in the larger mass range (>1,000 AMU) in comparison to the Athabasca asphaltene. The Cold Lake asphaltene has slightly more low-molecular weight material also in comparison to the Athabasca sample.

Previously, identification of electron ionized fragments of an asphaltene was reported to be in good agreement with the traditional elemental analysis, with the aromaticity being slightly underestimated(4) which significantly aids the validity of this type of approach. However, in that study over 90 % of the material was volatilized, while laser desorption in this study volatilized only a small fraction of the asphaltene. Here, only 100 or so of the major peaks have been examined. Furthermore, some calculated elemental assignments were equally valid so there was certain operator bias. The calculated atomic H/C ratios for the Cold Lake sample are shown in Table 1. The weighted atomic H/C ratio of 1.2 is in agreement with the bulk elemental for Cold Lake asphaltene. However, the calculated elemental composition over reports the heteroatom content for sulfur, nitrogen and oxygen (normalized to 100 carbon atoms bulk analysis is $C_{100}H_{120}N_3S_4O_2$ while the calculated weighted elemental composition is $C_{100}H_{116}N_3S_5O_3$). Additional calibration standards in the laser high-resolution mass spectroscopy might aid in closing this discrepancy.

Size-exclusion chromatography of Athabasca bitumen produced size fractions with essentially the same atomic H/C ratios of 1.4 over a molecular weight range of 900 to 3,000 AMU, (as measured by VPO(6)). A similar trend is seen over the much smaller mass range examined here for the Cold Lake asphaltene. This implies that the higher molecular weight structures are not undergoing circular ring condensation, as it would result in a significant reduction in the H/C ratios. Rather, it seems likely that higher molecular weight structures comprise of lower molecular weight structures linked together via sulfur, oxygen, and aliphatic chains(7) or directly via aryl-aryl bonds. Hence the approach of Murgich et al(8) of stinging small structures together without ring growth to produce an interconnected "island structure" seems reasonable. However, selection of these "binding structures" will have a significant influence on the structural model and their "behavior" and "coke formation" potential. It is the ultimate aim of structural modeling not only to present the structural features that are present in the asphaltene, essential the representation of chemical structure, but also the physical structure and provide a rational explanation of processing behavior occurring during cracking or hydrocracking. For example the Athabasca asphaltene sulfur linkages might be more important "binding structures" than in Cold Lake asphaltene which has a higher coke yield (55.4 in comparison to 47% (daf) for Athabasca). However, many other structural features such as differences in molecular weight distributions or differences in the fine chemical structure are also likely contributors. The current state of knowledge regarding Athabasca structural features is eloquently presented in the literature(7). Aromaticity results have been reported in the literature and are the same for both samples (0.49) for the C_7 -extracted asphaltene(3). The for the same sample the aliphatic hydrogen to carbon ratios were also in close agreement 2.16 and 2.10 for the Athabasca and Cold Lake asphaltenes, respectively(3). Hence, average parameters although useful in comparing materials do not necessarily provide insight into the behavior of the material. Molecular models produced should bare this in mind and should aim to produce chemically, physically accurate models with appropriate "reactivity" to processing.

CONCLUSIONS

Laser desorption high-resolution mass spectroscopy yielded information regarding the distribution of molecular mass in the range 100 to 1,500 AMU's for Cold Lake and Athabasca asphaltenes. Despite being close in bulk chemical composition (elemental analysis, carbon aromaticity) the asphaltenes differ in coking potential (as determined by thermogravimetric analysis). There are slight differences in the molecular weight distribution between the asphaltene samples. Cold lake has higher molecular weight material in the region of 1,000 to 1,500 amu in comparison to the Athabasca asphaltene, which has no significant contribution for molecular weights greater than 1,000 amu (in the analytical window of this technique). Weighted average molecular weights are 523 and 463 for the Cold Lake and Athabasca asphaltenes, respectively. This shows the opposite trend from vapor pressure osmometry, which yielded average molecular weights of 1,020 and 2,468 for the Cold Lake and Athabasca asphaltenes, respectively. Elemental analysis of carbon and hydrogen for Cold Lake was in reasonable agreement with calculated elemental analysis from high-resolution mass spectroscopy, however, other heteroatoms (S, O and N) were overestimated.

ACKNOWLEDGEMENTS

Thanks to A. Daniel Jones (Director, Penn State Intercollegiate Center for Mass Spectrometry) for running the laser desorption mass spectroscopy system and assistance in its interpretation.

REFERENCES

1. ASTM, Designation: D 4530-93, Standard test methods for determination of carbon residue (micro method), in Annual book of ASTM standards, Section 5, Petroleum products, lubricants and fossil fuels, 1998, 919.
2. Kotlyar, L. S., Ripmeester, J. A., Sparks, B. D. and Woods, J., *Fuel*, 1988, **67**, (11), 1529.
3. Suzuki, T., Itoh, M., Takegami, Y. and Watanabe, Y., *Fuel*, 1982, **61**, (5), 402.
4. Hunt, J. E. and Winans, R. E., *Am. Chem. Soc., Div. Fuel Chem. Prepr.*, 1997, **42**, (2), 427.
5. Artok, L., Su, Y., Hirose, Y., Hosokawa, M., Murata, S. and Nomura, M., *Energy & Fuels*, 1999, **13**, (2), 287.
6. Domin, M., Herod, A., Kandiyoti, R., Larsen, J. W., Lazaro, M. -J., Li, S. and Rahimi, P., *Energy & Fuels*, 1999, As soon as publishable web release, ef980065b, http://pubs.acs.org/subscribe/journals/enfuem/browse_asap.html.
7. Strausz, O. P., Mojelsky, T. W., Faraji, F., Lown, E. M. and Peng, P., *Energy & Fuels*, 1999, **13**, (2), 207.
8. Murgich, J., Abanero, J. A. and Strausz, O. P., *Energy & Fuels*, 1999, **13**, (2), 278.

Table 1. Molecular Ion Distribution and Average H/C ratio as Determined from High-Resolution Laser Desorption

M/z Range	Cold Lake %	Cold Lake H/C ratio*	Athabasca %
100-199	2		0
200-299	4	0.9	1
300-399	27	1.0	27
400-499	29	1.3	31
500-599	18	1.3	19
600-699	8	1.3	11
700-799	4	1.3	6
800-899	3		3
900-999	2		2
1,000-1,099	1		0
1,100-1,199	1		0
1,200-1,299	1		0
1,300-1,399	1		0
1,400-1,499	1		0
1,500-1,599	0		0
Average mw	523	Weighted H/C= 1.2	463

*Analysis of at least 10 major fragments in each average H/C calculation

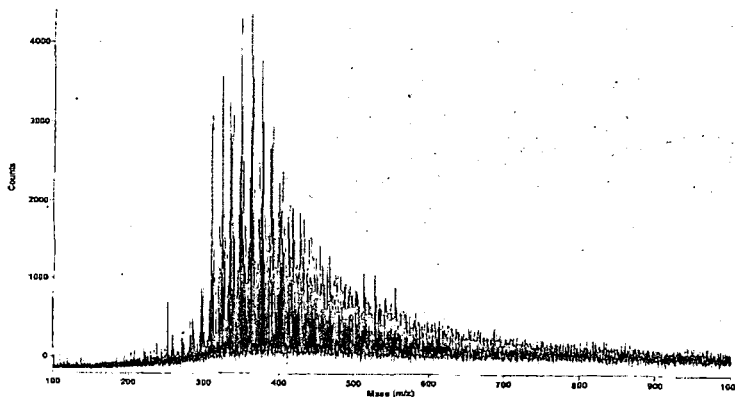


Figure 1. Laser Pyrolysis, High Resolution Mass Spectra Pyrogram of Athabasca Asphaltene

STRUCTURAL ANALYSES OF PETROLEUM ASPHALTENES AND RESINS AFTER HDM AND SUBSEQUENT HDS TREATMENTS

H. Seki and F. Kumata

Advanced Catalysts Research Laboratory, Petroleum Energy Center,
KSP D12F-1237, 3-2-1 Sakado, Takatsu-ku, Kawasaki, Kanagawa, 213-0012 Japan

Introduction

In our laboratory, we are developing a new two-stage process for upgrading petroleum residues, which consists of a slurry phase in the first stage and a fixed bed in the second stage. In this new process, the catalyst life in the second stage is one of the keys and its elongation is an important subject. Thus far we have been investigating the effects of operation conditions in the first stage on the fouling at the middle of run for the catalysts in the second stage, using a quasi two-stage process, *i.e.*, hydrodemetallization (HDM) and hydrodesulfurization (HDS) [1]. Consequently, we found followings: (i) a minimum fouling rate of the HDS catalysts existed around 400 °C of HDM temperature, (ii) the HDS catalysts were deactivated predominantly by coke rather than metals under the present conditions and (iii) effect of substances soluble in light gas oil (soft coke) on HDS catalyst deactivation could not be negligible under certain HDM reaction conditions.

In order to further understand the coke deactivation and to obtain a certain index which reflects coke deactivation, characterization of asphaltenes was performed since asphaltenes are likely to form coke and cause catalyst deactivation in resid hydrotreatings [2-4].

In this study, structural changes of asphaltenes after HDM and HDS treatments were examined, especially paying an attention to the change of polycondensed aromatic skeletons. In addition, resins were also characterized because some parts of resins might act as the soft-coke. We report the results of above characterization.

Experimental

Both HDM ($\text{Mo}/\text{Al}_2\text{O}_3$) and HDS ($\text{NiCoMo}/\text{Al}_2\text{O}_3$) catalysts were commercially available and supplied from a Japanese catalyst company. HDM treatments were carried out with a fixed-bed reactor using Kuwait atmospheric residue (KW-AR; S = 4.45 wt%, Ni/V = 20/61 ppm) as a feed under the following conditions; temperature 370 - 430 °C, pressure 14 MPa, LHSV 0.5 h⁻¹, H₂/Oil 2000 scfb. HDS treatments were subsequently conducted using the HDM product oils as feeds; temperature 390 °C, pressure 8 MPa, LHSV 0.5 h⁻¹, H₂/Oil 5000 scfb.

Asphaltenes were isolated from the HDM and HDS product oils as *n*-heptane-insoluble and toluene-soluble substances. Resins were separated from maltene by column chromatography.

LD-MS measurements were performed with Thermoquest Co., Ltd. Vision 2000 Spectrometer using angiotensin as a calibration standard. The details on the measurement were described elsewhere [5]. From the LD-MS measurement, we can obtain a molecular weight distribution as well as an average molecular weight (*M_n*). ¹H and ¹³C-NMR spectra (TMS base) were recorded on a JEOL JNM-

LA400 in a gated proton decoupled mode. Chromium acetylacetonate was added to obtain quantitative ^{13}C -NMR spectra. The assignments of chemical shift range for ^1H and ^{13}C -NMR spectra were made according to the literature [6-9].

The structural parameters listed in Table 1 for asphaltenes and resins were obtained with the data from ^1H and ^{13}C -NMR, LD-MS and elemental analyses, referring to the method by other workers [7-9]; In brief, *Cs*, *CCH3*, *Cn-ar* and *Coher* were directly obtained from ^{13}C -NMR, and *Cus* from ^1H -NMR with the combination of elemental analyses data. Then, *Cint*, *Cout*, *Csub*, *Ra* and *n* were calculated using above parameters.

Results and Discussion

1. Structural change of asphaltenes and resins after HDM treatment

Figure 1 shows the LD-MS spectra of asphaltenes after the HDM treatment with different temperature. A significant difference was observed in the molecular weight distribution; the shape of the broad band tailing to 5800 m/z was almost the same below 400 $^{\circ}\text{C}$, while it became polydispersed above 400 $^{\circ}\text{C}$. Especially, two peaks at 600 and 1100 m/z are clearly seen when HDM temperature is 430 $^{\circ}\text{C}$. On the other hand, the molecular weight distribution of resins became narrow as the HDM temperature increased. The *Mn* for asphaltenes and resins monotonously decreased with HDM temperature.

Variation of structural parameters for asphaltenes and resins with HDM temperature was described in Figure 2. The aromaticity (*fa*) of asphaltenes and resins changed with HDM temperature in a similar manner; the *fa* was almost unchanged up to 400 $^{\circ}\text{C}$ and steeply increased above 400 $^{\circ}\text{C}$. For asphaltenes, the *Csub* began to decrease around 400 $^{\circ}\text{C}$ while the *Ra* and *n* remained. For resins, on the other hand, the *n* decreased with HDM temperature without remarkable changes in *Ra* and *Csub*. These observations lead to the conclusion that the steep increase of *fa* for asphaltenes and resins is due to the decrease of the number of alkyl side chains and to the shortening of them, respectively. Variations of internal quarternary aromatic carbon (*Cint*) and outernal one (*Cout*) give us useful information on the aromatic skeleton. For asphaltenes, an increase of *Cint* from 10 to 17 and a decrease of *Cout* from 21 to 17 were observed with an increase of HDM temperature up to 410 $^{\circ}\text{C}$, indicating the structural change of the aromatic skeleton from cata- to peri-type. It might be because of the difference in the reactivities of cata- and peri-type polycondensed aromatics that this structural change appeared.

2. Structural change of asphaltenes and resins after HDS treatment

In our previous study, an increase in the fouling rate of HDS catalysts was observed when HDM temperature was raised from 390 to 400 $^{\circ}\text{C}$. It is, therefore, of interest to examine the structural changes of asphaltenes and resins by the HDS treatment. Variations of *fa* and *Ra* before (B) and after (A) the HDS treatment were shown in Figure 3. In this figure, the symbols, *As* and *Re*, indicate asphaltenes and resins, respectively, and the number is an HDM temperature. By the HDS treatment, the aromatic ring number (*Ra*) for asphaltenes increased while that for resins slightly decreased. This indicates that condensation reactions are more likely to occur for asphaltenes than resins during HDS treatments. Although significant difference by the HDM temperature was unfortunately not detected in the structural parameters, the LD-MS measurements for asphaltenes showed the clear difference: when the HDM temperature was 390 $^{\circ}\text{C}$, the *Mn* and molecular weight distribution were almost unchanged while 410 $^{\circ}\text{C}$, the *Mn* increased by HDS treatment and heavy fractions which were not detected before

the HDS treatment were observed, indicating that condensation reactions took place. Such condensation reactions of asphaltenes could cause the coke deactivation of HDS catalysts.

Conclusions

Heavy fractions (asphaltenes and resins) after HDM and HDS treatments were characterized to understand the deactivation of HDS catalysts. It was found that the increase of aromaticity (f_a) for both asphaltenes and resins by HDM treatment was attributed to the loss of alkyl chains and that polycondensed aromatic skeleton of asphaltenes changed toward peri-type. We confirmed that the asphaltenes tended to polycondense during the HDS treatments if the HDM temperature was over 400 °C.

Acknowledgements

This work has been carried out as a research project of Petroleum Energy Center with subsidy of the Ministry of International Trade and Industry. The authors are grateful to Drs. H. Iki and K. Hayasaka of Nippon Mitsubishi Oil Co. Ltd. for their kind help in NMR measurements.

References

1. H. Seki and F. Kumata, submitted to *Studies in surface science and catalysis* (The 8th International Symposium Catalyst Deactivation at Brugge)
2. D. S. Thakur and M. G. Thomas, *Apply. Catalysis*, **15**, 197 (1985)
3. P. E. Savage, M. T. Klein and S. G. Kukes, *Energy Fuels*, **2**, 619 (1988)
4. V. Calemma, P. Iwanski, M. Nali, R. Scotti and L. Montanari, *Energy Fuels*, **9**, 225 (1995)
5. M. Fujii, Y. Sanada, T. Yoneda and M. Sato, *Prepr. ACS Div. Fuel Chem.* **43**, 735 (1998)
6. A. Fonseca, P. Zeuthen and J. B. Nagy, *Fuel*, **75**, 1413 (1996)
7. S. Gillet, P. Rubini, J.-J. Delpuech, J.-C. Escalier and P. Valentin, *Fuel*, **60**, 221 (1981)
8. E. M. Dickinson, *Fuel*, **59**, 290 (1980)
9. M. F. Ali and M. Saleem, *Arab. J. Sci. Eng.*, **19**, 319 (1994)

Table 1. Structural parameters of average molecules for asphaltenes and resins.

Symbol	Definitions	Symbol	Definition
Car	aromatic carbons	Co _{ther}	carbons attached to oxygen
Cal	aliphatic carbons	C _{int}	internal quaternary aromatic carbons
C _{us}	unsubstituted aromatic carbons	C _{out}	external quaternary aromatic carbons
C _s	alkyl-substituted (methyl group excluded) aromatic carbons	C _{sub}	alkyl-substituted aromatic carbons
CCH ₃	methyl-substituted aromatic carbons	fa	aromaticity
C _{n-ar}	carbons at the junction of aromatic and naphthenic ring	R _a	aromatic ring number
		n	average length of alkyl side chain

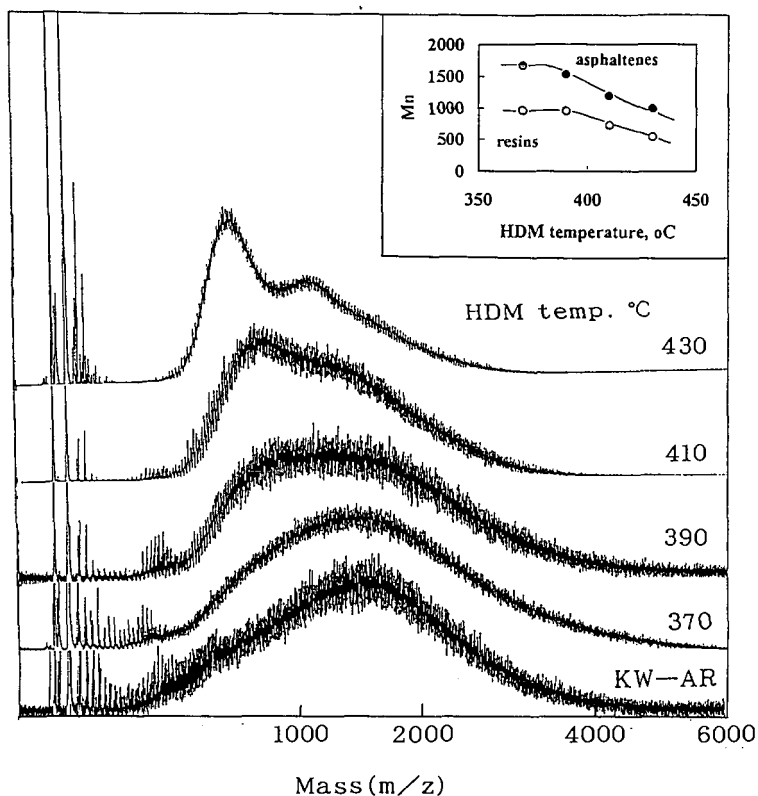


Figure 1. LD-MS spectra of asphaltenes after HDM treatments and average molecular weights of asphaltenes and resins.

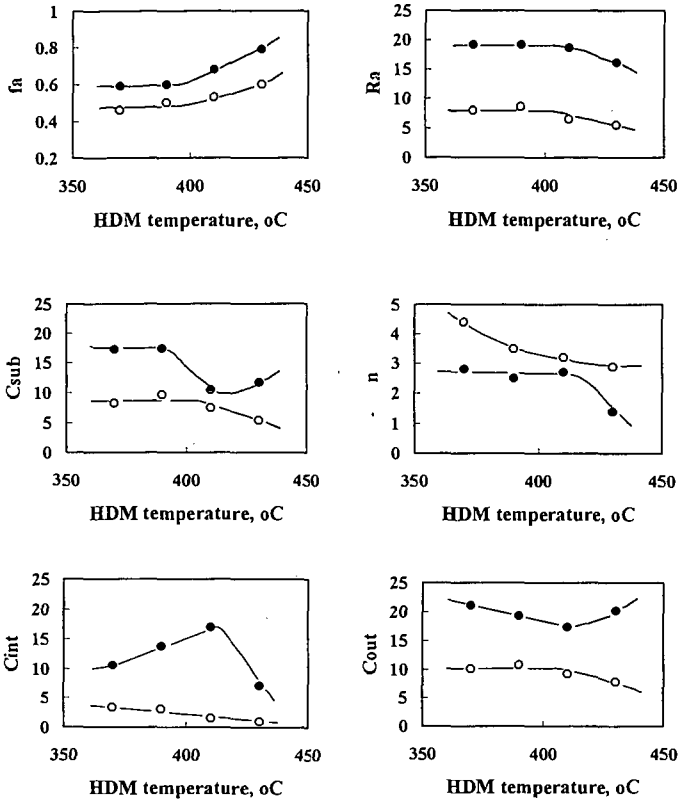


Figure 2. Structural parameters of asphaltenes and resins after HDM treatments; ● asphaltenes, ○ resins.

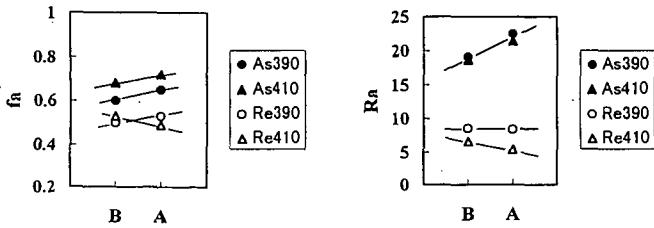


Figure 3. Structural parameters of asphaltenes and resins before (B) and after (A) HDS treatments

STRUCTURAL INSIGHTS TO HEAVY RESID AND COAL FOR DESIGNING UP-GRADING

Isao Mochida

Institute of Advanced Material Study, Kyushu University
Kasuga, Fukuoka 816-8580, Japan

Keywords: Molecular assemble, XRD, hydrotreatment

Objectives and Approaching of Resid Up-grading

Increasing demand for transportation fuel of higher performance and less environmental load and increasing dependence on heavy crude, resid, and coal require the development of more efficient up-grading technology in coming future. Several processes have been practiced for up-grading, which consists of depolymerization, aromatic hydrogenation and ring opening, metal and heteroatoms removals. The degrees of reaction severity varied the yield and quality of the product, charging the responsible cost. Such reactions are derived thermally and catalytically according to the severity of design and cost/performance balances.

Thermal up-grading is usually cheap in facility and running cost, but suffers the limited conversion, and selectivity to wanted products, insufficient quality of product and unwanted coke. Some coke can be designed to be the product of high quality such as those for blast furnace and electrode. Handling of solid coke is often energy-loss, dirty and tedious.

Catalytic process can drive the reactions as wanted, although the deactivation contaminants, and poisoning of the catalyst limit the advantage of the process, increasing the catalyst cost. Sometime cheap catalyst is obliged to use because of limited turn-over number and use of repetition. Combination of thermal and catalytic processes has been designed to optimize their advantages.

The design of up-grading is to define the reactions needed to convert the resid to transportation fuel, the best catalysts for the respective reactions, their optimum use and recovery for their repeated use. Hence the chemistry on the structural changes of organic substrates, catalyst surface, and active species should be described in details as much as possible.

Structural Images of Resid, especially Significance and Liberation of Molecular Assembles

Resid has been described as polyaromatic, polynuclear polymers. The aromatic rings are connected directly (aryl-aryl linkage) or through methylene bridges to form polynuclear chains, carrying heteroatoms within the ring and alkyl substituent on the rings as imaged from the structure of depolymerized units. The alkyl chains in the substituents are basically normal and very long up to 30-40 carbons. The hetero-cyclics such as pyrrole, pyridine, and thiophenes carry heavy metals such as vanadium and nickel as observed in porphyrins.

The primary polyaromatic polynuclear chains form three dimensional network through the non-covalent as well as covalent linkages. The non-covalent bonds link the chains through alkyl chain entanglement, π - π stacking of aromatic rings, acid-base or hydrogen bonding, coordinative bridge of the metal cations, and charge transfers among the heterocyclic rings. Such intermolecular assemble sometime forms micelle, influencing strongly the solubility in the matrix of smaller partners and reaction solvent and reactivity through governing the contact of the

reactive sites with the reagent as well as active site on the catalyst, and favoring the intermolecular condensation.

The asphaltene in the resid which is defined by the solubility in hexane and benzene is a target of up-grading. Its coking/fouling reactivity, inertness for depolymerization and tendency for phase separation and precipitation are ascribed to the structure of its chains and their intermolecular assembles. Liberation of molecular assemble by breaking intermolecular linkage through solvation, ring hydrogenation, removal of bridging cations and heterogroups. Such liberation enhances solubility and the reactivity for depolymerization, reducing the coking reactivity and irreversible adsorption.

Detection of Molecular Assemble

Molecular assemble in resids and coals has been accessed by XRD, NMR and ESR through diffraction of aromatic stacking, different relaxation and rotational narrowing of metal porphyrins, respectively. XRD of slow step scan provides two broad diffraction peaks at 20° (γ -band) and 26° (π -band), receptively, which are believed to reflect alkyl entanglement and π -stacking. Figure 1 illustrates XRD profiles of a vacuum residue and its fractions. The intensity of π -band increases in the order of saturate, aromatic, polar, and asphaltene fractions, indicating increasing significance of π - π stacking. In addition to two broad bands, very sharp peaks are observable at 22° and 24° , which are attributable to n-paraffin's crystals.

Liberation of Molecular Assemble

High temperature and solvents moderate both stacking. Higher temperature reduced the π -stacking and shifted γ -band to the lower angle. Figures 2 and 3 show XRD of VR in toluene and swollen Beulah-Zap coal by DMF and THF. Both bands of VR were weakened according to the amount of solvent although the γ -band reduced its intensity more rapidly. In contrast, solvent swelling of coal appears to moderate the π -stacking more selectivity.

Removal of cationic bridges in coal liberates the aliphatic entanglement in the coal producing weaker hydrogen bond.

Extraction and Adsorption of Asphaltene

Asphaltene in the VR is the target of conversion while it is a troublemaker in the catalytic conversion. Hence its removal prior to the up-grading of heavy resid is an approach to avoid the trouble. Asphaltene can be selectivity extracted by liquid propane under supercritical conditions.

Some carbon materials adsorb asphaltene rather selectively. Their pore must be larger than 10A. Carbon blacks of nanoparticulate adsorb selectively the asphaltene at a high capacity. Selective and deep removal of metals in VR is most wanted since the demetalation is the first step in a series of hydrotreatment stages, where the capacity of demetalation agent and its completeness govern efficiency of the process.

Inflence of Hydrotreatment on Molecular Assemble

Hydrotreatment produces distillate and more saturate, converting the polar and asphaltene fractions. Aromatic rings are hydrogreated and polymer chains are broken down by such treatment. Hydrogenation reduces intensities of both γ and π bands.

Configuration and Catalyst for Hydrotreatment of Resid and Coal

Hydrotreatment consists of metal removal, hydrogenation, hydrocracking, hydrodesulfurization and hydrodenitrogenation. Hydrogenation is believed to moderate the coking and sludge formation and enhances the reactivity for cracking. Since the hydrogenation favors thermodynamically the lower temperature, while the cracking does higher temperature. The active catalyst is preferably used at a separate step of lower temperature for the pretreating hydrogenation.

Aromatic and hydrogen donor solvents often help the hydrotreatment by dissolving heavier components and suppressing on retrogressive reactions. Dry sludge produced in the hydrocracking is successfully suppressed by the two stage hydrocracking and added solvent to achieve a high distillation yield.

Catalysts of fine particles are appreciated in the moving bed hydrotreating. Recovering and repeated use as well as penetration into micelle or coal grain are concerned. Carbon black of nano-particles is a candidate support to solve the problems. NiNo/carbon black has been reported to give the very high activity for coal liquefaction NiFe/carbon black shows comparable activity, although its activity for ring hydrogenation is limited, requiring donor solvent in the liquefaction.

Unfortunately such catalysts adsorbs strongly the asphaltene to be insoluble during the hydrotreatment. Some modification of the support is necessary to reduce its surface polarity for limited adsorption, maintaining the dispersion form against sulfide active species.

Molecular Identification of Gas Oil and Vacuum Gas Oil for Desulfurization and Denitrogenation

Gas chromatograph equipped with atomic emission detector can separately identify hydrocarbons, sulfur, nitrogen, oxygen and even metal containing species. Molecular separation by a suitable column and every identification are now in progress. Nevertheless the reactivity of the respective species inhibiting and deactivation factors of partner species are measured very easily. Figure 4 illustrates typical chromatographs of hydrocarbons, sulfur, nitrogen and oxygen species in the coal derived gas oil. Analyses before and after the hydrotreatment tell us their reactivity. Some intermediate products are also identified to establish the reaction scheme in the presence of competitors and inhibitors in the same oil.

The desulfurization schemes of its most refractory 4,6-dimethyldibenzothiophene have been proposed as shown in Figure 5. Based on the scheme, natures of the active site and inhibitors are identified and better catalyst and reaction configuration can be designed. Denitrogenation of nitrogen species in the gas oil is studied by the same approach.

Another significance of the molecular identification is that the products in the hydrotreated resid suggest us the unit molecular structure of the building blocks of the polymeric substances.

Aromatic Ring Opening

Heavy feed and coal tend to yield highly aromatic products. Aromatic rings are hopefully opened into alkylnaphthenes for clean and efficient combustion. Selective hydrogenation of aromatic ring by noble metal catalyst and selective C-C bond fission by adequate zeolite catalyst appear most promising. Pore, crystal sizes, and crystallinity of the wall and zeolite content in the synthesis are necessary to be improved.

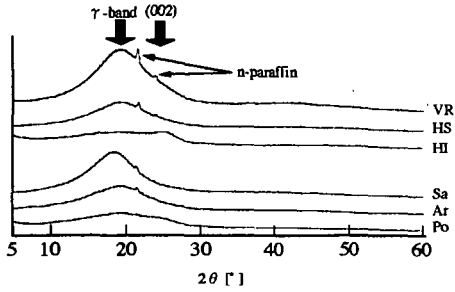


Figure 1 XRD of AM-VR fractions (Step Scan 4 sec. / 0.01°)

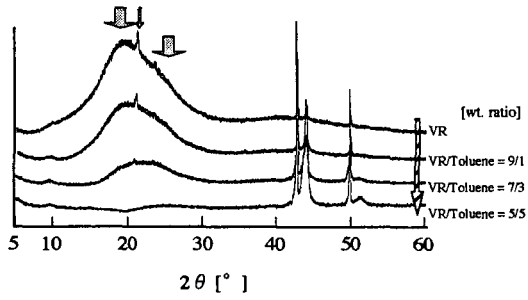


Figure 2 XRD of VR in toluene (Step Scan 4 sec. / 0.01°)

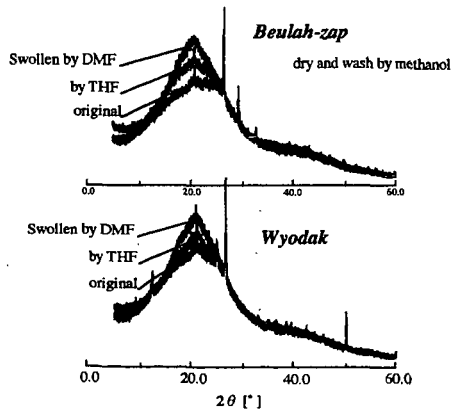


Figure 3 XRD of Swollen coals with DMF and THF (Step Scan 3 sec. / 0.01°)

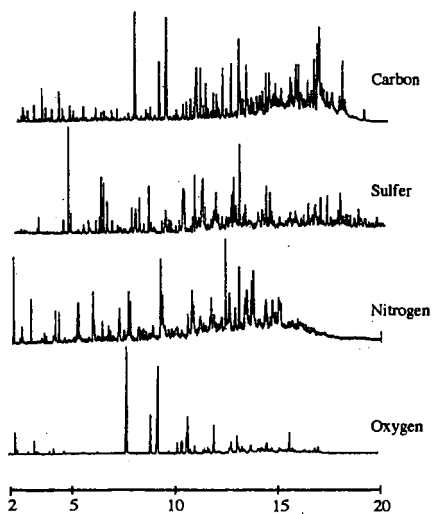


Figure 4 GC-AED chromatograms of C, S, N, O species in South Banko Coal Liquids

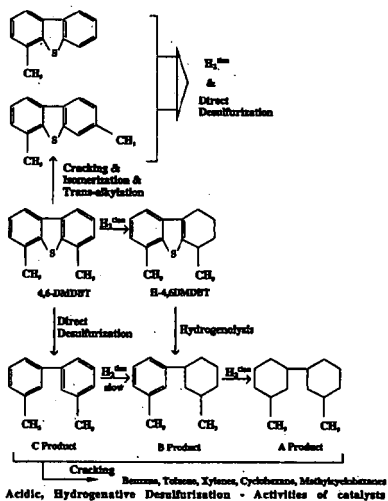


Figure 5 Hydrodesulfurization Reaction Schemes for 4,6-Dimethyldibenzothiophene

SEPARABILITY OF COLD LAKE BITUMEN AND ARABIAN HEAVY VACUUM RESID

Irwin A. Wiehe*
Soluble Solutions
3 Louise Lane
Gladstone, NJ 07934

KEYWORDS: heavy oil, separability, molecular limits

INTRODUCTION

While refinery separation of heavy oil is usually restricted to distillation, fluid catalytic cracking (FCC) feed is not required to be volatile, only containing acceptable levels of catalyst poisons: Conradson carbon residue, vanadium, nickel, and basic nitrogen. One method for achieving this objective is to physically separate the higher quality fraction. Therefore, the laboratory separation of Cold Lake bitumen and Arabian Heavy vacuum resid was done to determine the potential for a more molecularly selective separation. The combination of distillation, deasphalting, and adsorption was used to determine the ultimate separation that is possible in order to approximate the molecular limits, or the molecular separability.

The feed specifications for fluid catalytic cracking of resid containing oils depend greatly on the design and practice of the FCC unit, on the catalyst, and on other feeds available for blending. Nevertheless, the typical guidelines of Barnes (1), shown in Table 1 will be used. Of these, Conradson carbon residue, vanadium content, and nickel content are often the most critical and will be emphasized.

Table 1
Feed Specifications for Resid FCC (1)

<u>Feed Property</u>	<u>Limit</u>
Conradson Carbon Residue	3 - 8 wt%
Vanadium Content	10 - 15 ppm
Nickel Content	20 - 25 ppm
Sodium Content	5 - 10 ppm
Basic Nitrogen	800 ppm
Sulfur Content	3 wt%
Maximum Density	0.940 g/cc
Minimum Hydrogen	11.5 wt%

EXPERIMENTAL

The general procedure used for separating heavy oils as shown in Figure 1 is a variation of that published previously (2). The first possible step was batch distillation at 1.4 mm Hg that was done directly out of tubing bombs immersed in a sand bath at 315° C. The second and third steps were repeated using several solvents but the same solvent for each step for a given trial. The second step removed the solvent insolubles by mixing 25 parts solvent to one part oil, waiting eight hours, and filtering. In the third step Attapulugus clay was mixed with the oil dissolved in the solvent and let sit for eight hours. This mixture was filtered with a fine glass frit and washed with additional solvent until the solvent passed through clear of any color. The heavy oil dissolved in the solvent was recovered by rotary evaporation and vacuum drying. The fraction remaining on the clay was recovered by washing on the glass frit with a mixture containing 50% acetone and 50% toluene followed with 10% methanol and 90% toluene. Finally, the adsorbed fraction of heavy oil was recovered from the solvents by rotary evaporation and vacuum drying. The solvents used in the separation trials included n-pentane, n-heptane, cyclohexane, toluene, and carbon disulfide. Once collected, analytical data were measured on each of these fractions.

RESULTS AND DISCUSSION

Separation of Heavy Oils

For the separation of each heavy oil, each quality measurement: Conradson carbon, vanadium, nickel, etc., in the higher quality fraction was plotted versus the yield of the higher quality fraction. Since the highest quality fraction was the distillable liquids, it was the point at the lowest yield for Cold Lake bitumen. The soluble, but unadsorbed, fraction was the next highest quality fraction for each trial solvent. Thus, the quality measurement and yield were calculated as if this fraction and the distillable liquids were mixed to form the second point for each trial

* Research was done at Exxon Corporate Research, Annandale, NJ 08801-0998

solvent. Likewise, the soluble adsorbed fraction and the insolubles were added. This type of data for Conradson carbon residue is shown in Figure 2 for Cold Lake bitumen and in Figure 3 for Arabian Heavy Vacuum resid. In each case a curve is drawn through those of highest yield at a given quality measurement as this determines the best way the heavy oil could be split into two fractions, the separability.

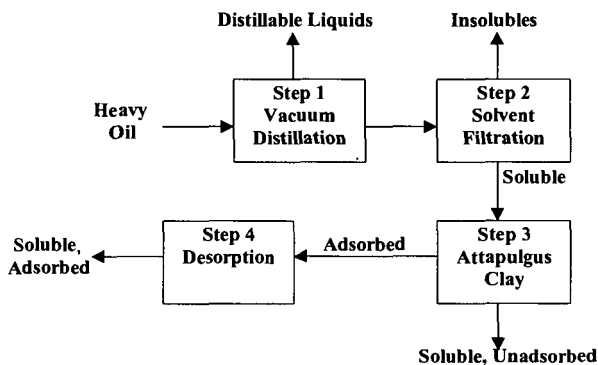


Figure 1. General Procedure for Laboratory Selective Separation

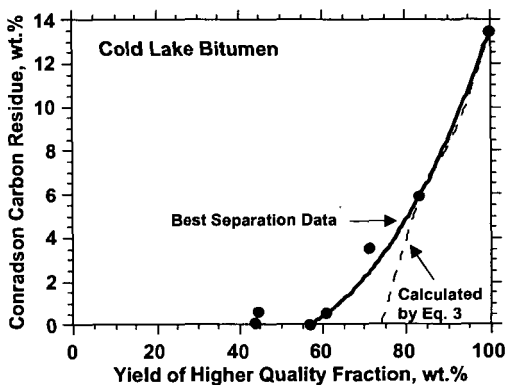


Figure 2. Selective Separation of Conradson Carbon for Cold Lake Bitumen

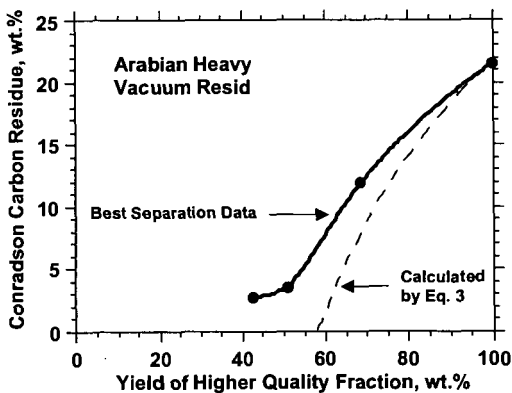


Figure 3. Selective Separation of Conradson Carbon for Arabian Heavy Vacuum Resid

Of the solvents tried, cyclohexane is the best because it gives a high yield of a high quality fraction without insolubles. The yields and analytical data for the cyclohexane separations are shown in Table II and compared with the starting feed data. Thus, for Arabian Heavy vacuum resid that does not require distillation, the separation is achieved in two steps, adsorption and desorption, and about half of the resid would meet the specifications for resid FCC feed in Table I except for sulfur. On the other hand, combining vacuum distillation with cyclohexane adsorption separates 71% of Cold Lake bitumen into a fraction that only slightly misses the example specifications for sulfur and hydrogen.

Table II
Cyclohexane Separations: Yields and Analytical Data

Fraction	Yield wt.%	C wt.%	H wt.%	N wt.%	O wt.%	S wt.%	V ppm	Ni ppm	Conradson
									Carbon wt.%
Cold Lake Bitumen									
Distillable Liquids	44.5	85.14	11.67	0.09	0.00	2.63	0.6	0.0	0.57
Soluble, Unadsorbed	<u>26.7</u>	<u>84.08</u>	<u>10.96</u>	<u>0.17</u>	<u>0.60</u>	<u>4.11</u>	<u>29</u>	<u>10</u>	<u>8.4</u>
Dist. Liq. + Sol. Unadsorb.	71.2	84.74	11.40	0.12	0.22	3.18	11	4	3.5
Soluble, Adsorbed	30.2	81.07	8.73	0.99	2.39	6.55	359	138	43.8
TOTAL	101.4	83.57	10.60	0.38	0.87	4.19	115	41	15.5
Full Feed	100	83.82	10.46	0.38	0.68	4.57	152	62	13.5
Arabian Heavy Vacuum Resid									
Soluble, Unadsorbed	50.9	85.07	11.47	0.030	0.50	3.57	0.0	0.0	3.4
Soluble, Adsorbed	50.1	82.63	8.53	0.80	1.63	6.78	451	112	36.9
TOTAL	101.0	83.86	10.01	0.41	1.06	5.16	224	56	20.2
Full Feed	100	83.51	9.93	0.45	0.57	5.80	165	40	21.5

Conradson Carbon Separability Limit

Here we will focus on the problem of maximizing the yield of a low Conradson Carbon fraction. 100 parts of heavy oil of C_F Conradson carbon is separated into β parts of a higher quality fraction containing a Conradson carbon of C_H and $100 - \beta$ parts of a lower quality fraction containing a Conradson carbon of C_L . Since Conradson carbon is conserved for separations (3):

$$100 C_F = \beta C_H + (100 - \beta) C_L \quad [1]$$

Solving for β :

$$\beta = 100 [1 - (C_F - C_H) / (C_L - C_H)] \quad [2]$$

This shows that to maximize the yield of a high quality fraction meeting a Conradson carbon specification from a given heavy oil feed, one needs to concentrate the Conradson carbon in the low quality fraction. Therefore, for Cold Lake bitumen (Conradson carbon = 13.5 wt.%) to separate 85 wt.% of a fraction meeting a specifications of 5 wt.% Conradson carbon, one would need to isolate 15 wt.% containing 61.7 wt.% Conradson carbon. However, the highest Conradson carbon fraction that was isolated from Cold Lake bitumen is the 14.1 wt.% yield of n-heptane insoluble asphaltenes with a Conradson carbon of 52.5%. Thus, it is unlikely that 85 wt.% of a fraction of Cold Lake bitumen with a Conradson carbon of 5 wt.% or less exists because significant fractions of Conradson carbon much greater than 50 wt.% Conradson carbon are not present in heavy oils. This is because the coke precursors are chemically linked to distillable liquid precursors in the same molecule. In terms of the pendant - core building block model (3), all molecules that contain cores also contain significant fractions of pendants. For instance, Arabian heavy vacuum resid with a Conradson carbon of 21.5 wt.% and an asphaltene Conradson carbon of 51.6 wt.% at a specification of 5 wt.% Conradson carbon:

$$\beta = 100 [1 - (21.5 - 5) / (51.6 - 5)]$$

$$\beta = 64 \text{ wt.}\%$$

Thus, the separation of 64 wt.% of Arabian Heavy vacuum resid with a Conradson carbon of 5 wt.% or less is not possible because there are only 20 wt.% asphaltenes and not the 36 wt.% required. As a result, Eq. 2 with the asphaltene Conradson carbon substituted for C_L is an upper limit on the yield of a fraction of a given Conradson carbon value. Eq. 1 can be rearranged and the asphaltene Conradson carbon, C_A , substituted for C_L to give:

$$C_H = \{C_F - (1 - \beta/100) C_A\} / \{\beta/100\}$$

[3]

This upper limit, Eq. 3, is plotted on Figures 2 and 3 as a dashed curve. The curve through the best separation data approaches the upper limit at high yields of the higher quality fraction for Cold Lake bitumen. On the other hand, a gap remains between the two curves for Arabian Heavy vacuum resid, indicating further improvements in separability of this heavy oil may be possible.

Separation of Vanadium and Nickel from Heavy Oils

Unlike for Conradson carbon, the separability of vanadium and nickel is not limited much by the heavy oil macromolecules. Vanadium with an atomic weight of 50.9, even as part of the largest macromolecules, the asphaltenes of average molecular weight of 3000, would be 1/60 the weight of the molecule bonded to it. Thus, in Cold Lake bitumen that contains 152 ppm vanadium and Arabian Heavy vacuum resid that contains 165 ppm vanadium, all of the vanadium is in less than 1 wt.% of each heavy oil. Likewise, nickel at 62 ppm in Cold Lake bitumen and 56 ppm in Arabian Heavy vacuum resid must be contained in less than 0.5 wt.% of each heavy oil. Nevertheless, the vanadium and nickel containing molecules physically associate with the Conradson carbon precursors, the polynuclear aromatics. As a result, they tend to separate together. Figure 4 and 6 demonstrates for Cold Lake bitumen and Figures 5 and 7 for Arabian Heavy vacuum resid that only a little more low vanadium and nickel fractions can be separated than low Conradson carbon fractions (Figures 2 and 3). Thus, precipitation and/or Attapulugus clay adsorption do not provide the desired selective separation for vanadium and nickel.

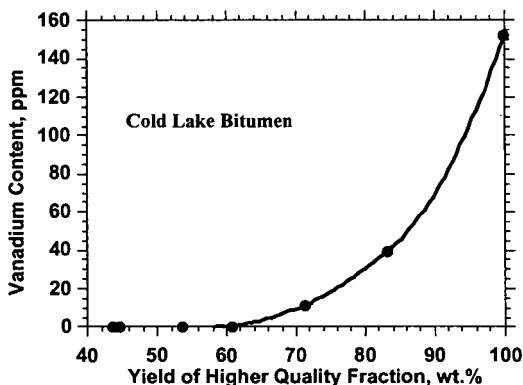


Figure 4. Selective Separation of Vanadium in Cold Lake Bitumen

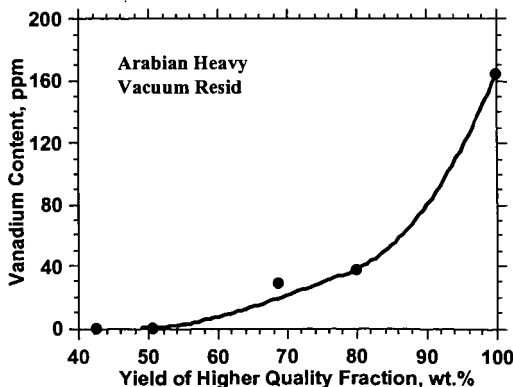


Figure 5. Selective Separation of Vanadium in Arabian Heavy Vacuum Resid

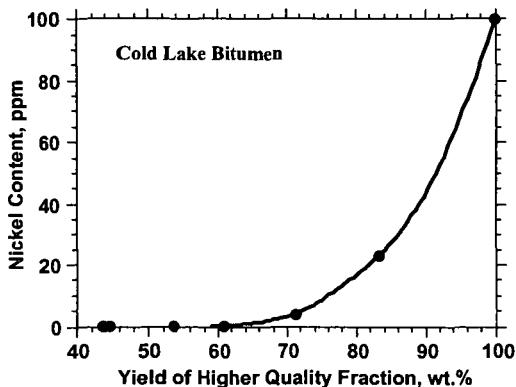


Figure 6. Selective Separation of Nickel in Cold Lake Bitumen

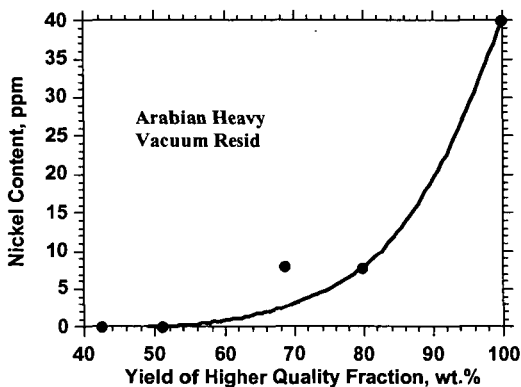


Figure 7. Selective Separation of Nickel in Arabian Heavy Vacuum Resid

CONCLUSIONS

Selective separation has the potential to provide substantial fluid catalytic cracking feed from heavy oils that could compete with resid conversion processes. Further separation of Conradson carbon is limited by heavy oil molecules in which Conradson carbon precursors are chemically bonded to significant fractions of distillable liquid precursors. On the other hand, there are no molecular limitations to the much greater separation of vanadium and nickel. Vanadium is in less than 1 wt.% of heavy oils and nickel is in less than 0.5 wt.%. Although sufficient for resid FCC specifications, physical association with Conradson carbon precursors tends to cause vanadium and nickel to separate with the Conradson carbon precursors in precipitation and adsorption separations. Thus, devising a molecularly selective separation method for attaining the full potential of metals removal from heavy oils remains to be a significant challenge.

REFERENCES

1. Barnes, P.H., AIChE, International Conference on Refinery Processes, Preprints, 1998, 227.
2. Wiche, I. A., *Ind. Eng. Chem. Res.* 1992, 31, 530.
3. Wiche, I. A., *Energy Fuels* 1994, 8, 536.

The Promotional Effect of Initiators in Hydro-thermal Cracking of Resids

Jie Chang, Li Fan* and Kaoru Fujimoto

Department of Applied Chemistry, School of Engineering, The University of Tokyo,
Hongo 7-3-1, Bunkyo-ku, Tokyo, 113-8656, Japan Email: lfan@hongo.ecc.u-tokyo.ac.jp

1 Introduction

Based on cracking mechanism, there are three main industrial processes to produce middle distillate from resid. They are thermal cracking, catalytic cracking and hydrocracking. Hydro-thermal cracking, the combination of thermal cracking and catalytic hydrogenation, is a novel method developed by the present authors to upgrade resids aiming at maximum middle distillate (Fujimoto et al., 1988; Yang et al., 1998). The following elementary steps are important during hydro-thermal cracking reactions: (1) Initiation free radical (homolytic cleavage of a hydrocarbon molecule into two free radicals). (2) Free radical dissociation (β scission). (3) Hydrogen transfer (between H_2 , radical and hydrocarbon). H transfer from H_2 to radical can suppress the secondary cracking of hydrocarbon, therefore, suppress the yields of coke and gas. It is considered that some effective initiators may enhance the conversion of resids by increasing the concentration of free radicals. Much research has been carried out on catalyst development, reaction mechanism, process design and optimization in the above refinery processes until now. But the issue of adding initiators in the cracking of resids was very rarely addressed. The present work shows the promotional effect of initiators in hydro-thermal cracking of resids as well as its model compound.

2 Experimental

Experiments were carried out in a 75 cm³ batch reactor. The reaction conditions were as follows: temperature, 673-703K; initial pressure, 5.0 MPa; reaction time, 0-60 min; catalyst/oil ratio, 0.05-0.2. Canadian bitumen (B) and Arabian heavy vacuum resid (AVR) were used in experiments. Their properties are shown in Table 1.

Sulfur and $(CH_3)_2COOC(CH_3)_2$ (DTBP) were used here as initiators to promote heavy oil conversion.

Gas products were analyzed by gas chromatography (Shimadzu GC-8A). Liquid products were separated by a distillation gas chromatography (Shimadzu GC-14A) into 5 components: naphtha (initial boiling point -343K), kerosene (343-503K), gas oil (503-616K), vacuum gas oil (616-798K) and residue (>798K). The conversion of resid was calculated by the following formula:

$$\text{Conversion (wt\%)} = \left(1 - \frac{\text{residue in product}}{\text{residue in feed}}\right) \times 100\%$$

When alkylbenzene was pyrolyzed or cracked on solid acid catalyst, the selectivities of benzene and toluene were so different that it could be used as a model compound to distinguish a reaction proceeding via carbonium mechanism or free radical mechanism (Szwarc 1950; Mochida and Yoneda 1967; Nakamura et al, 1997). Study on liquid-phase thermolysis of 1-phenyldodecane (PhDD) demonstrated that PhDD pyrolysis entirely proceeded through free radical mechanism (Savage and Klein, 1987). The reaction of PhDD was used as a probe reaction to study the mechanism of initiator promotional effect. In these experiments, the liquid products were determined by GC-MS (Shimadzu GCMS 1600) and analyzed by gas chromatography (Shimadzu GC-14A).

3 Results and Discussion

3.1 Effect of initiators addition in resids

1 wt% of DTBP was added into bitumen to study the effect of initiator. The properties of products are listed in Table 2. It was obvious that this peroxide was very effective to increase the conversion of bitumen from 59.1% to 91.9% (runs 1 and 2 without catalyst) and from 68.4% to 78.5% (runs 3 and 4 with catalyst) respectively. Coke yield was greatly suppressed by catalyst (runs 3 and 4).

It also was seen from Table 2 that in the cases of adding DTBP, the selectivity of iso-butane was higher than that without DTBP. It is well known that thermal cracking of hydrocarbon molecule proceeded via the chain reaction of free radicals generated from C-C cleavage or hydrogen atom abstraction from C-H bond. In bitumen hydro-thermal cracking, free radicals were generated from C-C cleavage at initial stage. But when DTBP was added into bitumen, it decomposed at high temperature and produced tertiary butoxy radical. This free radical could abstract hydrogen from bitumen and initialized chain reactions at initial stage besides the conventional initiation path, therefore the concentration of radical was higher and the conversion of bitumen was increased.

3 wt% of sulfur was added into AVR to test the effect of initiator addition. The results were compared in Table 3. When catalysts were used, the addition of sulfur increased the conversion from 63.6% to 81.1% (runs 5 and 6). In absence of catalyst, the addition of sulfur raised the conversion from 15.7% to 32.5% (runs 7 and 8). Similarly, sulfur was an effective initiator to the hydro-thermal cracking of AVR.

3.2 Study on model compound

The conversions in different case at different reaction time are depicted in Fig.1. It is clear from Fig.1 that the conversion was obviously enhanced by adding initiator with or without catalyst. Without catalyst and with initiator, when the reaction time was one hour, the conversion increased from 40.1% to 51.9%. In absence of initiator, catalyst greatly decreased the conversion from 40.1% to 16.8% in one-hour reaction. It seemed that free radicals were hydro-quenched over catalyst. After adding initiator to catalyzed reaction, the conversion restored to 40.2% even if the reaction time was just half of an hour. If the reaction time was extended to one hour, the conversion of the catalyzed reaction with addition of peroxide was further enhanced to 47.5%. The selectivities of part products are shown in Table 4. It was found from Table 4 that the ratios of toluene to benzene were about 18.0-22.2 in all of these cases. This indicated that hydro-thermal cracking of PhDD proceeded via free radical mechanism and hydrogenation quench. In the cases of adding peroxide, iso-butene, acetone and tertiary butyl alcohol were detected in products and selectivity of C₁ species was also increased. In run 11, the feed was heated from room temperature to 683K in 10 min and cooled down immediately, to 573K in 5 min and to room temperature in another 15 min (reaction time = 0). The yield of acetone was high. It should be derived from decomposition of tertiary butoxy radical, with the corresponding formation of C₁ species (Fan et al., 1998). This provided the evidence that the decomposition of DTBP was the initial stage of the chain reactions.

The above results suggested that the hydro-thermal cracking of PhDD related with free radical chain reactions. It was considered that in the chain reactions, the initiation step of PhDD molecule dissociation, forming free radicals, was the slowest one, the overall reaction rate was readily controlled by this step. If the concentration of free radicals in reactants was increased, the reaction rate could be elevated. When DTBP was added into PhDD, it easily produced free radicals during hydro-thermal cracking conditions, therefore increased the overall concentration of free radicals, enhanced the conversion of PhDD. If effective free radical initiators are available, the conversion of resid in hydro-thermal cracking, thermal cracking or hydrocracking will be raised and the reaction temperature may be lowered. The experiments showed that DTBT and sulfur are effective promoters to resid conversion.

4 Conclusions

DTBP remarkably enhanced the conversion of resid and its model compound during hydro-thermal cracking. This resulted from tertiary butoxy free radical produced by the decomposition of peroxide at reaction condition. Similarly, sulfur was an effective promoter to the hydro-thermal cracking of AVR.

5 References

- Fan, L.; Watanabe, T.; Fujimoto, K. *Stud. Surf. Sci. Catal.* 1998, 119, 581.
 Fujimoto, K.; Nakamura, I.; Tominaga, H. *Chem. Lett.* 1988, 167.
 Mochida, I.; Yoneda, Y. *J. Catal.* 1967, 7, 386.
 Nakamura, I.; Yang, M.; Fujimoto, K. *Preprints Div. Petrol. Chem., ACS* 1997, 42(2), 401.
 Savage, P. E.; Klein M. T. *Ind. Eng. Chem. Res.* 1987, 26, 374.
 Szwarc, M. *Chem. Rev.* 1950, 47, 171.
 Yang, M.G.; Nakamura, I.; Fujimoto, K. *Catal. Today* 1998, 43, 272.

Table 1 Properties of feedstock

	B	AVR
API Gravity	6.0	5.9
CCR, wt%	14.8	22.4
C, wt%	82.89	84.80
H, wt%	10.14	10.20
S, wt%	4.90	4.02
Ni, wtppm	75	53
V, wtppm	192	180
Naphtha, wt%	0	0
Kerosene, wt%	0	0
Gas oil, wt%	6.8	0
VGO, wt%	28.0	0
Residue, wt%	65.2	100.0

Table 2 Effect of DTBP addition on hydro-thermal cracking of bitumen

Run number	1	2	3	4
Catalyst	no	no	Ni/Al ₂ O ₃	Ni/Al ₂ O ₃
DTBP	no	adding	no	adding
Conversion, %	59.1	91.9	68.4	78.5
yield, wt%				
C ₁ -C ₄	4.3	5.4	4.2	5.0
iC ₄ H ₁₀ /nC ₄ H ₁₀	0.50	0.84	0.50	1.46
Naphtha	9.1	12.4	7.4	9.6
Kerosene	9.4	11.9	8.0	9.1
Gas oil	22.6	28.4	22.7	25.0
Vacuum gas oil	21.8	29.9	31.8	32.3
Residue	26.7	5.3	20.6	14.0
Coke	4.6	5.1	3.0	2.8

Temperature 703K, pressure 5.0MPa, Bitumen 10.00g, catalyst 2.00g , DTBP 0.10g

Table 3 Effect of sulfur addition on hydro-thermal cracking of AVR

Run number	5	6	7	8
Catalyst	NiMo/Al ₂ O ₃	NiMo/Al ₂ O ₃	no	no
Initiator	no	0.3g S	no	0.3g S
Time, min.	60	60	0	0
Conversion, %	63.6	81.1	15.7	32.5
yield, wt%				
C ₁ -C ₄	3.3	4.9	0.1	0.1
Naphtha	4.8	9.2	0.2	1.1
Kerosene	6.1	9.7	0.5	1.4
Gas oil	16.5	21.6	2.3	6.3
Vacuum gas oil	28.6	27.8	12.7	23.6
Residue	34.5	18.8	84.3	67.6
Coke	3.2	6.4	-	-

Temperature 703K, pressure 5.0MPa, AVR 10.00g, catalyst 2.00g

Table 4 Effect of DTBP addition on model compound

Run number	9	10	11	12
Conversion, %	40.1	51.9	19.5	47.5
Selectivity, %				
acetone	0.0	2.86	9.83	0.0
t-butyl alcohol	0.0	0.0	1.56	0.0
n-olefin C ₅ -C ₈	3.03	3.22	0.63	0.0
n-paraffin C ₅ -C ₈	5.76	6.69	0.75	7.03
n-olefin C ₉ -C ₁₃	18.8	7.62	13.8	4.36
n-paraffin C ₉ -C ₁₃	22.2	24.4	15.8	33.9
toluene / benzene	21.3	22.2	18.0	19.2

Temperature 683K, pressure: 5.0MPa

Run 9: reaction time 60 min. no catalyst and no peroxide

Run 10: reaction time 60 min. adding 0.40g peroxide only

Run 11: reaction time 0 min. adding 0.40g peroxide only

Run 12: reaction time 60 min. adding 0.40g peroxide and 0.50g catalyst

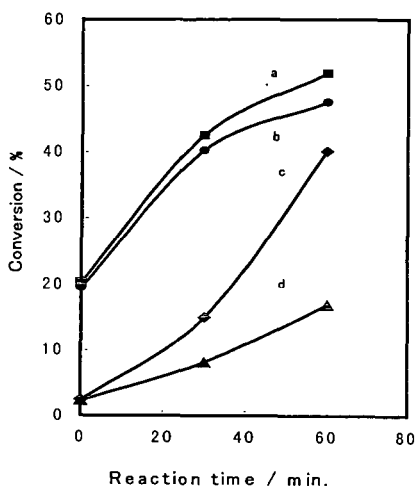


Fig.1 Effect of DTBP on conversion of PhDD

Feed: PhDD 10.00g, temperature 683K

pressure 5.0MPa

a: adding 0.40g DTBP only

b: adding 0.40g DTBP and 0.50g catalyst

c: no DTBP and catalyst

d: adding 0.50g catalyst only

EFFECT OF STEAM ON COKING CHEMISTRY OF ATHABASCA BITUMEN

Richard Dutta, William McCaffrey and Murray Gray

Dept. of Chemical and Materials Eng., University of Alberta,
Edmonton, Alberta, Canada

Key Words: fluid-coking, bitumen, free-radical stabilization

INTRODUCTION

Fluid-coking is an important technology used in upgrading of bitumen and petroleum residues. The process uses a fluidized bed of hot coke particles to crack the feedstock. The bed is fluidized by steam, which also acts as a stripping medium to remove the distillate from the surface of the coke particles. Steam has long been thought of as chemically 'inert' in this process, in that it does not effect the product quality or yields. The use of other fluidizing media has been considered as an alternative to steam, including methane or nitrogen. Therefore, the question as to the chemical influence of steam is an important one and this study was undertaken to determine this on a micro-lab scale and on a larger pilot scale.

Much of the previous research into the effect of steam on hydrocarbons has been limited to the lower temperature regime associated with thermal maturation of kerogen in aqueous environments (<400°C). Research has focussed on hydrous pyrolysis experiments using kerogens and stable isotope analysis^{1,2}. The chemical transformation of kerogen to bitumen, oil and gas has been studied to assess the role of water in these reactions. Studies at low temperatures (<150°C) conclude that water-hydrogen may exchange with certain labile organic hydrogen sites, e.g., those bound to nitrogen, sulfur and oxygen³. There is some evidence of hydrogen exchange with aromatic hydrogen and alkyl-hydrogen via carbonium ion mechanisms^{4,5}. However, the higher temperatures of fluid-coking (530°C) and other upgrading processes, lead to free-radical reactions. Studies by Hoering⁶, Lewan⁷, and Stalker et al.⁸, have shown that at higher temperatures, exchange between water-hydrogen and organic-hydrogen is due to quenching of free organic radical sites. Thermodynamically, the reactions of steam and free-radicals have been shown to be favorable under certain reaction conditions⁹.

Song et al.⁹ have studied the effect of water on the process of coal liquefaction. Water was seen to have three effects on liquefaction; chemical, physical and surface interactions. The increase in coal conversion was attributed to increased removal of oxygen functionalities in the presence of water, and therefore a reduction in retrogressive reactions. Tse et al.¹⁰ suggested that water can reduce retrogressive reactions such as crosslinking of hydroxy groups. Siskin et al.^{11,12} have observed that water may increase depolymerization by cleavage of ether linkages. Clark and Kirk studied the upgrading of bitumen with water at temperatures up to 415°C¹³. Their results show that water has an effect in decreasing insoluble material produced and also decreasing the sulfur content of the liquids produced. This enhancement of product quantity and quality was improved even further in the presence of an iron-based catalyst.

The objective of this research project was to determine the extent to which steam exchanges/donates hydrogen to the reacting bitumen molecules under coking conditions. Experiments were carried out with water doped with D₂O to trace any exchanged deuterium atoms. Comparisons of experiments carried out with and without water were made to ascertain the effect that steam may have on coking chemistry.

EXPERIMENTAL

The feedstock used in this study was Athabasca Bitumen obtained from Syncrude Canada. A 5.6 wt% solution of deuterium oxide (D₂O) in water was used for all reactions. The coking reactions were carried out in 15 ml microautoclave reactors heated in a fluidized sand bath to temperatures in the range of 350-480°C. 3g of bitumen was accurately weighed into the reactor along with 0.6g D₂O solution. The reactor was closed and purged with nitrogen to atmospheric pressure. For the reactions without D₂O solution (dry), the nitrogen pressure in the reactor was increased to account for the pressure generated by steam in the reactions with water. The reactor was lowered into the sand bath for a pre-determined reaction time and then quickly quenched in cold water. Gases were vented from the reactor and analyzed for hydrocarbon composition by Gas Chromatography. The products in the reactor were extracted in toluene to give coke (toluene insolubles) and liquids (toluene solubles). The coke was dried and weighed to give coke yield. The liquids were analyzed by elemental analysis for C, H, N and S content. ¹H and ²H liquid NMR were used to quantify the % deuterium in the liquid samples.

In order to determine the deuteration of bitumen under conditions more applicable to fluid coking conditions (530°C, fluidized bed, short residence time), the 3" coking pilot plant at Syncrude Research Center was utilized for two reactions. A 5% solution of D₂O in water was used as the fluidizing medium. Liquid products were analyzed by NMR to give %D.

RESULTS

In order to determine the extent to which steam changes the chemistry of the coking process, several analytical procedures were utilized. This section will show the major findings from each of these, followed by a discussion of the possible mechanism that can explain these changes.

Coke Yield: The yield of toluene insoluble material (coke) at various reaction times at 450°C is shown in Figure 1. The MCR of Athabasca bitumen is 14%. The figure shows that coke yield with and without water exceeds 20% after 60 minutes. This is because a closed reactor is used for this study. At 450°C, volatiles produced in the cracking of bitumen can further crack to produce gas or recombine to produce coke. In the presence of steam, coke yield is reduced from 24% to 21%.

Gas Composition: Figure 2 shows the hydrocarbon gas composition after bitumen coking at 450°C and 60 minutes reaction time. The most striking result is the reduction in methane produced when steam is used in the reaction. The presence of steam appears to reduce the cracking of alkyl-aromatics leading to a reduction in methane formation.

Sulfur Analysis: Figure 3 shows the wt% sulfur in the liquid products from bitumen coking at 450°C. Desulfurization of bitumen proceeds by thermal cleavage of C-S bonds (aliphatic sulfides). These bonds are relatively weak (compared to C-C bonds) and are therefore the first to crack, which is observed in that most of the desulfurization takes place in the first 10 minutes of the reaction. In the presence of steam, removal of sulfur is reduced.

¹H and ²H Liquid NMR: This technique was used to quantify the percentage of deuterium atoms per total hydrogen atoms (%D) in various liquid products from bitumen coking. The technique also shows the preferred position that exchanged deuterium will attach to bitumen and its products. Figure 4 shows an example of the ²H spectra of bitumen liquid products detailing the areas used to quantify the data. The spectra has been split into 3 sections, namely aromatic protons, α -CH₂ (benzylic) and α -CH₃ protons (i.e., located on carbon atoms adjacent to aromatic rings), and β - and γ - protons (i.e., located on carbon atoms one and two positions removed from an aromatic ring). Figure 5 shows %D at various reaction conditions. The data shown at 530°C is from liquids taken from the Syncrude coking pilot unit discussed in the experimental section of this paper. It should be noted that in the control experiment (530°C, no D₂O), the %D was 0.014% (natural abundance of deuterium is 0.015%). Exchange of deuterium atoms from D₂O with organic protons from the bitumen occurs mostly at the α -position. Aromatic and γ -carbon deuterations occur but to a lesser extent than α -carbon deuteration

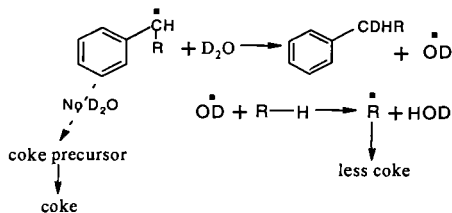
DISCUSSION

The results show that steam is reducing coke yield, methane formation and sulfur removal. The most likely explanation of these observations is by considering radical-stabilization by water-hydrogen exchange. This will cause a reduction in radical-recombination reactions that will lead to coke, stabilization of alkyl-aromatic radicals leading to reduction in methane, and stabilization of C-S radicals leading to reduction in sulfur removal. A second stage of sulfur removal has also been postulated by Kakimura et al.¹⁴. Hydrothermal cracking of C-S bonds in aromatic structures led to increased removal of sulfur and reduction in viscosity. Based on the limited sulfur analysis taken in this study, it is impossible to back-up the ideas put forward by Kakimura. However, the data does agree with conclusions made previously when considering the coke yield and gas composition.

The data obtained by NMR of the liquid samples shows preferential exchange of deuterium at the α -position (benzylic). This would be expected if conclusions from our previous results are correct, in that, water-hydrogen is stabilizing free-radicals in the coking process. Benzylic radicals are resonance-stabilized and are therefore more likely to exist as reactive intermediates in the coking reaction. Stabilization of these radicals can occur more readily and this is shown with the preferential deuteration of benzylic carbons. This hypothesis can be backed up when considering the coking reaction at 350°C. This reaction temperature does not give rise to many free-radicals (compared to >425°C) and the preferential deuteration of the benzylic position does not occur. The %D data obtained for the pilot plant data taken at 530°C does show a decrease in overall deuterium incorporation into the liquids due to the much decreased residence time of the bitumen cracking products in the reactor. The pilot unit also operates at a much lower pressure than the closed reactors used in the other experiments, which could also explain the decrease in deuteration. The results still show evidence for the radical stabilization behavior that is inferred from the results obtained at lower temperatures and in closed microautoclave reactors.

Figure 6 shows a comparison of the coke yield (divided by 100) and %D in the liquids produced under increasing reaction severity. The data shows that increasing reaction severity give increasing coke yield and an overall trend of increasing deuteration. The decrease at the highest severity conditions is probably due to excess hydrocarbon gas formation that will remove some of the deuterium from the liquid fraction. The relationship between coke yield and %D implies that a similar mechanism can account for the effect of steam on these two parameters.

Proposed Mechanism: Steam is changing the chemistry of the coking process by 'stabilizing' free-radicals that are produced by thermal cleavage of C-C and C-S bonds. This process of free-radical 'stabilization' has to be carefully defined. Free-radical 'capping' is a term that has been used to explain termination reactions by gas-phase hydrogen or hydrogen transferred from donor solvents^{15,16}. This mechanism does not particularly apply to this system because the hydroxyl radical will tend to abstract a hydrogen from the bitumen. This concept of 'stabilization' is more applicable because it is possible that the radical produced in the stabilization of the hydroxyl radical will not recombine to produce coke.



Scheme 1. Mechanism of 'stabilization' of free-radicals produced by cracking of bitumen

CONCLUSIONS

The purpose of this study was to find evidence for the chemical interaction of steam and bitumen under coking conditions. Through various analytical techniques, namely, coke yield, elemental analysis, gas analysis, and liquid NMR, the concept of free-radical stabilization by water-hydrogen has been explored. This free-radical stabilization process can also be inferred by comparing the gas composition and the liquids sulfur content for reactions with and without steam. Water is exchanging/donating hydrogen to the radicals to reduce methane formation and sulfur removal. NMR data has shown preferential deuteration of the benzylic carbons, which would suggest that free-radical stabilization is occurring (benzylic radicals are very stable). Coking reactions carried out in a pilot-unit under conditions similar to real fluid-coking conditions, show this preferential deuteration of the benzylic carbons and suggest that even with the short residence time and low pressures of fluid-coking, water-hydrogen may be exchanged/donated to the reacting bitumen.

ACKNOWLEDGEMENTS

The authors would like to thank the staff of the NMR facility, Dept. of Chemistry, University of Alberta, for NMR analysis of the products. Dr. Karlis Muehlenbachs, Dept. of Earth and Atmospheric Sciences, University of Alberta, has provided the authors with valuable insight into stable isotopes. Thanks to Scott Gillis, Iftikhar Huq and Murray Noble for running the reactions on the pilot plant unit at Syncrude Research Center, Edmonton. Thanks to Dr. Ed. Chan (Syncrude Research Center) for many useful discussions. The work was supported by Syncrude Canada.

REFERENCES

- Siskin, M. and Katritzky, A. R. *ACS, Div. Fuel. Chem. Prep.* 44(2), 324, 1999
- Lewan, M. D., *Geochim. Cosmochim. Acta.* 61, 3691-3723, 1997
- Koepp, M. in *Short papers of the Fourth International Conference, Geochronology, Cosmochronology, Isotope Geology*, 1978
- Alexander, R., Kagi, R. I., and Larcher, A. V., *Geochim. Cosmochim. Acta.*, 46, 219-222, 1982
- Werstiuk, N. H., and Ju, C., *Can. J. Chem.* 67, 812-815, 1989
- Hoering, T. C., *Org. Geochem.* 5, 267-278, 1984
- Stalker, L., Larter, S. R., and Farrimond, P. *Org. Geochem.* 28, 238-253, 1998
- Lewan, M. D., *ACS, Div. Fuel. Chem. Prep.* 44(2), 420, 1999
- Song, C., Saini, A. K., and Schobert, H. H., *Energy Fuels* 8, 301-312, 1994
- Tse, D. S., Hirschon, A. S., Malhotra, R., McMillen, D. F., and Ross, D. S., *ACS, Div. Fuel. Chem. Prep.* 36(1), 23, 1991
- Siskin, M., Katritzky, A. R., Balasubramanian, M., *Energy Fuels* 5, 770, 1991
- Siskin, M., Bron, G., Vaughn, S. N., Katritzky, A. R., Balasubramanian, M., *Energy Fuels* 4, 488, 1991
- Clark, P. D. and Kirk, M. J. *Energy Fuels* 8, 380-387, 1994
- Kakimura, H., Takahashi, S., Kishita, A., Moriya, T., Hong, C. X., and Enomoto, H., *ACS Div. Fuel. Chem. Prep.* 43(3), 741, 1998
- Curran, G. P., Struck, R.T., Gorin, E. *Ind. Eng. Chem. Proc. Des. Dev.* 6, 167, 1967.
- Wiser, W.H. *Fuel.* 47, 475, 1968

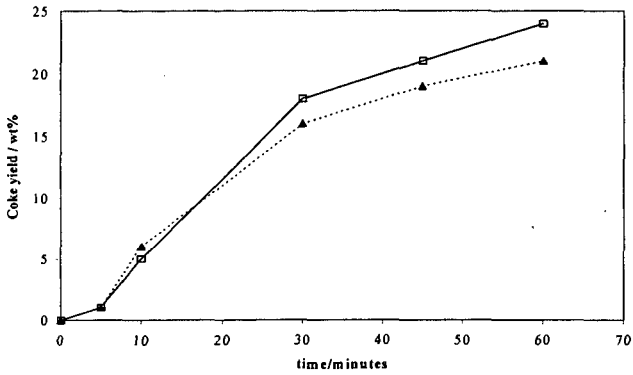


Figure 1. Effect of steam on toluene insoluble (coke) yield from bitumen coking at 450C (▲-steam; □-Dry)

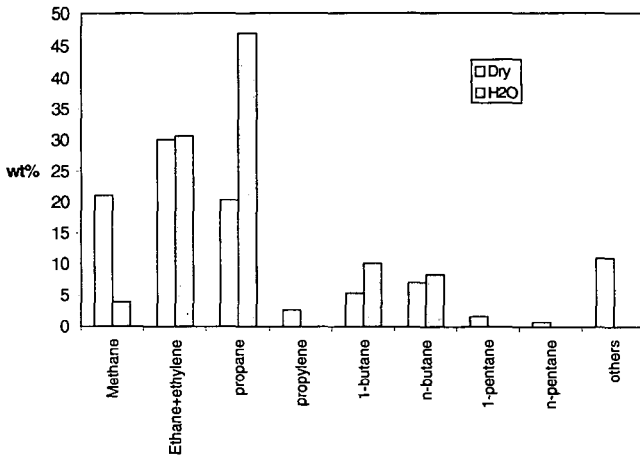


Figure 2. Hydrocarbon gas composition from bitumen coking at 450C and 60 minutes

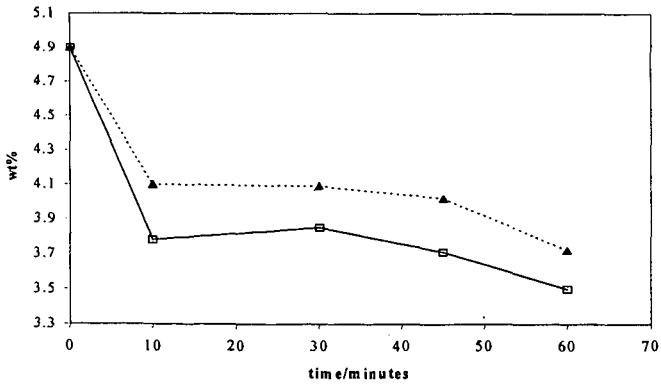


Figure 3. Sulfur content of liquid products from bitumen coking at 450C (▲-steam; □-Dry)

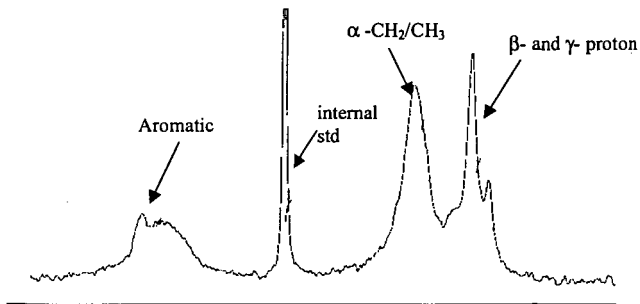


Figure 4. ^1H NMR spectra of liquid products from bitumen coking – 450C 60min 5% D_2O in H_2O

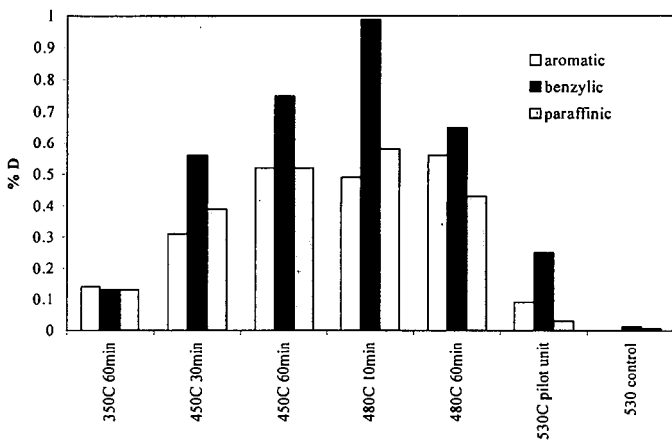


Figure 5. %D in liquid products from bitumen coking (5% D_2O in H_2O)

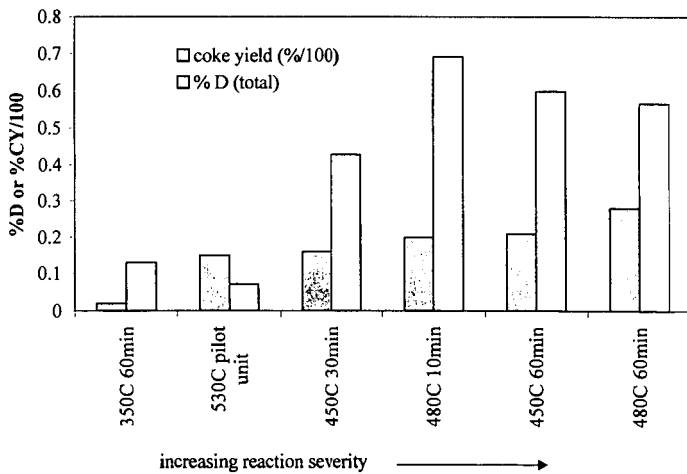


Figure 6. Comparison of %D in liquids and coke yield for bitumen coking at increasing severity

PROCESSABILITY AND THERMAL BEHAVIOUR OF ATHABASCA BITUMEN WITH VARYING ASPHALTENES CONCENTRATION

Thomas Gentzis and Parviz Rahimi. National Centre for Upgrading Technology (NCUT),
1 Oil Patch Drive, Suite A202, Devon, Alberta, Canada T9G 1A8

ABSTRACT

The coking propensity and thermal hydrocracking of extra heavy Athabasca bitumen vacuum bottoms fractions obtained by a short path distillation were investigated using hot-stage microscopy and microautoclave. The microscopy results indicated that the initial boiling point of the feedstocks (ranging from +525°C to +675°C) and asphaltene content (varying from 32 to 56wt%) did not significantly affect the mesophase induction period. However, the coke yield obtained at different severities using a microautoclave correlated with the asphaltene content and the molecular weight of the feedstocks.

INTRODUCTION

The production of synthetic crude oil from Athabasca bitumen in Alberta is increasing from the current 450 K bbl/day to approximately 1.2 MM bbl/day by the year 2005. The main upgrading technologies presently used to convert the vast reserves of oil sands bitumen to SCO are delayed coking at Suncor Energy Inc. and fluid coking at Syncrude Canada Ltd. Both plants process atmospheric bottoms. Recently, Suncor Energy Inc. has installed a vacuum tower and Syncrude Canada Ltd. will soon install a vacuum tower to process vacuum bottoms.

Upgrading by a coking process results in the production of volatile liquids, gases and coke. Heavier and larger molecules present in the vacuum bottoms would have a greater tendency to form macroscopic particles of solid coke by free radical polymerization reactions in the absence of hydrogen and catalyst. Even in a hydrogen addition process semisolid sediment, sometimes referred to as "incompletely polymerized coke," is formed.¹ According to Wiehe² heptane insoluble asphaltenes are the main culprit in coke formation. These asphaltenes, under coking temperatures, are first converted to pseudocomponents called "asphaltene cores" the concentration of which may exceed the solubility limit in the reaction medium. Once these asphaltene cores are produced, phase separation takes place which leads to irreversible polymerization forming solid coke.

Changing the cut point of the feedstocks from atmospheric to vacuum bottoms will affect their chemical composition which in turn will alter the chemistry of the process. It is well known that the ratio of resins to asphaltenes is an important factor in keeping asphaltenes in solution and thus preventing phase separation.³

The present work addresses how the changes in the feedstocks as a result of removing lighter boiling point materials by distillation would affect the upgrading of Athabasca bitumen during thermal processing.

EXPERIMENTAL

Athabasca bitumen atmospheric bottoms (+343°C) was distilled using the automated ASTM D1160 procedure to produce vacuum residue (+525°C) to be used as feed to a short path distillation unit (Leybold-Heraeus model KDL4-P). The system pressure and the temperature of the evaporator were adjusted to produce the desired distillate cuts. The yields and some properties of the residue fractions (+525°C, +575°C, +625°C, and +675°C) are shown in Table 1. Thermal hydrocracking experiments were performed in duplicate in a semi-batch 18-mL microautoclave for 30 min with 13.9 MPa hydrogen pressure and 3.0 L/min (STP) hydrogen flow rate. The reaction temperature and residence time were kept constant at 440°C and 32 min respectively. The product distribution is shown in Fig. 1. In this work, coke is defined as methylene chloride insolubles, asphaltenes as pentane insolubles, and maltenes as pentane soluble fractions.

The coking propensities of these fractions were determined using hot-stage microscopy. The detailed experimental procedures can be found elsewhere.⁴ Briefly, the experiments were conducted at a pressure of 750 psi at 440°C in the presence of nitrogen and hydrogen gases in order to determine the differences in mesophase induction period, mesophase size and growth rate as a function of gas used. The heating rate used was 11°C/min and the flow rate of the gas was kept at 35 mL/min. Photomicrographs were taken at regular intervals to illustrate the mesophase growth rate and optical texture. The long axis of each photo is 300µm.

RESULTS AND DISCUSSIONS

The bitumen upgrading chemistry is significantly influenced by the composition of the feedstocks. The understanding of the chemical transformation is difficult because of the complex nature of the resid. One way to simplify this complexity is by fractionating the resid into narrow distillate cuts and solubility classes. Some of the properties of the distillation residues from Athabasca bitumen are shown in Table 1. The data in this table show that as the distillate cuts increased, the molecular weight, MCR, asphaltenes, sulphur, nitrogen and the metals also increased. On other hand, there is only a small change in the aromaticity of the fractions as a function of boiling point.

The product distribution from the autoclave experiments is shown in Fig. 1. In this figure the coke yield is based on the weight percent of the feed processed. In general the coke, asphaltenes, and gas yield increased with increasing boiling point of the feedstocks. Since the asphaltenes are the major component of the residues, their conversion was

plotted as a function of boiling point. The asphaltene conversion [defined as $[\text{wt}\% \text{ asphaltene (in)} - \text{wt}\% \text{ asphaltene (out)}] / \text{wt}\% \text{ asphaltene (in)}$] is shown in Fig. 2. This figure shows that asphaltene conversion increases as boiling point increases. Obviously, some of the asphaltene is converted to coke (Fig. 3) but some liquid products can also be obtained from asphaltene decomposition. Production of liquid from asphaltene is in agreement with the findings of Speight,⁵ which showed that the thermal decomposition of asphaltene from Athabasca bitumen produced not only 40wt% coke but also produced a high yield of volatile products.

The coking propensity of the residues was also studied using hot-stage microscopy.⁶ The induction period, which is the period of time before the coke precursors (mesophase) are observed, is known to depend on the composition of the feedstock and most importantly on the concentration of asphaltene.² As shown in Table 1, the C₅ asphaltene content of the residues increased from approximately 32wt% to 56wt% (although not shown there is a corresponding decrease in the maltene fraction). Mesophase induction period as a function of boiling point is shown in Fig. 4. The results indicate that within the experimental error, the induction period for the boiling point fractions remained relatively constant under either hydrogen or nitrogen atmospheres. Although the asphaltene content of the fractions increased, no shortening of the mesophase induction period was observed. The maltene, although present at a relatively low concentration in the highest boiling point fraction, still has the ability to peptize asphaltene thus keeping them in the solution and prolonging the induction period.

Another important observation worth noting is the size and the optical texture of mesophase. Under hydrogen atmosphere, large mesophase were formed in all fractions. The ultimate result was the development of bulk mesophase having large domains and vacuoles (Fig. 5). Under nitrogen atmosphere, the size of mesophase remained small and the optical texture was fine-grained.⁷

REFERENCES

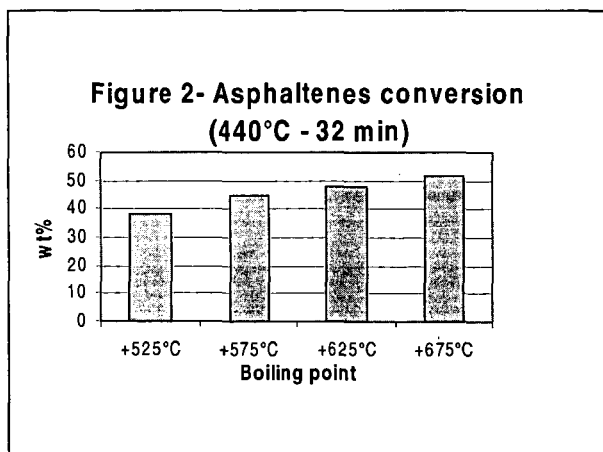
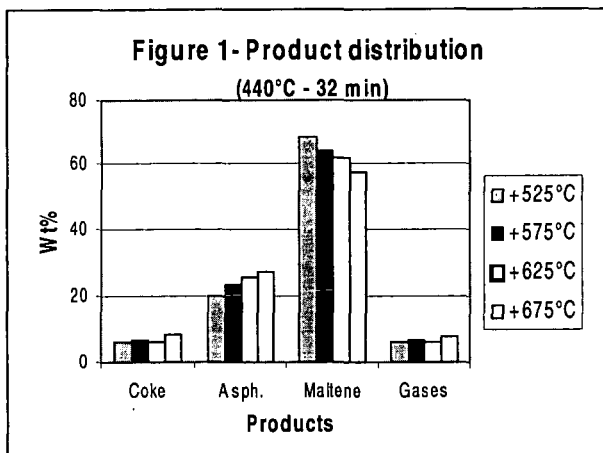
- 1- Storm, D.A., Barresi, R.J., Sheu, E.Y., Bhattacharya, A.K. and DeRosa, T.F. "Microphase behavior of asphaltic micelles during catalytic and thermal upgrading", *Energy & Fuels*, 1998, 12, 120-128.
- 2- Wiehe, I. A. "A phase separation kinetic model for coke formation", *Industrial Engineering Chemical Research*, 1993, 32, 2447-2454.
- 3- Clarke, P.F. and Pruden, B.B. "Asphaltene precipitation from Cold Lake and Athabasca bitumens", *Petroleum Science and Technology*, 1998, 16, 287-305.
- 4- Rahimi, P., Gentzis, T., Dawson, W.H., Fairbridge, C., Khulbe, C., Chung, K., Nowlan, V. and DelBianco, A. "Investigation of coking propensity of narrow cut fractions from Athabasca bitumen using hot-stage microscopy", *Energy & Fuels*, 1998, 12, 1020-1030.

- 5- Speight, J.G., "Thermal cracking of Athabasca bitumen, Athabasca asphaltenes, and Athabasca deasphalted heavy oil", Fuel, 1970, 49, 134-145
- 6- Rahimi, P., Gentzis, T., Khulbe, C., Fairbridge, C., Nowlan, V. and Cotté, E. "Effect of boiling point on the mesophase induction period during thermal treatment of Athabasca bitumen", 2nd International Conference on Refinery Processes, AIChE 1999 Spring National Meeting, Houston, TX, March 14-18, 515-519.
- 7- Rahimi, P., Gentzis, T. and Fairbridge, C. "Interaction of clay additives with mesophase formed during thermal treatment of solid-free Athabasca bitumen fraction", Energy & Fuels, 1999, in press.

Table 1. Properties of Athabasca bitumen distillate residues

Cut point	ASTM (D1160)	Distact Distillation*			
		+525 °C	+575 °C	+625 °C	+675 °C
Yield, wt%	50.8	75.6	67.6	62.2	
Mw, Dalton (VPO)	862	1890	2010	2565	
MCR, wt%	26.7	31.8	34.0	36.0	
Asphaltene, C ₅ , wt%	32.7	41.5	48.7	56.2	
Aromaticity, fa	0.41	0.38	0.40	0.40	
Sulphur, wt%	6.53	6.83	6.91	7.20	
Fe, ppm	994	989	1088	1217	
V, ppm	364	462	471	509	
Ni, ppm	148	183	186	209	

* The yield of distillate residues are based on +525°C feed



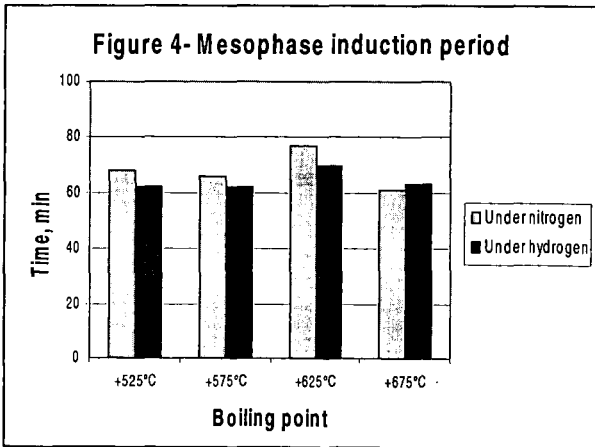
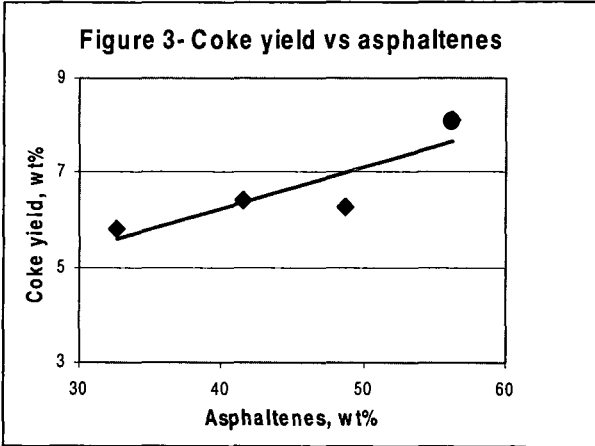
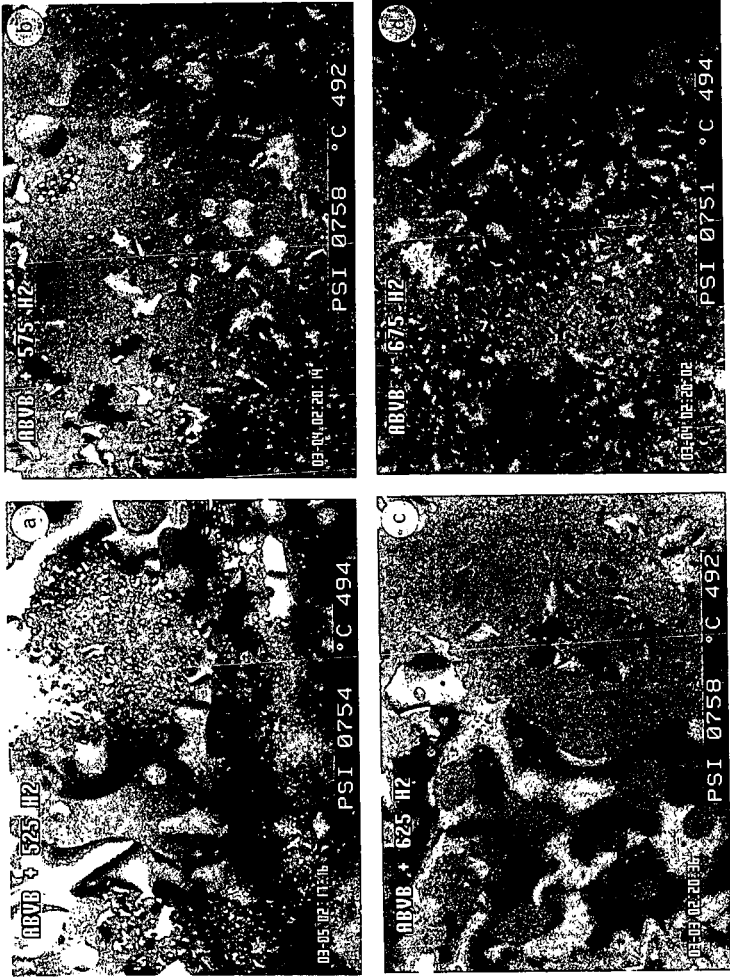


Figure 5 - Mesophase formation under hydrogen



THE INFLUENCE OF CARBONACEOUS ADDITIVES ON MESOPHASE FORMATION FROM ATHABASCA BITUMEN

Thomas Gentzis and Parviz Rahimi, National Centre for Upgrading Technology, 1 Oil Patch Drive, Suite A202, Devon, Alberta T9G 1A8 CANADA; and Ripudaman Malhotra and Al Hirschon, SRI International, 333 Ravenswood Ave, Menlo Park, CA 94025

ABSTRACT

The effect of carbonaceous additives (soot and coke) on the mesophase induction period, growth and coalescence of Athabasca bitumen vacuum bottoms fraction was investigated using hot-stage microscopy. Two types of soot materials and coke from a delayed coking operation at Fort McMurray, Alberta were used in this study. The soot #1 additive did not have a pronounced effect on the mesophase induction period and growth whereas soot #2 additive prolonged the induction period and resulted in very small mesophase (2-4 μ m) after 120 min. The results were rationalized in terms of the physical interaction between the soot particles and the mesophase spheres. Addition of coke resulted in the shortening of the mesophase induction period and the formation of relatively larger domains.

INTRODUCTION

During bitumen upgrading by thermal treatment for the production of synthetic crude oil, an undesirable by-product known as coke which is insoluble in most organic solvents is formed. Coke formation is believed to be the result of physical and chemical processes. In the process leading to coke formation, phase separation (Cartlidge et al. 1996) and asphaltenes flocculation (Storm and Sheu 1996) are known to occur initially. These occurrences are followed by chemical reactions such as radical polymerization and/or cyclization/dehydrogenation reactions (McMillen et al. 1994). Prior to coke formation, an intermediate phase known as mesophase is formed. The initial time of mesophase formation is referred to as *induction period* which is strongly dependent on the chemical composition of feedstocks (Rahimi et al 1998). Petroleum residua rich in asphaltenes are expected to have a very short induction period (Wiehe 1993) whereas materials containing no asphaltenes generally show a longer but variable induction period for mesophase appearance (Rahimi et al. 1998). Prolonging the induction period during bitumen upgrading has important implications for the upgraders as shown below:

- 1- Provides longer operation between scheduled shutdowns
- 2- Results in higher liquid yields (less coke)
- 3- Leads to a more efficient plant operation
- 4- Results in less GHG emissions

During thermal conversion of petroleum residua containing asphaltenes to distillable liquid products, an induction period prior to coke formation has been observed by numerous investigators. Prolonging the induction period has been attempted in a number of ways, such as the addition of a hydrogen donor (H-donor) to the feed, the addition of an aromatic gas oil, or the introduction of a donor-refined bitumen in

a pretreatment step (Speight 1999). Using hot-stage microscopy, the effect of a clay additive (kaolinite) on the mesophase induction period during the thermal treatment of Athabasca bitumen was studied at the National Centre for Upgrading Technology (Rahimi et al. 1999). The results showed that there was a small or no effect on the induction period. In the presence of kaolinite the size of mesophase was significantly smaller compared with the experiments where no additive was used. Furthermore, the work by Tanabe and Gray (1997) on the thermal hydrocracking of Athabasca bitumen vacuum bottoms at a relatively short reaction times (20-30 min) using an autoclave showed that the presence of solid additives also resulted in a 7-9wt% reduction in coke yield.

The objective of this study was to investigate the effect of solid carbonaceous additives such as soot and coke on the mesophase induction period during the thermal treatment of Athabasca bitumen vacuum bottoms.

EXPERIMENTAL

The Athabasca bitumen vacuum bottoms fraction (ABVB) used in this study was obtained by supercritical extraction using pentane (Rahimi et al. 1998). Soot #1 was obtained from Material and Electrochemical Research Corporation and used as received. Soot #2 was an experimental soot received from TDA Research and was extracted with toluene to remove the soluble portion prior to use. The coke sample used in these experiments was obtained from a delayed coking operation in Alberta.

The mixtures of additives and bitumen fraction were prepared first by dissolving bitumen in methylene chloride, then adding the appropriate concentration of soot #1 at 1wt%, soot #2 at 5wt% and coke at 5wt%, and then sonicating each mixture for 60 min. The mixtures were then allowed to dry under nitrogen stream and left in a vacuum oven at 60°C for 3h.

For hot-stage microscopy tests, small quantities of each mixture (5-10 mg) were placed in aluminum cups at the centre of the heated cell. The experiments were conducted in the presence of hydrogen atmosphere, at a flow rate of 35 mL/min. The gas pressure was 750 psi and the final temperature (dwelling temperature) was 440°C and 450°C. The rate of heating was kept constant at 11°C/min from room temperature to the desired temperature. For a detailed description of the experimental procedure, the reader is referred to Rahimi et al. (1998).

RESULTS AND DISCUSSION

The descriptions of photomicrographs obtained from hot-stage microscopy experiments on ABVB without and with additives are given below and shown in Fig. 1a-d.

ABVB fraction with no additive

The mesophase induction period ranged from 61 min at 450°C to 67 min at 440°C. Mesophase spheres formed, grew, and coalesced to produce large domains (Figure 1a). As was shown previously (Rahimi et al. 1998), in the presence of hydrogen gas, mesophase grew without restrictions. The formation of

mesophase from this solids-free residue may indicate that the presence of dispersed solids is not a prerequisite for the formation of anisotropic mesophase via the nucleation process as proposed by Tillmanns et al. (1978).

Mixture of ABVB with Coke

The mixture was characterized by a very short mesophase induction period: 45 min at 450°C and 53 min at 440°C. The sample appeared to be very reactive and fluid throughout the experiment. The results showed that, in contrast to the presence of clay additives (Rahimi et al. 1999), the presence of coke did not increase the viscosity of the isotropic matrix and did not restrict the movement of mesophase spheres. Mesophase was high viscoelastic and formed large optical domains (Figure 1b). The observed fluidity requires further investigation since it may be related to the role of the chemical composition of the coke (radical scavenging via hydrogen transfer).

It was further observed that in the early stages of the experiment, some mesophase disappeared in the isotropic matrix and reappeared shortly after which may indicate sinking and floating of the particle as its density changed relative to that of the isotropic matrix.

Mixture of ABVB with Soot #1

The mixture of the ABVB fraction and soot #1 at 1wt% resulted in the following mesophase induction period: 62 min at 450°C and 70 min at 440°C. These data indicate that the presence of soot at the above concentration did not have a significant effect on prolonging or shortening the induction period prior to mesophase formation. Mesophase spheres grew almost uninhibited and coalesced to form larger domains (Figure 1c). The observed mesophase texture shown in Fig. 1c is consistent with that reported by Matsumoto et al. (1977): the concentration of soot particles was too small to cover the surface of mesophase spheres completely. As a result the mesophase grew to form larger spheres.

Mixture of ABVB with Soot #2

The addition of soot #2 to the ABVB fraction resulted in a slight prolongation of the mesophase induction period. In this case, mesophase spheres first became visible at about 67 min at 450°C and 75 min at 440°C. The addition of this soot had a significant effect on the size, growth, and coalescence of mesophase and resulted in very small mesophase even after 120 min (Figure 1d). The apparent viscosity of this mixture was higher than the viscosity of bitumen-soot #1 mixture. This observation can simply be the result of the higher concentration of soot #2 used in the current experiment. As the concentration of soot increased from 1wt% to 5wt%, the size of mesophase became smaller and the size distribution more uniform because of the limited coalescence of the spheres (compare Figure 1c with Figure 1d).

Based on the above observations, it was concluded that the use of carbonaceous materials may have beneficial effects in terms of mesophase induction period (soot #2 additive) and in terms of possible chemical reactions that may reduce radical-radical combination (coke additive).

REFERENCES

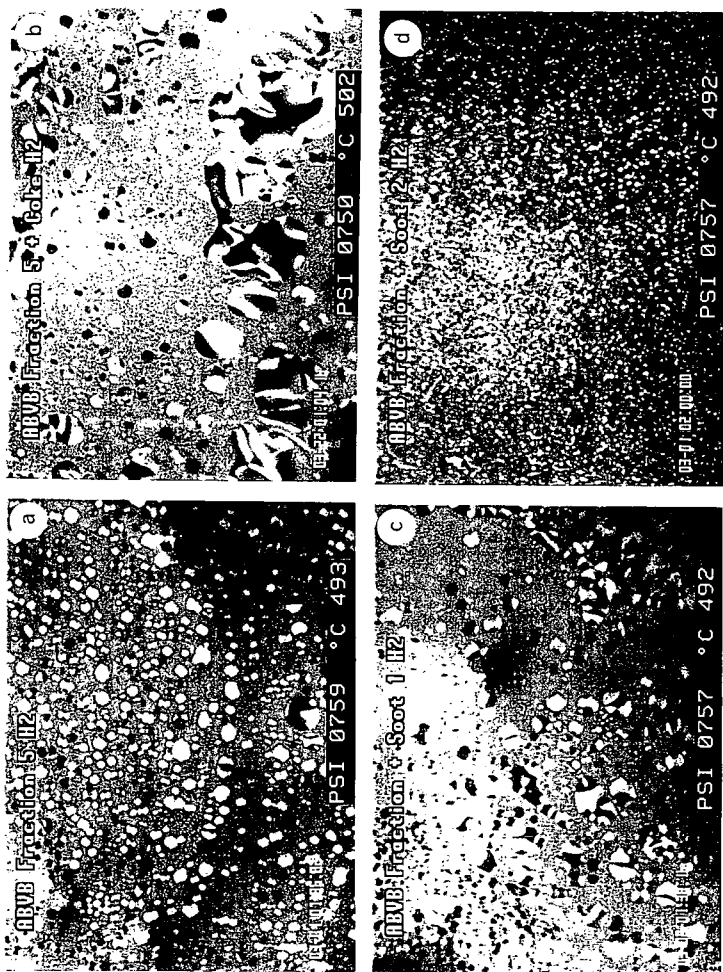
1. Carlidge, C.R., Dukhedin-Lalla, L., Rahimi, P.M., and Shaw, J.M. 1996. Preliminary phase diagram for heavy oil and bitumen mixtures, *Fuel Science and Technology International*, vol. 14, 1-2, p. 163-178.
2. Matsumoto, S., Oi, S., Inamura, T., Nakamizo, N., Yamada, Y., and Honda, H. 1977. Influence of a magnetic field on the molecular arrangement of mesophase spherules, 13th Biennial Conference on Carbon, July 12-18, Irvine, CA, U.S.A., p. 201-202.
3. McMillen, D.F., Manion, J.A., Tse, D.S., and Malhotra, R. 1994. Hydrogen transfer promoted ring growth during catalytic resid hydroprocessing, Preprints, ACS Division of Petroleum Chemistry, vol. 39, no. 3, p. 422-425.
4. Rahimi, P., Gentzis, T., and Fairbridge, C. 1999. Interaction of clay additives with mesophase formed during thermal treatment of solid-free Athabasca bitumen fraction, *Energy & Fuels*, *In Press*.
5. Rahimi, P., Gentzis, T., Dawson, W.H., Fairbridge, C., Khulbe, C., Chung, K., Nowlan, V., and Del Bianco, A. 1998. Investigation of coking propensity of narrow cut fractions from Athabasca bitumen using hot-stage microscopy, *Energy & Fuels*, vol. 20, no. 10, p. 1020-1030.
6. Speight, J.G. 1999. *Properties and Upgrading of Oil Sand Bitumen*, Course Material, February 1999.
7. Storm, D.A., and Sheu, E.Y. 1996. Flocculation of asphaltenes in heavy oil at elevated temperatures, Symposium on Thermodynamic of Heavy Oils and Asphaltenes, *Fuel Science Technology International*, vol. 14, p. 243-260.
8. Tanabe, K. and Gray, M. R. 1997. Role of fine solids in the coking of vacuum residues, *Energy & Fuels*, vol. 11, p. 1040-1043.
9. Tillmanns, H., Pietzka, G., and Pauls, H. 1978. Influence of the quinoline-insoluble matter in pitch on carbonization behaviour and structure of pitch coke, *Fuel*, vol. 57, p. 171-173.
10. Wiehe, I.A. 1993. A phase-separation kinetic model for coke formation, *Industrial & Engineering Chemistry Research*, vol. 32, no. 11, p. 2447-2454.

DESCRIPTION OF PHOTOMICROGRAPHS

All photos were taken in reflected light. The long axis of each photo is 300 μ m.

- Figure 1a: Formation of anisotropic mesophase spheres from the ABVB fraction in the absence of additives.
- Figure 1b: The presence of coke in the ABVB fraction resulted in the development of larger domain bulk mesophase in a highly fluid matrix.
- Figure 1c: Soot #1 did not influence the formation or the size of mesophase from the ABVB fraction.
- Figure 1d: The addition of Soot #2 to the ABVB fraction resulted in the formation of much smaller mesophase spheres than with either Soot #1 or coke.

Figure 1 – Mesophase formation in the absence and presence of coke and soot additive



MAXIMIZING CYCLE LENGTH OF VACUUM RESIDUE HYDRODESULFURIZATION UNIT

S. Kressmann¹, V. Harlé², S. Kasztelan², J. Guibard¹, P. Tromeur³, F. Morel¹

IFP,

¹ Centre d'Études et de Développement Industriel "René Navarre",
B.P. 3, 69390 Vernaison, France.

² Division Cinétique et Catalyse, 92852 Rueil-Malmaison Cedex, France.

³ Division Industrielle, 92852 Rueil-Malmaison Cedex, France.

ABSTRACT

Achievement of long cycle length is an important objective for the refiner operating a vacuum residue hydrodesulfurization unit. The fixed bed technology generally used for this purpose requires a specific design such as swing/permutable reactors as well as the use of sophisticated associations of catalysts to reach a long cycle length and constant low sulfur content in the products. In particular, it is shown that the stability of the refining catalyst is a key parameter to improve the run length while keeping a high level of hydrodesulfurization. An efficient HDS catalyst has been designed to respond to this demand and also recommendations to conduct the operation of the VRDS unit have been mentioned.

INTRODUCTION

Atmospheric residue (AR) and vacuum residue (VR) are the most difficult feed to be treated catalytically under hydrogen pressure because they contain all the impurities present in the crude oil and among them, asphaltens and metals (1-3).

The hydrodesulfurization of vacuum residue is nowadays carried out with well-established upgrading process using usually fixed bed technology (4-6). The objectives of the refiner are mainly to desulfurize and to convert the vacuum residue in order to produce a stable low sulfur fuel oil (LSFO) according to the specifications of the market. This objective is driven by an increasing demand for LSFO, residue FCC feed and an increasing needs for clean transportation fuels (gasoline and diesel).

One main aim of the refiner is to maintain cycle length of the Vacuum Residue DeSulfurization (VRDS) unit as long as possible. This is a major challenge for fixed bed technology because, as it is well known, the asphaltens and metals are concentrated in the still bottom and therefore the deactivation of conventional hydrotreating catalysts is strongly enhanced during the treatment of vacuum residue.

Several process technologies have been introduced to improve cycle length of VRDS units such as the moving bed technology (7-8), ebullated bed technology (11) and Swing/Permutable fixed bed reactors (4-6, 9). To increase the cycle length on vacuum residue and improve the protection of downstream HDS catalyst, a concept of fixed bed VRDS process including a permutable-swing guard reactors system has been developed by IFP (HYVAHL process, Figure 1, see also reference 9) and is industrially proven. The process scheme includes permutable fixed bed guard reactors that can be switched in operation allowing the possibility to isolate temporally one reactor for change out of the guard HDM catalyst.

However, in order to maximize the HDM and HDS performances of the unit and to maintain the stability, it is now well recognized that associations of several catalysts with different functions are also mandatory (9). One typical association comprises three types of catalysts :

- a HDM catalyst for the metal removals in front of the unit,
- a HDM/HDS catalyst with balanced HDS and HDM activities,
- a very active and stable HDS catalyst in the last section.

The HDM catalyst has the objective to remove the metals contained in the feed and as a consequence to protect the downstream catalysts from metal deposits. A special porous structure designed for this purpose is the so-called "chestnut-burr" structure (10) in which the porosity has been adjusted to allow access of the heavy molecules to the active phase and to get a high porous volume to accommodate metals deposits accumulated during a minimum of one year of operation. In addition, the coke deposit due to the conversion of asphaltens and resins is minimized by using a low acidity alumina base (10) The stability of this system has been already

reported (5, 6, 10) and can maintain during a long period a good HDM activity on vacuum residue (4-5).

The aim of the second HDM/HDS catalyst is to continue with the demetallization and to begin the desulfurization step. It is in general a large mesoporous monomodal catalyst. The HDS catalyst located in the third and last section is the catalyst for deep refining which remove the sulfur content in the effluent.

In this paper we shall discuss the need for a specifically designed HDS and also the optimum way to carry out this catalyst for improving the cycle length of VRDS unit.

EXPERIMENTAL

HDS Catalyst has been tested in a pilot unit using a demetallized feedstock obtained after the demetallization section and the equilibrium HDM/HDS catalyst section. The pilot unit is a one-liter reactor working in isothermal configuration. The average temperature is calculated from the temperature measurements made in the catalyst bed.

The Arabian vacuum residue (Table 1) previously demetallized contain 3.6 wt% of sulfur and 100 wt ppm of Ni+V. Different severities have been applied to this primary feed in order to obtain three level of demetallization. The analyses of these three demetallized feeds are shown in Table 1 (references : charges 1, 2 and 3). The metals content are ranging from 9.3 to 16.5 wppm and the sulfur content varies from 0.98 to 1.8 wt % depending of the severity of the HDM and equilibrium HDM/HDS section.

The demetallized feeds (charges 2 and 3) with high sulfur and metals content was used to age quickly the HDS catalyst. Dimethyl disulfide was added to the demetallized feeds to generate H₂S in order to be representative of the gas phase composition at the outlet of the previous reactors.

The sulfur compounds of the demetallized feeds are mainly present in asphaltens and aromatics and are therefore very difficult to be desulfurized. Thus, the residence time of the HDS section is around twice more important than in HDM and HDM/HDS section (Figure 2). This residence time of the HDS section must be optimized depending of the HDS done in the two first sections. Thus, for HDS section, we have carried out some variations of LHSV for kinetic studies. The catalyst deactivation for HDS has been evaluated by a correction of LHSV using a kinetic order of reaction. Moreover, for each change of demetallized feeds, we have checked the catalyst activity by using the same Arabian light straight run atmospheric residue feed. The temperature was adjusted in order to maintain on A.L. A.R. a minimum of 90 % of HDS. This procedure was done all along the test and also has the aim to evaluate the reactivity of each demetallized vacuum residue.

RESULTS AND DISCUSSION

HDS catalysts are often based on high specific surface area carriers with monomodal pore size distribution. It has been found that monomodal catalysts have different selectivities for the HDM and HDS functions depending on the size of the mesopores (HDM=60 %, HDS=90 % on A.L. A.R. for HDS catalyst). An increase of the mean average mesopore diameter leads to a decrease of the HDS and an increase of the HDM performance (HDM=77, HDS=85 %, on A.L. A.R.). This change HDS vs. HDM activity results from the variation of BET surface area and also the change in the level of diffusional limitations. In addition, as the mean average mesopores increases, the penetration of resins, which contain metals, is more important leading to an increase of HDM and therefore a higher rate of deactivation of HDS function. A compromise in term of mean mesopore diameter has to be found between high activity and high diffusional limitations. This has be done to develop a specific HDS catalyst. Performances on demetallized vacuum residue that can be reached with this catalyst are developed in the following.

In Figure 3, the sulfur content of the product from the HDS reactor is plotted versus hours on stream (HOS). The reactor temperature increase is also plotted in Figure 3 showing the deactivation of the HDS catalyst. We have tried during the run to maintain the severity of the HDS section to reach a sulfur content at the reactor outlet around 0.4 to 0.5 wt %. For the first 2000 hours and also during 75% (in hours) of the test, the LHSV is the same than the base. By consequent, 25 % of the points had to be corrected for the LHSV variation.

In Figure 3, we have indicated when we have switched on A.L. A.R. in order to check the catalyst activity for the temperature adjustment if necessary. The total HOS using demetallized feeds from vacuum residue can be evaluated to around 5600 hr, so 75 % of the overall H.O.S.

The overall deactivation of the HDS catalyst on demetallized feed can be estimated if we compare the activity on the same charge (charge 1) from the end of run to the start of run. We begin at 360°C and finish at 390°C for 5600 hours of run on demetallized vacuum residue. The behavior of this HDS catalyst is in line with the expected cycle length of an industrial unit. The end of run temperature of an industrial unit is usually around 415°C. So, the HDS catalyst could reach at least one year of cycle length on pure A.L. V.R.

The use of charges 2 and 3 (metals content around 16 wppm) shows that the slope of deactivation for HDS catalyst doesn't increase even during 4000 HOS on these charges. The HDS catalyst achieves this task because of its monomodal structure protecting the catalyst sites for HDS. This system demonstrates its flexibility in case of problem in HDM section.

Figure 4 shows the calculated temperature to obtain a constant sulfur content (0.45 wt %) of the reactor outlet effluent from HDS section. This temperature was calculated by assuming a constant activation energy along the test.

After 2000 hours, the HDS catalyst is more stabilized and the deactivation becomes lower. An interpretation could be that the A.L. A.R. washes the catalyst by removing one part of the coke. In Figure 4, we have observed that we recovered the slope of HDS deactivation on demetallized vacuum residue after only 200 hour. This effect has been observed at 3000 HOS and 4000 HOS. Thus, we expect to extend the cycle length of the HDS catalyst by suggesting to work in block operation (switch between A.R. and V.R.). We also observed that the slope of desactivation for HDS is lower after this washing period than during S.O.R. This observation confirms also that overall deactivation of HDS catalyst must be calculated only on demetallized vacuum feeds (75 % HOS of the run).

CONCLUSION

The upgrading of vacuum residue to obtain a constant fuel oil quality can be improved by using a complex association of catalysts with particle size, pore size distribution and activity grading. The improvements come from a better optimization of each catalyst and the association of different selectivity in term of HDM/HDS. The synergy effect has been demonstrated and two commercial units are running under this concept. The use of adapted design HDM catalysts and monomodal catalysts for HDS objective insure the stability of the system. Monomodal catalysts for HDS section permit to achieve the goal of a constant sulfur in fuel oil with a run length cycle of at least one-year on Arabian vacuum residue feedstock. The possibility for the refiner to work by block operation (switch between A.R. and V.R.). has certainly a good impact for increase the cycle length.

REFERENCES

1. T. Ohtsuka, *Catal. Rev. Sci. Eng.*, 16, 291, (1977).
2. W.I. Beaton; R.J. Bertolacini, *Catal. Rev. Sci. Eng.*, 33, 281, (1991).
3. H. Koyama, E. Nagai, H. Torii, H. Kumagai, *Stud. Surf. Sci. Catal.*, 100, 147, (1996).
4. F. Morel, S. Kressmann, V. Harlé, S. Kasztelan, *Stud. Surf. Sci. Catal.*, 106, 1, (1997).
5. A. Billon, J.P. Peries, M. Espeillac, T. des Courrieres, NPRA 89th Annual Meeting, San Antonio, March 17-19, 1991.
6. A. Billon, G. Henrich, A. Hennico, *Pétrole et Techniques*, n°388, mai-juin 1994.
7. B.E. Reynolds, J.L. Rogers, R.A. Broussard, NPRA Annual Meeting, San Antonio, March 16-18, 1997.
8. B. Scheffer, K.W. Robschlagel, F.C. de Boks, Preprints of ACS San Francisco CA, April 13-17, 1997, 347-350
9. S. Kressmann, F. Morel, V. Harlé, S. Kasztelan, *Catalysis Today*, 43, 1998, 203-215
10. H. Toulhoat, R. Szymansky, J.C. Plumail, *Catal. Today*, 7, 1990, 531.
11. S. Kressmann, J. Colyar, E. Peer, A. Billon, F. Morel, 7th Unitar Conference, Beijing, China, October 27-30, 1998, 857-866

Table 1

FEEDS :	S.R. Arabian A.R.	SR Arabian V.R.	Charge 1	Charge 2	Charge 3
Specific gravity	0.959	1.017	0.967	0.980	0.982
Sulfur (wt %)	3.34	3.68	0.98	1.23	1.80
Nitrogen (wppm)	2075	3610	3305	3200	3000.0
Hydrogen (wt %)	11.20	10.48	11.32	11.36	11.23
Nickel (wppm)	9.3	20.0	5.5	7.8	7.7
Vanadium (wppm)	35.0	80.0	3.8	8.7	8.1
Total of metals (wppm)	44.3	100.0	9.3	16.5	15.8
Viscosity @ 100°C	25.6	1028	90.6	182	138
Conradson carbon (wt %)	9.5	19.8	11.3	13.2	13.0
Asphaltenes C5 (wt %)	5.6	12.9	4.3	5.4	5.6
Asphaltenes C7 (wt %)	3.1	6.2	1.6	1.5	1.8
Saturates (wt %)	30.7	10.2	22.4	18.1	18.2
Aromatics (wt %)	47.5	45.8	47.8	51.2	50.4
Resins (wt %)	17.6	34.6	22.9	26.0	25.4
ASTM D2887					
IBP (°C)	300	385	182	223	234
T(°C) for 5 wt %	325	533	330	433	403
T(°C) for 10 wt %	358	554	426	498	468
T(°C) for 20 wt %	404	580	514	546	518
T(°C) for 30 wt %	436		553	572	547
T(°C) for 40 wt %	468		577	594	572
T(°C) for 50 wt %	503		602		596
EBP (°C)	720	600	620	613	614
wt % EBP	92	25	58	49	57

Figure 1

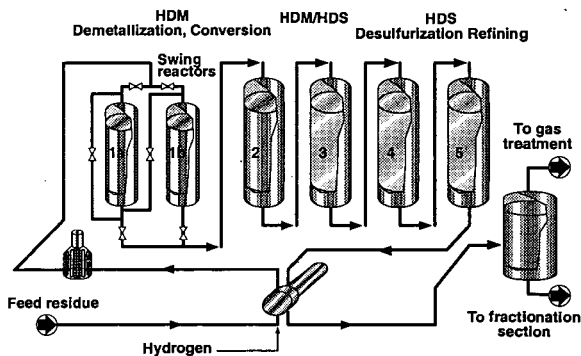


Figure 2

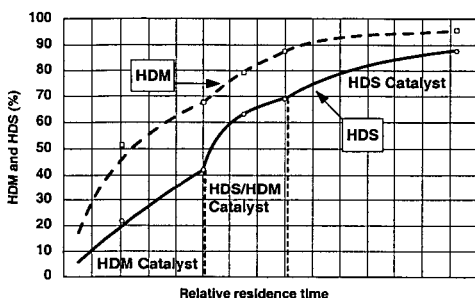


Figure 3

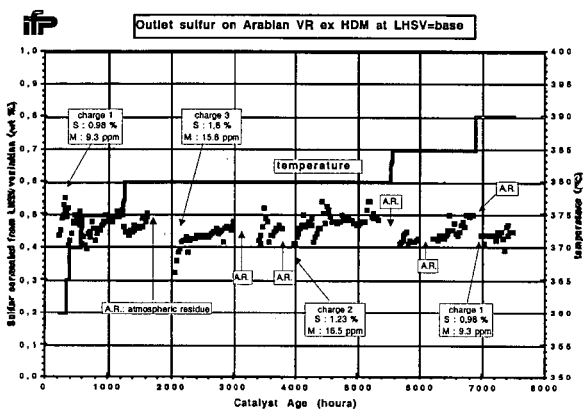
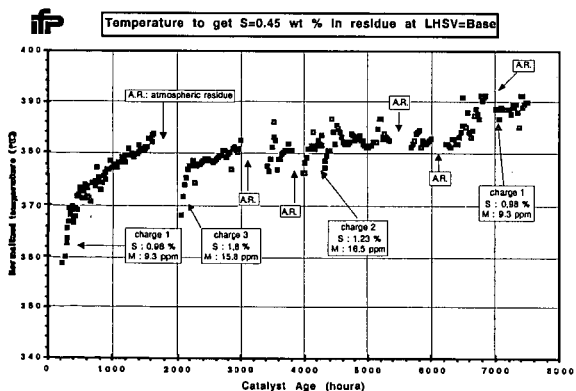


Figure 4



PILOT PLANT STUDY OF THE PERFORMANCE OF AN INDUSTRIAL $\text{MoO}_3/\text{Al}_2\text{O}_3$ CATALYST IN HYDROTREATMENT OF KUWAIT ATMOSPHERIC RESIDUE

A. Stanislaus¹, S.Fukase², R. Koide², A. Al-Barood¹, A. Marafi¹, F. Al-Jasem¹,
and M. Absi-Halabi¹.

- (1) Petroleum Technology Department, Kuwait Institute for Scientific Research, P.O.Box 24885, Safat, 13109, Kuwait
(2) Kuwait Branch Laboratory, Petroleum Energy Center Japan, C/O Kuwait Institute for Scientific Research, P.O.Box 24885, Safat, 13109, Kuwait

INTRODUCTION

Graded catalyst systems with two or more types of catalysts are used in recent years in multiple reactor fixed-bed residue hydrotreaters to achieve demetallation (HDM), desulfurization (HDS) and denitrogenation (HDN) together with conversion of residues to distillates at desired levels(1,2). Rapid catalyst deactivation is reduced and the on-stream efficiency is increased with such multiple catalyst systems. Since the overall performance of the process with regard to various conversions and catalyst life is strongly tied up with the performance of the catalysts in different reactors, information on the activity, selectivity and deactivation rate of individual catalysts is highly desirable for optimizing reactor loading with such multiple catalyst systems. In the present work, we have examined the performance of an industrial HDM catalyst containing MoO_3 alone on alumina in hydrotreating Kuwait atmospheric residue in a fixed-bed pilot plant. Systematic studies were conducted to assess the activity and selectivity of the catalyst for various reactions such as HDM, HDS, HDN, asphaltenes conversion and hydroconversion of the residual oil feed to distillates. The reaction kinetics in residual oil hydrotreating was also investigated as part of the study.

EXPERIMENTAL

The hydrotreating experiments were conducted in a fixed-bed reactor unit (manufactured by Vinci Technologies) using Kuwait atmospheric residue as feed. The feedstock contained 4.3 wt% sulfur, 69 wtppm vanadium, 22 wtppm nickel, 0.31 wt% nitrogen, 3.6 wt% asphaltenes and 12.2 wt% CCR. A commercial HDM catalyst containing 4.3 wt% MoO_3 on alumina (surface area = 200 m^2/g ; pore volume = 0.67 ml/g) was used in all experiments. 50 ml catalyst charge diluted with an equal amount of carborundum was used for each run. The catalyst was presulfided using straight run gas oil containing 3 wt% dimethyl disulfide (DMDS) by a standard procedure before injecting the feed. The run conditions used for different studies are summarized in Table 1. During the course of each run, product samples were collected every 12 hours and analyzed for sulfur, metals (V and Ni), nitrogen, asphaltenes, CCR, viscosity, density and distillates yield.

Table 1. Run Conditions for Temperature and LHSV Effect Studies

Process Parameter	Range	
	Temperature Effect Study	LHSV Effect Study
Temperature ($^{\circ}\text{C}$)	360 - 420	380
Pressure (bar)	120	120
LHSV (h^{-1})	1	0.5 - 4.0
H_2/Oil Ratio (ml/ml)	570	570
Time-on-stream(h)	120	120

RESULTS AND DISCUSSION

In the first set of experiments reactor temperatures were varied in the range 380 – 420 °C to investigate the performance of the HDM catalyst in promoting various reactions such as HDM, HDS, HDN, asphaltenes conversion, CCR reduction and hydrocracking of residues to distillates as well as to examine the deactivation behavior of the catalyst at different temperatures.

In Fig. 1 the desulfurization data for different temperatures are plotted as a function of time-on-stream. It is seen that the extent of desulfurization is very low (around 20%) at 360 °C and increases substantially with increasing temperature reaching about 65% at 420 °C. An interesting observation that can be made in the results presented in Fig. 1 is a gradual increase in the degree of HDS with increasing time-on-stream. The HDS activity is usually expected to decrease with time during the early period of operation due to rapid initial deactivation of the catalyst. But in the present study the HDS activity shows an increase with increasing run time, probably because of the accelerating effect of nickel deposited on the catalyst surface.

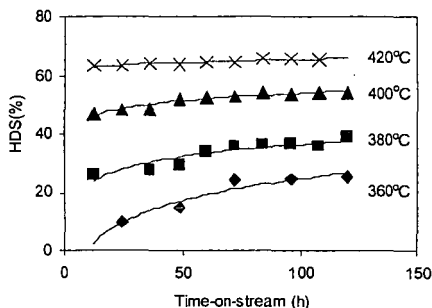


Fig. 1 Sulfur removal vs time-on-stream at different reactor temperatures

The data presented in Fig. 2, which compares the catalysts activity for various reactions such as HDS, HDV, HDNi, HDN and asphaltenes conversion that occur during residual oil hydrotreating shows the following order:



The low activity catalyst containing unsupported MoS_2 on alumina with large pores used in the present study appears to favor HDM and asphaltenes cracking reactions which are more diffusion limited than other reactions. The higher activity of the catalyst for HDM and asphaltenes conversion reactions can, thus, be attributed to the large pores in the catalyst which facilitates the diffusion of large metal containing molecules and asphaltenes into the catalyst pellet. The enhanced reactivity of vanadium relative to nickel may be attributed to a combination of factors resulting from the chemistry of oxygen ligand in vanadyl (VO^{2+}) group(3).

In the second set of experiments, the liquid hourly space velocity (LHSV) of the feed was varied in order to investigate the kinetics of various reactions in residual oil hydrotreating. The kinetics of petroleum residue hydrotreating is highly complicated due to the complex composition of the residues which includes high concentrations of asphaltenes, sulfur, nitrogen and metals (V and Ni). The low diffusivities and reactivities for these large molecular species make the kinetics of the process further complicated.

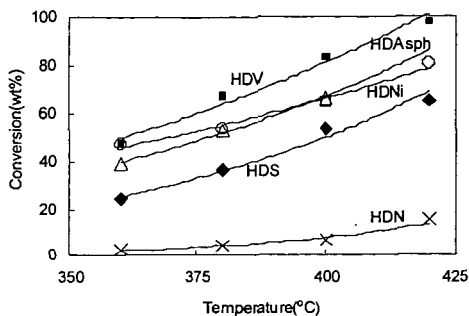


Fig. 2 Comparison of catalyst's activity for various reactions in hydrotreating of Kuwait atmospheric residue

In the present studies, the conversion data generated for various reactions at different space velocities were used to determine the reaction order for different reactions such as HDS, HDV, HDNi and asphaltenes cracking that occur during residual oil hydrotreating. The results presented in Fig. 3 show that HDS and asphaltenes cracking reactions obey second order kinetics. The activation energies calculated from the Arrhenius plots in Fig. 4 are 26.1 kcal/mole for HDS and 23.6 kcal/mole for asphaltenes eracking reactions.

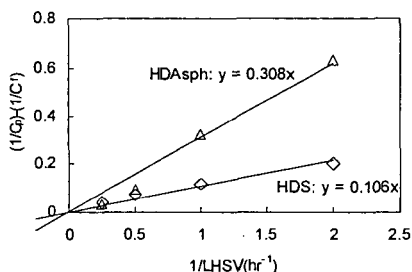


Fig. 3 Second-order plot of kinetic data for HDS and HDAsph of Kuwait atmospheric residue

The plots of kinetic data for vanadium and nickel removal shown in Figs. 5 indicate that a reaction order of 1.5 gives the best fit in correlating kinetic data for HDM reactions. Demetallation kinetic orders varying from 1.0 to 2.0 have been reported by different workers(3). In the case of model compound demetallation studies with pure metalloporphyrins, first order kinetics have been reported for both vanadium and nickel removal. In the present work a reaction order of 1.5 is observed for vanadium removal from Kuwait atmospheric residue. Just as in hydrodesulfurization, several first order reactions with different rates can occur due to the presence of more than one class of metal compounds in the residual oil. This can lead to an apparent order greater than unity.

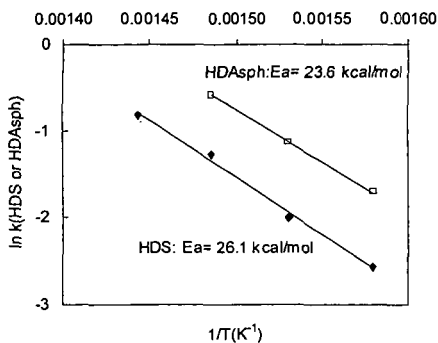


Fig. 4 Arrhenius plot for HDS and HDA sph

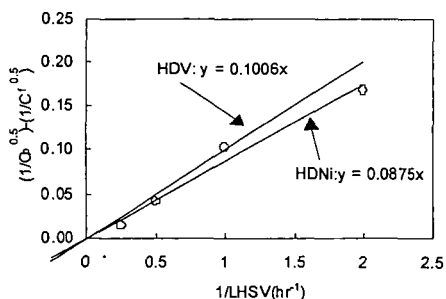


Fig. 5 1.5-order plot of kinetic data HDV and HDNi of Kuwait atmospheric residue

The Arrhenius plots of $\ln k$ vs $1/T$ for both vanadium and nickel removal reactions (Fig. 6) show a sharp increase in the reaction rate at temperatures above 400 °C with two different activation energy values, namely 27.7 and 62.2 kcal/mole for vanadium and 12.5 and 28.9 kcal/mole for nickel.

Apparent activation energy values reported in literature for vanadium removal from residues by HDM reaction range from 10 to 38 kcal/mole depending on the reaction order(3). The discrepancies observed in the activation energy values may reflect differences in crude source resulting in different reactivities of metal containing species and different rate limiting steps. The sharp increase in activation energy for HDM reactions at temperatures above 400 °C is considered to be due to a combination of factors such as improved diffusion and change in reaction mechanism.

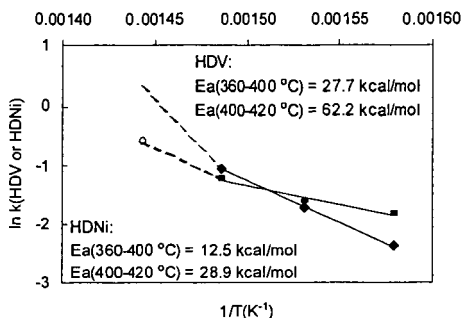


Fig. 6 Arrhenius plots for HDV and HDNi

CONCLUSIONS

Pilot plant studies were conducted to investigate the activity and selectivity of an industrial HDM catalyst for various reactions such as HDS, HDM, HDN, asphaltenes conversion and hydroconversion of residual oil feed to distillates as well as to examine the reaction kinetics in residual oil hydrotreating. The catalyst showed a remarkably high activity for HDM and asphaltenes cracking reactions and a moderate activity for HDS. Its activity for HDN, hydrogenation and hydroconversion reactions was very low. HDS activity increased with time on stream probably because of the promotional effect of nickel deposited on the catalyst surface. Kinetic data analysis showed 2nd order for HDS and asphaltenes cracking and 1.5 order for HDV and HDNi reactions. The apparent activation energies for HDS and asphaltenes cracking reactions were, respectively 26.1 and 23.6 kcal/mole. Arrhenius plots for HDV and HDNi reactions showed a sharp increase of the reaction rate constants at temperatures above 400 °C with two different activation energy values, namely, 27.7 and 62.2 kcal/mole for nickel. The increase in the activation energy of the HDM reactions above 400 °C is considered to be due to a combination of factors such as improved diffusion and change in reaction mechanism.

ACKNOWLEDGEMENT

This work is a joint research project between Petroleum Energy Center (funded by the Ministry of International Trade and Industry), Japan, and Kuwait Institute for Scientific Research, Kuwait. It bears the KISR Project No. PF010C.

REFERENCES

- (1) Bartholdy, J. and Cooper, B. H., *Stud. Surf. Sci. Catal.*, 100, p.117(1996)
- (2) Yamamoto, U., Mizutami, Y., Shibata, Y., Kitou, Y., Yamazaki, H., *Stud. Surf. Sci. Catal.*, 100, p.181(1996)
- (3) Quan, R. J., Ware, R. A., Hung, C. W., Wei, J., *Adv. Chem. Eng.*, 14, p.95(1988)

CHARACTERISATION OF COKE ON DEACTIVATED HYDRODESULFURISATION CATALYSTS AND A NOVEL APPROACH TO CATALYST REGENERATION

Colin E. Snape, Youva R. Tyagi, Miguel Castro Diaz, Peter J. Hall, Ian P. Murray and Shona C. Martin.

University of Strathclyde, Department of Pure and Applied Chemistry,
Thomas Graham Building, 295 Cathedral Street,
Glasgow G1 1XL, Scotland, UK

Keywords: Hydrodesulfurisation catalysts, coke, hydropropylolysis

ABSTRACT

The soft (chloroform-extractable) and hard coke fractions from a suite of deactivated Co/Mo hydrodesulfurisation (HDS) catalysts with carbon contents ranging from 5 to 18% have been characterised. The hard coke accounted for between 50 and 70% of the total carbon, but was responsible for much less of a reduction in BET surface area as the carbon content increased. Indeed, significant variations in structure were revealed by solid state ^{13}C NMR with the aromaticity ranging from 0.6 to over 0.9 with increasing carbon content and time on stream. The relatively high aliphatic contents and atomic H/C ratios for the hard cokes obtained at low levels of carbon deposition (5-7%) suggested that much of the carbon should be removed under reductive conditions. Indeed, hydropropylolysis, in which the deactivated catalysts were heated from ambient to 500°C under a hydrogen pressure of 15 MPa, removed over 90% of the carbon and recovered 70% of the BET surface that had been lost.

INTRODUCTION

Deactivation via coke deposition affects all the catalysts used in hydrocarbon conversion processes with the timescale varying from just a few seconds for fluid catalytic cracking (FCC) of heavy petroleum feeds to several months for naphtha reforming and gas oil hydrotreating. For the latter, controlled oxidation is the established means of regeneration to remove coke (see, for example, refs. 1-3 for hydroprocessing catalysts). However, despite the use of slow heating rates and low oxygen environments, some loss of surface area is inevitably encountered for Ni/Mo and Co/Mo γ -alumina-supported hydroprocessing catalysts and other deleterious effects have been observed, including the loss of Ni promoter due to spinel NiAl_2O_4 formation⁽⁴⁾.

Thus far, non-oxidative treatments in the form of reductive heating⁽⁴⁾ and solvent extraction⁽⁴⁻⁶⁾ have received very little attention because they only remove the adsorbed oil that comprises the soft or soluble portion of the coke. For example, Teixeira daSilva *et al.*⁽⁴⁾ using a nitrogen/hydrogen mixture for reductive heating after acetone extraction reduced the carbon content of a spent catalyst from hydroprocessing shale oil by approximately 35%. Traditionally, the insoluble or hard coke is considered to be highly intractable aromatic in character even for hydrotreating catalysts operating at relatively low temperatures. To investigate whether or not this is the case, the soft (chloroform-extractable) and hard coke fractions have been characterised for a suite of deactivated Co/Mo HDS catalysts with carbon contents ranging from 5 to 18%. The fact that solid state ^{13}C NMR indicated that the hard coke is normally quite aliphatic and contains small aromatic clusters prompted us to use fixed-bed hydropropylolysis for the reductive regeneration of the catalysts where they were heated from ambient to 500°C under a hydrogen pressure of 15 MPa. This technique typically gives rise to conversions of over 90% for sedimentary organic matter, including low-rank coals and petroleum source rocks (type I and II kerogens)⁽⁷⁾. It has been adapted as an analytical procedure for determining the distribution of organic sulfur forms from H_2S evolution profiles^(7,8) and for covalently-bound biomarkers^(7,9,10). Since the temperatures used in hydropropylolysis are potentially lower than in oxidative combustion regeneration, there is the potential that the irreversible loss of surface area can be reduced which offers the possibility of extending catalyst lifetimes and helping to solve the ever-growing disposal problem for spent catalysts.

EXPERIMENTAL

Ten deactivated Co/Mo HDS catalysts, differing in terms of the run time and catalyst bed position, were supplied by BP/Amoco. The carbon contents of the catalysts investigated are listed in Table 1. Samples 1-7 are at different bed heights in the same operation. The final sample (no. 10) with a carbon content of 18% was obtained from a unit that had been left running for 8 years. All the catalysts were extracted in chloroform under reflux to recover the soft coke for

characterisation (designated soft coke I). To isolate the hard coke, one of the low (no. 8) and the high carbon (no. 10) chloroform-extracted catalysts were demineralised using HF/HCl as used previously on FCC catalysts^(11,12). A final wash with dilute nitric acid (2M at 70°C) was required to dissolve the metal sulphides. The hard coke concentrates (carbon contents > 50%) were then extracted in chloroform with the extracts being designated soft coke II.

Carbon, hydrogen and nitrogen contents of the initial deactivated catalysts, the soft coke fractions and the hard coke concentrates were determined using a Perkin-Elmer 2400 analyser and sulphur contents were measured using the Sulphazo III method. BET measurements were carried out using a Micromeritics ASAP 2000 apparatus on the deactivated catalysts before and after chloroform extraction and on two of the hard coke concentrates. A Bruker 250 MHz instrument was used to obtain the ¹H NMR spectra of the soft cokes in chloroform-d. HPLC analysis was carried out using Shandon Scientific Hypersil CTA column in conjunction with a Waters 486 UV detector. The soft cokes were separated into aliphatic, aromatic and polar fractions by open column adsorption chromatography using activated silica gel. Size exclusion chromatography (SEC) was carried out to estimate the number and weight average molecular masses (M_n and M_w) of the soft cokes based on polystyrene standards, a mixed bed PL gel column being employed with RI detection and chloroform as the eluting solvent.

The solid state ¹³C NMR measurements on the hard coke concentrates were carried out at 25 MHz on a Bruker MSL 100 spectrometer with MAS at 4.5-5.0 kHz to give spectra in which the sideband intensities are only ca. 6-7% of the central aromatic bands. A contact time of 1 ms was used for the cross polarisation (CP) measurements and the ¹H decoupling and spin-lock field was ca. 60 kHz. The FIDs were processed using a Lorentzian line broadening factor of 50 Hz. To determine the fraction of protonated and non-protonated carbon, four delay periods between 1 and 100 μ s were employed in dipolar dephasing experiments.

Fixed-bed hydrolysis tests at 15 MPa were conducted using either ca. 0.5 or 1 g of sample for the low and high carbon deactivated catalysts selected for detailed investigation. For some tests, the deactivated catalysts (extrudates) were ground and diluted in sand. The procedure used has been described elsewhere^(7,9,10), a slow heating rate of 5°C min⁻¹ being used to maximise conversion.

RESULTS AND DISCUSSION

Characteristics of the soft coke

The soft coke obtained from the as-received catalysts accounts for between 25 and 50% of the total carbon with the mean being close to 35% (Table 1). Thus, the high carbon in the case of sample no. 10 does not markedly affect the distribution of soft to hard coke. After demineralisation, further extract was obtained (soft coke II) but the yield was typically no more than ca. 3% of the total carbon. Table 2 summarises the analytical data obtained for the chloroform extracts obtained from both the as-received catalysts (soft coke I) and after the demineralisation treatment (soft coke). Overall, the H/C ratios, heteroatom contents, molecular masses and compound class distributions indicate that the easily extractable soft coke can be described as "heavy and generally polar gas oil" (Table 2). The gas chromatographic profiles comprised broad unresolved shoulders containing small peaks from *n*-alkanes. ¹H NMR indicated that the soft cokes have low aromaticities (6-8 mole % aromatic hydrogen) consistent with their relatively high aromatic H/C ratios (Table 2). Both HPLC and ¹H NMR indicated that the average ring size is quite small (1-2 rings as for initial gas oil).

The relatively small quantities of soft coke physically entrapped within the pore structure that were amenable to extraction after demineralisation (soft coke II) have considerably higher molecular masses, lower atomic H/C ratios and higher heteroatom contents than their easily extractable counterparts (Table 2). If the adsorbed soft coke is the major precursor of hard coke, then it is a case of concentrating the polars as opposed to the large polycyclic aromatic hydrocarbon moieties from the initial gas oil. Further, the aliphatic nature of the soft coke indicates that considerable condensation is required to form large aromatic structures.

Characteristics of the hard coke

The CP/MAS ¹³C NMR spectra of the hard coke concentrates from the low and high carbon catalysts (nos. 8 and 10, respectively) are shown in Figure 3. The aromaticities and the average ring sizes derived from the normal and dipolar dephasing ¹³C NMR spectra are listed in Table 3. There is a remarkable difference between the two samples. The concentrate from the low carbon catalyst is quite aliphatic in character (aromaticity of ca. 0.6) and contains relatively small aromatic clusters. In contrast, the hard coke from the high carbon catalyst has a high aromaticity and contains large clusters (Table 3). In fact, it is quite comparable in bulk structural terms to catalytic coke obtained in FCC^(11,12). These results indicate that aromatisation to large cluster sizes proceeds extremely slowly under hydrotreating conditions (relatively low temperature, high hydrogen pressure). Further, the aliphatic nature and small aromatic ring

cluster size for the hard coke obtained under typical operating conditions suggests that it should readily be converted into oil by hydrolysis under the conditions where high conversions are achieved for type I and II kerogens and low-rank coals⁽⁷⁾.

Reductive regeneration using hydrolysis

Figure 2 compares the carbon contents of the received, the chloroform-extracted and the hydrolysed samples for the low and high carbon samples. Carbon conversions of over 90% were achieved for the low carbon catalyst consistent with the bulk structural characteristics of the hard coke concentrate (Table 3). In contrast for the high carbon sample, hydrolysis removed only ca. 60% of the carbon which corresponds to ca.40% of the hard coke (Figure 2). Neither sample size nor grinding and diluting the samples in sand had a significant effect on the levels of carbon removal, the differences being below 5% of the total carbon.

Figure 3 indicates that the surface area recovery for the low carbon sample (ca. 70%) is comparable to that achieved by controlled combustion. In contrast, for the high carbon sample, the surface area recovery is considerably less than that by combustion (by ca. 30 m² g⁻¹) due to the low carbon conversion. For this catalyst, extraction of the soft coke alone gives rise to approximately 70% of the surface area recovery compared to controlled combustion (Figure 3). Thus, the soft coke is proportionally responsible for a much greater loss of surface area than in the case of the low carbon catalyst.

It is probable that a combination of a lower temperatures (450°C) and higher pressures to those employed in this initial study should probably represent the optimum conditions for maintaining catalyst surface area. It was observed that hydrolysis gave rise to sulfur reductions of up to 2% w/w. In order to prevent reduction of the promoter to the corresponding metal (Ni/Co), hydrolysis should be carried out in the presence of a small amount of hydrogen sulphide to help maintain the catalyst to remain in a reasonably fully sulfided form. Hydrolysis for virtual complete carbon removal will need to be carried out off-line since the combination of temperature, pressure and flow rate required cannot be achieved in hydrotreating units. In terms of potential applications, carbon-supported catalysts may represent the major area since these cannot be regenerated oxidatively.

CONCLUSIONS

Soft coke accounts for typically about one-third of the carbon on deactivated catalysts from gas oil hydrotreating units. The soft coke is highly polar in nature, but possesses significant aliphatic character. The hard coke obtained in normal operating situations (5-7 % carbon) has a carbon aromaticity of not much more than 50% and comprises small clusters. However, prolonged usage (carbon content > 15%) leads to a vast increase in aromaticity (>0.90) and ring cluster size. The majority of the hard coke obtained under normal operating conditions (> 80%) can be effectively removed by carrying out fixed-bed hydrolysis at 15 MPa and 500°C. This gives rise to a recovery in surface area comparable to that achieved oxidatively. Further improvements in hydrolysis in terms of surface area recovery are likely by operating at lower temperatures and higher pressures.

ACKNOWLEDGEMENTS

The authors thank EPSRC for financial support and Dr. K. Holder and colleagues at BP/Amoco for supplying the suite of deactivated HDS catalysts.

REFERENCES

1. Arteaga, A.; Fierro, J.L.G.; Dellanay, F.; Delmon, B. *Appl. Catal.* **1986**, *26*, 227.
2. George, Z.M.; Mohamed, P.E.; Tower, R. *Proc. Int. Congr. Catal.*, *9th 1988*, 230.
3. Teixeira da Silva, V.L.S.; Frety, R.; Schmal, M. *Ind. Chem. Eng. Res.* **1994**, *33*, 1692.
4. Teixeira da Silva, V.L.S.; Lima, F.P.; Dieguez, L.C.; Schmal, M. *Ind. Eng. Chem. Res.* **1998**, *37*, 882.
5. Maraf, M.; Stanislaus, A. *Appl. Catal.* **1989**, *47*, 85.
6. Babcock, K.E.; Hiltzik, L.; Ernst, W.R.; Garruthers, J.D. *Appl. Catal.*, **1989**, *61*, 295.
7. Rocha, J.D.; Brown, S.D.; Love, G.D.; Snape, C.E. *Journal of Anal. and Appl. Pyrolysis* **1997**, *40-41*, 91.
8. Brown, S.D.; Sirkecioglu, O.; Snape, C.E.; Eglinton, T.I. *Energy & Fuels* **1997**, *11*, 532.
9. Snape, C.E.; Love, G.D.; Murray, I.P.; Bailey, N.J.L. *Organic Geochem.* **1998**, *29*, 1487.
10. Love, G.D.; McAulay, A.D.; Snape, C.E.; Bishop, A.N. *Energy & Fuels* **1997**, *11*, 522.

11. Snape, C.E.; McGhee, B.J.; Andrése, J.M.; Hughes, R.; Koon, C.L.; Hutchings, G.
12. Snape, C.E.; McGhee, B.J.; Martin, S.C.; Andrése, J.M. *Catalysis Today* 1997, 37(3), 285.

Table 1 Coke contents for the suite of deactivated HDS catalysts

Sample no.	%C	%Soft coke 1 (carbon basis)
1	5.6	30
2	6.1	25
3	5.3	33
4	6.5	36
5	6.4	28
6	6.5	39
7	7.4	32
8* (3 months)	8.2	49
9	6.8	43
10* (8 years)	17.8	31

Samples 1-7 from the same unit, 1 at top and 7 nearest bottom of bed.

* selected for detailed characterisation.

Table 2 Summary of the soft coke composition for the suite of deactivated HDS catalysts

	Soft Coke I	Soft Coke II
Atomic H/C	1.60 - 1.85	1.5
% N	0.5-0.8	1.3
% S	< 0.2	< 0.2
%O (by difference)	3-6	>10
% Aliphatics	<10	n.d.
% Aromatics:	<20	n.d.
% Polars:	>70	n.d.
M _n :	200-300	240-340
M _w :	270-380	420-460

n.d. = not determined.

Table 3 Summary of structural parameters for the hard coke concentrates

Parameter	Low carbon (no. 8)	High carbon (no.10)
Carbon aromaticity	0.58	0.42
Fraction of aromatic C that is non-protonated	0.56	0.53
Fraction of aromatic C that is bridgehead	0.1-0.2	0.44
Inferred ring size	1-2	8

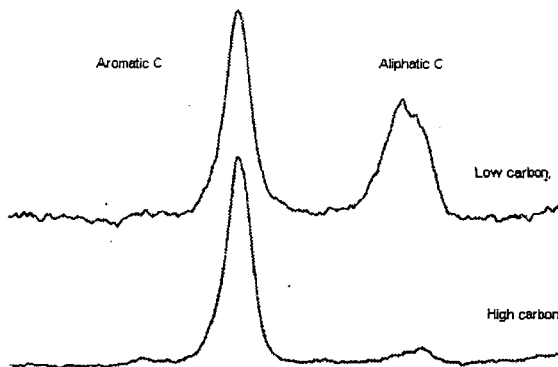


Figure 1. Solid state CP/MAS ¹³C NMR spectra of hard coke concentrates from low carbon (top) and high carbon (bottom) deactivated HDS catalysts.

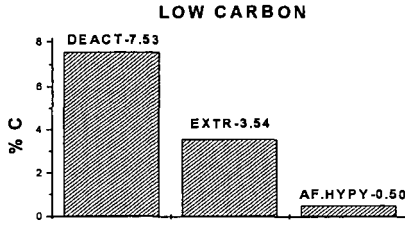
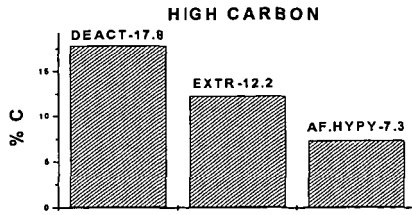


Figure 2. Carbon contents for the low and high carbon deactivated HDS catalysts – as received, after chloroform extraction and after hydropyrolysis.

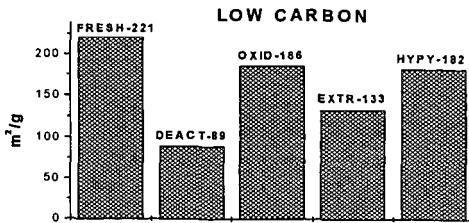
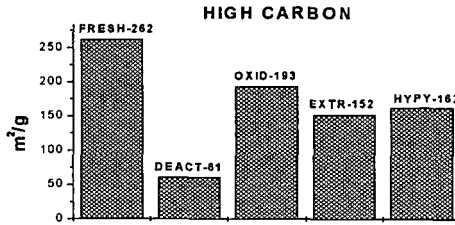


Figure 3. BET surface areas for the low and high carbon deactivated HDS catalysts – as received, after chloroform extraction and after hydropyrolysis.

HYDROGENATION OF PETROLEUM RESIDUA IN DIFFERENT FLUID MEDIA

Ming-Gang Yang¹, Qing-Feng Zha² and Semih Eser^{1,3}

1. Lab. for Hydrocarbon Proc. Chem., The Energy Institute, Penn State Univ., 209 Acad. Proj. Bldg.

2. The Institute of Coal Chem., Chinese Academy of Sciences, P.O. Box 165, Taiyuan, China

3. Dept. of Energy and Geo-Environmental Eng., Penn State Univ., 154 Hosler Building,
University Park, PA 16802

KEYWORDS: Hydrogenation, Residua, Supercritical fluid

INTRODUCTION

In recent decades, hydroprocessing has played a very important role in upgrading petroleum heavy oils. Compared to thermal processes, hydroprocessing gave distillates not only in higher yield but also in higher quality^{1,2} to meet the environmental constraints on petroleum products. In hydroprocessing, the chemical reactions, such as hydrodesulfurization, hydrogenation, and hydrocracking, occur among the three phases that are gaseous hydrogen, liquid heavy oils and solid catalysts. In order to promote diffusion of hydrogen from gas phase into the surface of catalysts and prolong the catalyst life, high operating pressure is necessary in hydroprocessing. Upgrading petroleum heavy oils in supercritical fluids has been studied in recent years to improve diffusion of reactants and products in reaction systems and to prolong catalyst life. A recent study showed that coke deposits on catalysts were decreased and heteroatom removal was increased when hydrotreating shale oils in supercritical fluids such as toluene and n-heptane³. In such supercritical reaction processes, however, a large amount of supercritical fluid medium (4 times larger than the amount of reactants) has to be used to see the benefits.

Some researchers^{4,5} studied the effects of adding some solvents, for example, on reducing coke formation and increasing heteroatom removal. The solvents used are usually polynuclear aromatics with partial hydrogen saturation. These solvents are considered to facilitate hydrogen transfer by donating or shuttling hydrogen. The conclusions derived from these studies are still controversial. It appears that the effects of the solvents depend strongly on the feedstocks.

In this study, we investigated the effects of adding small concentration of different fluids, e.g., toluene, hexane and pyridine, on catalytic hydrogenation of pyrene and two petroleum distillation residua. Ammonium tetrathiomolybdate was used as a catalyst precursor in the hydrogenation experiments.

EXPERIMENTAL

Pyrene (99% purity) was supplied by Aldrich Chemical Company Inc. The properties of the petroleum residua used in the present work, an atmospheric residue (AR) and a vacuum residue (VR), are listed in Table 1. Hydrogen gas used in the experiments was ultra high purity hydrogen supplied by MG Industries. Ammonium tetrathiomolybdate (ATTM) supplied by Aldrich Chemical Company Inc. was used as a catalyst precursor. Its purity is 99.97%. ATTM decomposes to amorphous MoS₂, H₂S and NH₃ when heated in hydrogen. MoS₂ has catalytic activity for pyrene and petroleum residua hydrogenation.

Table 1. Properties of petroleum residua

	Asphaltene content wt %	H/C atomic ratio	Sulfur content wt %	Residue fraction (525 °C+) / wt %
AR	9.2	1.58	3.9	55.7
VR	14.0	1.33	4.8	88.2

The n-hexane, toluene, pyridine and water were used in the present work to investigate the effect of the fluid media on the pyrene and petroleum residua hydrogenation. The n-hexane and toluene were supplied by J. T. Baker Inc. The purity was more than 95 and 99.9 % for n-hexane and toluene, respectively. Deionized water with high purity was used in the experiments.

Reactions were carried out in 316 stainless steel batch reactors (20 mL) heated in a fluidized-sand bath. Except for investigating the effect of the amount of the fluid media, the quantity of the media used in the experiments was kept a constant at 2 mol % with respect to the quantity of hydrogen initially present. For instance, approximately 0.16 g of toluene was added per 0.083 mol hydrogen. ATTM of 3.8 wt% based on reactant (pyrene or petroleum residue) was added into the reactor in each run, which corresponds to a metal loading of 1.5 wt %. After adding the reactant (pyrene, AR

or VR), ATTM catalyst precursor and liquid fluid medium, the headspace gas in the reactor was replaced three times with hydrogen before the reactor was charged with hydrogen to the desired cold pressure. Then, the reactor was plunged into a preheated sand bath. The reactor contents reached the desired reaction temperature within 3 minutes. At the end of the reaction, the reactor was quenched in cold water. Products and catalyst mixtures were washed with toluene. Then the catalyst was separated from the toluene solution by filtration. After evaporation in Rotavapor, the toluene solvent and the fluid medium were separated and the product mixture was recovered.

Products resulted from pyrene hydrogenation were characterized by GC-MS using standard compounds, and measured quantitatively by GC-FID with a DB-17 capillary column. Products from residue hydrogenation were analyzed by CHN-600 elemental analyzer and LECO sulfur analyzer to determinate H/C atomic ratio and sulfur content of the product mixture. Asphaltene (here defined as materials insoluble in n-hexane) contents of the products were measured by treating the sample (0.2 ± 0.02 g) with n-hexane (20 mL) in an ultrasonic water bath for 5 minutes, followed by setting for another 10 minutes before vacuum filtration through a previously weighed GF/A filter paper. The filtration residue was washed with excess n-hexane (about 30 mL). The solid residue and the sample vial (as some residue remains adhered to the vial wall) were dried in a vacuum oven and then weighed to determine the asphaltene content of the sample.

RESULTS AND DISCUSSION

Pyrene hydrogenation. Products of pyrene hydrogenation were mainly composed of dihydroxyrene, tetrahydroxyrene and hexahydroxyrene. At high pyrene conversion, some amount of decahydroxyrene was also found in the product mixture. Pyrene conversion was defined as the difference of pyrene content in reactant and product mixture in percent. Figure 1 compares pyrene conversion obtained in four binary mixtures of hydrogen with n-hexane, toluene, pyridine, and water (containing 2 mol % of each compound in the starting mixtures with respect to the hydrogen) to that obtained in pure hydrogen at 375 °C and 90 min. The cold hydrogen pressure in the reactor determines the hydrogen mole content in the reactant mixture, and changes the initial total pressure at the reaction temperature, as shown in Table 2. A pyrene conversion 23 % was obtained at 0.083 mol hydrogen in pure H₂ gas, reaching the thermodynamic equilibrium. It is notable that a much higher conversion was obtained with the addition of the second compound at the same hydrogen mole content, except in the case of adding pyridine at a relatively high pressure. The highest conversion (64%) was obtained with the addition of toluene, followed by the addition of water (61%) and n-hexane (56%). Although it is not clear why conversion decreases from 42% to 24% there were signs of pyridine hydrogenation at 1750 psi when the total pressure was increased from 1400 to 1750 psi in pyridine + hydrogen mixtures. It is clearly shown in Figure 1 that the addition of toluene, n-hexane or water strongly promoted the pyrene hydrogenation at the some partial pressure of H₂ initially.

Table 2. Changes of cold hydrogen pressure and corresponding hydrogen molar content and initial total reactor pressure at 375 °C

H ₂ mole	H ₂ cold Pressure /psi	Initial reactor pressure / psi			
		H ₂	H ₂ +n-hexane	H ₂ +toluene	H ₂ +pyridine
0.017	200	400	350	430	350
0.034	400	800	700	810	780
0.052	600	1200	1100	1060	1150
0.069	800	1700	1460	1520	1400
0.083	1000	2000	1919	1850	1750

The effect of increasing the toluene concentration in the binary mixture on pyrene conversion is shown in Figure 2. A significant increase in the conversion was observed upon adding a small amount of toluene and the conversion quickly leveled off with further addition of toluene. Toluene, as a mono-ring aromatic compound, does not act as a hydrogen shuttle, like some polynuclear aromatics that transfer radical hydrogen to hydrogen acceptors⁵. The trend in Figure 2 clearly shows that a step increase was obtained in pyrene conversion upon incremental addition of toluene, related most likely to large changes in critical properties of the H₂ and toluene mixture compared to those of H₂ alone. Further increase in toluene concentration may not cause much change in the critical properties of the mixture.

Residua hydrogenation. The change in the n-hexane insoluble components (HI, asphaltenes) content of the residua samples was used as a preliminary measure for the extent of hydrogenation. Figure 3-4 shows the change in HI of AR and VR residua as a function of hydrogen mole content in pure hydrogen and three binary mixtures. The reaction conditions were the same as those of pyrene hydrogenation. For the mixture of hydrogen with toluene, water, and pyridine, the concentration of the second fluid was kept constant at 2 mole % of the initial hydrogen. The trends

are remarkably similar to those obtained with pyrene hydrogenation in the same fluid mixtures. The H₂ + toluene mixtures produced the highest conversion and all binary mixtures gave higher conversions than that achieved with hydrogen alone. The trends of asphaltene reduction in the mixtures of H₂ + water were similar to those with H₂ + toluene mixtures and also gave higher reductions in asphaltenes than those obtained by pure hydrogen. Comparing Figure 3 with 4, under the present reaction conditions, it is clearly shown that the asphaltene reduction by hydrogenation depends strongly on the addition of the second compound for both residua, AR and VR.

Table 3 shows for both residua the H/C atomic ratio and sulfur content of the products obtained by hydrogenation of AR and VR in pure hydrogen, and in mixtures of H₂ + toluene. There was not much change in the elemental composition under the present reaction conditions, and only slight increases were observed in the H/C ratios of the hydrogenated products in the case of H₂ + toluene. The reductions in sulfur contents were small, and showed, in general, that ATTM has little desulfurization activity under the reaction conditions.

Table 3. Comparison of H/C ratio and sulfur content in hydrogenated products

Feedstock	Fluid media	H/C atomic ratio	Sulfur content wt %
AR	H ₂	1.58	3.61
	H ₂ + Toluene	1.60	3.62
VR	H ₂	1.33	4.73
	H ₂ + Toluene	1.37	4.60

CONCLUSIONS

The addition of a small amount of fluids (toluene, water or n-hexane) strongly promotes the hydrogenation of pyrene with ATTM. In hydrogenation of petroleum residua, the addition of the fluids reduced the asphaltene content of the products and increased the H/C ratio of hydrogenated products. These promotional effects could result from the changes in the supercritical properties of the fluid media (mixture of hydrogen and the added second compound).

ACKNOWLEDGMENTS

This study was supported by funding from Marathon Oil Company. Many helpful discussions with Dr. Mark A. Plummer and Mr. Rolf R. Schroeder of Marathon Oil are gratefully acknowledged.

REFERENCES

- Sonnemans, J. W. M. In *Catalysts in Petroleum Refining and Petrochemical Industries* 1995; Stud. Surf. Sci. Catal., Elsevier Sci. B. V. 1996, Vol. 100, p99-115.
- Yang, M.-G.; Nakamura, I.; Fujimoto, K. *Catal. Today* 1998, 43, 273.
- Low, J. Y. In *Supercritical Fluids*, ACS Symposium Series 329, Sep.8-13, 1985, p.281.
- Aaarts, J. J. B., Ternan, M., Parsons, B. I., *Fuel*, 1978, 57, 473.
- Kubo, J., *Energy & Fuels*, 1996, 10, 474.
- Arends, I. W. C. E., Mulder, P. *Energy & Fuels*, 1996, 10, 235.

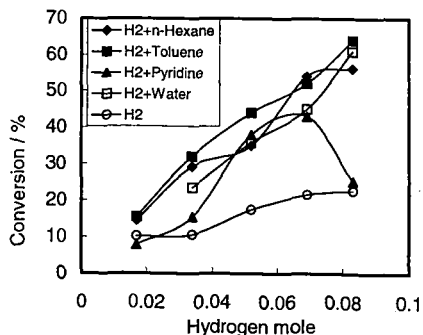


Figure 1. Pyrene hydrogenation in different fluid media. 375 °C, 90 min.

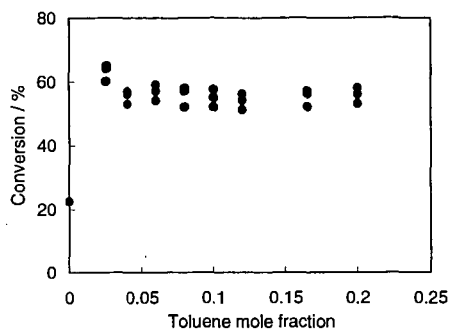


Figure 2. Pyrene conversion as a function of toluene mole fraction in mixtures of H₂-Toluene (H₂ = 0.083 mole). 375 °C, 1000 psi H₂ (cold), 90 min.

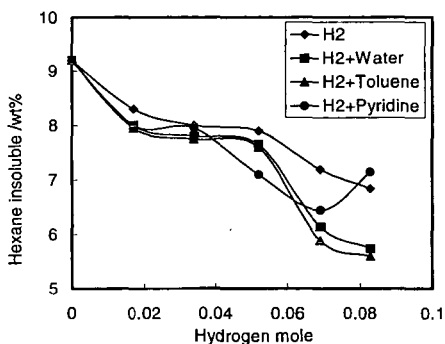


Figure 3. Asphaltene content in products from hydrogenation of AR in different fluid media. 375 °C, 1000 psi H₂ (cold), 90 min.

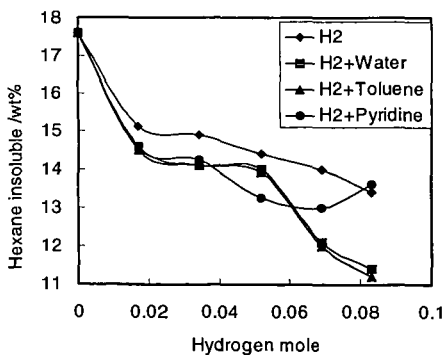


Figure 4. Asphaltene content in products from hydrogenation of VR in different fluid media. 375 °C, 1000 psi H₂ (cold), 90 min.